Preparation and Properties of Long Persistent $Sr_4Al_{14}O_{25}$ Phosphors Activated by Rare Earth Metal Ions

March 2010

Department of Energy and Materials Science
Graduate School of Science and Engineering
Saga University

HOM NATH LUITEL

Preparation and Properties of Long Persistent $Sr_4Al_{14}O_{25}$ Phosphors Activated by Rare Earth Metal Ions

By

Hom Nath LUITEL

Supervisor: Professor Dr Takanori Watari

A Dissertation Presented in Partial Fulfillment of the Requirements for the Degree of Philosophy in Applied Chemistry

Doctor of Philosophy

Department of Energy and Materials Science

Graduate School of Science and Engineering

Saga University

March 2010

APPROVAL

Preparation and Properties of Long Persistent $Sr_4Al_{14}O_{25}$ Phosphors Activated by Rare Earth Metal Ions

by

Hom Nath Luitel

A Dissertation Presented in Partial Fulfillment of the Requirements for the Degree of Philosophy in Applied Chemistry

Doctor of Philosophy

Department of Energy and Materials Science
Graduate School of Science and Engineering
SAGA UNIVERSITY

Dissertation Committee:

Takanori Watari 3/9/2010

Supervisor, Prof. Takanori WATARI Date
Department of Applied Chemistry

H Noguchi 3/9/2010

Co-supervisor, Prof. Hideyuki NOGUCHI Date

Hiroyoshi Nakamura 3/9/2010

Member, Prof. Hiroyoshi NAKAMURA Date

Mitsunori Yada 3/9/2010

Member, Prof. Mitsunori YADA Date

ABSTRACT

Preparation and Properties of Long Persistent $Sr_4Al_{14}O_{25}$ Phosphors Activated by Rare Earth Metal Ions

Chairperson of the Supervisory Committee: Professor Takanori WATARI
Department of Energy and Materials Science, Saga University

This work comprises of several aspects of phosphor materials, especially, strontium aluminate phosphor activated with rare metal ions. The 1st chapter gives a brief and general background of phosphor materials, its synthesis methods and underlined phosphorescence mechanisms.

In 2nd chapter, long persistent $Sr_4Al_{14}O_{25}:Eu^{2+}/Dy^{3+}$ blue-green phosphor was prepared by solid state reaction method. The effect of synthesis parameters like calcinations temperature and time, calcinations environment and effect of additives like addition of boron and rare earth ions (Eu^{2+}, Dy^{3+}) were studied in detail. When the phosphor was prepared adding 4 mol% H_3BO_3, it showed dense microstructure composed of pure $Sr_4Al_{14}O_{25}$ phase showing higher emission intensity. But in the samples containing less than 3.5 mol% H_3BO_3, mixed phases consisting of Al_2O_3, $SrAl_{12}O_{19}$ and $SrAl_2O_4$ were observed, while if higher H_3BO_3 content (8 mol%) was used, $SrAl_2B_2O_7$ phases predominated. The phosphor showed blue-green emission centered nearly at 500 nm. However, the emission maxima and its intensity depend on the Eu^{2+} and Dy^{3+} concentrations. Both the initial intensity and afterglow duration increased and reached maximum at 4 at% Eu^{2+} and 8 at% Dy^{3+}, respectively, and then decreased above that value. The decay curve fitting results revealed that the phosphor with the aluminium to strontium ratio (Al/Sr) of 3.7 has deeper trap depths and hence showed the longer afterglow duration over other compositions. Addition of 3 mol% Ag^+ as charge compensator effectively enhanced the brightness of the phosphor. Substitution of part or whole of strontium sites by calcium or barium ions can effectively monitor the emission light color and CIE values of it. When 0.7 to 0.8 mole fraction of strontium was substituted by calcium, a bluish white luminescence was observed, however the persistent white afterglow achieved was very short. Use of γ-alumina of 0.05μm size as a raw powder during the synthesis of phosphor was found to be effective for the formation of regular particles with smaller particles size over other alumina type and showed better photoluminescence characteristics.

In chapter 3, the $Sr_4Al_{14}O_{25}:Eu^{2+}/Dy^{3+}$ phosphor was synthesized by solid state, solution combustion and sol-gel reaction methods. Their microstructures variation and its effect on the photoluminescence properties were studied. X-ray diffraction (XRD) patterns revealed that the same $Sr_4Al_{14}O_{25}$ phase was formed irrespective of the synthesis method used. Scanning electron microscopy (SEM) observations showed that regular morphology and fine particles were achieved by sol-gel and solution combustion methods at lower firing temperatures. Obviously, much bigger, agglomerated particles with higher crystallinity can be obtained by solid phase method at high calcination temperature. The photoluminescence properties were found to be dependent on the firing temperature. However, even at the same firing temperature, solution combustion samples showed better photoluminescence properties.

In chapter 4, Cr^{3+} doped $Sr_4Al_{14}O_{25}$: Eu^{2+}/Dy^{3+} persistent phosphor was synthesized by cheap, easy and efficient combustion method. Persistent phosphorescence in blue-green (495nm) by Eu^{2+} emission and in red (695 nm) by Cr^{3+} emission was observed in this phosphor. The persistent time for blue-green emission was over 10 h but for red emission, it was comparatively short. Red phosphorescence was evinced through the persistent energy transfer from Eu^{2+} to Cr^{3+}, converting the blue-green emission to the red. The energy transfer rate increased on increasing the Cr^{3+} ions concentration and reached optimum at 4 at%. Comparative results revealed that the relatively regular morphology, smaller particle size and narrow size distribution can be achieved for the phosphor synthesized by the combustion method.

In chapter 5, $Sr_4Al_{14}O_{25}:Sm^{3+}$ phosphor was prepared by high temperature solid state reaction method. UV-visible absorption and photoluminescence emission spectra were investigated for the phosphor at different annealing temperatures and various doped concentrations of Sm^{3+} ions with different amount of H_3BO_3 as a flux. The phosphor showed the orange-red emission consisting of several peaks due to transition from $^4G_{5/2}$ level to the $^6H_{5/2}$, $^6H_{7/2}$, $^6H_{9/2}$ and $^6H_{11/2}$ levels of Sm^{3+} ion. The emission intensity of Sm^{3+} ions in the $Sr_4Al_{14}O_{25}$ host largely enhanced with the amount of flux, concentration of dopant (Sm^{3+}) and addition of some trivalent metal ions. The maximum intensity was observed in the phosphor prepared using 3.5 mol% boric acid as a flux, 2 at% of Sm^{3+} as a activator and 4 at% Bi^{3+} as co-activator at 1350^{o}C. The detail conclusions are summarized in chapter 7.

TABLE OF CONTENTS

Chapter **Page**

LIST OF FIGURES

LIST OF TABLES

ACKNOWLEDGEMENT

I would like to express my heartfelt gratitude and sincere indebtedness to my supervisor Prof. Takanori Watari who kindly accepted me as a student in the Ceramics laboratory. His continuous guidance, constructive criticism, valuable comments and suggestions were indispensable for the completion of my degree.

I am deeply indebted to Prof. Hideyuki Noguchi, Prof. Mitsunori Yada and Prof. Hiroyoshi Nakamura for their constructive and invaluable suggestions during the revision of the dissertation. I also wish to convey my sincere thanks to Prof. Chao-Nan Xu and Dr. Kazuhiro Nanoka (AIST Tosu) for their generous assistance in my research work.

I am grateful to Mr. Toshio Torikai and Ms. Yuki Inoue for their continuous support and help in various aspects. I am thankful to all the members of the Ceramics Laboratory for their contentious help and comments during the completion of my doctorate course.

I am deeply grateful to Prof. M.B. Gewali and Prof. K.N. Ghimire at Tribhuvan University, Nepal, for their innovative encouragement during my research periods.

I am particularly indebted to the teachers and Profs. of Saraswati Lower secondary school, Triveni High school, National School of Sciences, Kathmandu Valley College, Amrit Science College and Central Department of Chemistry, Tribhuvan University. It is my pleasure to remember Mr. Swagat Shrestha, Mr. Ramesh Dhakal, Dr. Durga Parajuli, Dr. Chaitnaya R. Ahikari and Dr. Arjun K. Thapa for their supports during my study. Especial thanks goes to Mr. Bishnu Prasad Bastakoti for TEM measurements.

Thanks are also due to many Japanese personalities in and around Saga and all Nepalese friends in Saga for their kind hospitality, friendly treatment and assistance in various matters.

I gratefully acknowledge 'The Japan Science Society' for granting me The Sasagawa Scientific Research Grant.

I would like to express my indebtedness to my parents, brothers and sisters for their encouragement and moral support. Last but not least, I would like to thank my dear Rumi for her inspiration and emotional support during the completion of my doctorate course.

I would like to dedicate this dissertation to my **late mother**.

Hom Nath Luitel
April, 2010

Chapter I

General Introduction

1.1. Phosphor Terminology

The term *Phosphor* was invented in the early 17th century in Italy by an alchemist Vincentinus Casciarolo [1]. He fired a heavy crystalline stone with a gloss at the foot of a volcano to obtain a novel metal. Instead, he found that the sintered stone emitted red light in the dark after exposure to the sun light. From the knowledge now known, the stone was $BaSO_4$ and the fired product was BaS ($BaSO_4 + 2C \rightarrow BaS + 2CO_2$) which is now known to be a host for phosphor materials. Later phosphor developments occurred in 1768 when Canton obtained CaS and then in 1866 when Sidot formed the first ZnS, green emitting luminescent material. An understanding of the luminescence from these materials begin in 1886 when Verneuil proved that pure CaS did not luminance and a trace of Bi was necessary for light emission. Later, it was found that a trace of Cu was necessary for emission from green ZnS and Cr for red BaS.

Literally, the term phosphor means “light bearer”. In general, a phosphor is a solid that converts certain types of energy into electromagnetic radiation over and above the thermal radiation [1]. The word *Phosphorescence*, which means persistent light emission from a substance after the excitation source is ceased, was also derived from the word phosphor. The term *Fluorescence* was introduced to denote the imperceptible short afterglow of the materials after excitation. This is to distinguish the emission from the phosphorescence which is used to denote a long afterglow [2-3]. The term fluorescence and phosphorescence had created controversy centered on the duration of the afterglow after excitation was ceased. But, in the modern usage, light emission from a substance during the time when it is exposed to excitation source is called fluorescence whereas the afterglow if detected by the human eye after the cessation of the excitation is called phosphorescence (The term is different in organic molecules where light emission from singlet and triplet excited states are called fluorescence and phosphorescence, respectively). The term

Luminescence, which includes both fluorescence and phosphorescence, is defined as a phenomenon in which the electronic states of substance is excited by some kind of external energy and the excitation energy is given off as light of various wavelengths [1].

1.2. Fundamental of luminescence

A phenomenon of emission of light by certain materials after exposure of it to the excitation source is called luminescence. Depending on the type of excitation sources, luminescence is broadly classified as: Photoluminescence is excited by electromagnetic radiations, Cathodoluminescence by energetic electrons, Electroluminescence by electric voltage, Chemiluminescence by the energy of chemical reaction and Triboluminescence by the mechanical energy [2-3]. In this dissertation, we concern especially on the photoluminescence and hence the other types of luminescence will not be discussed onward.

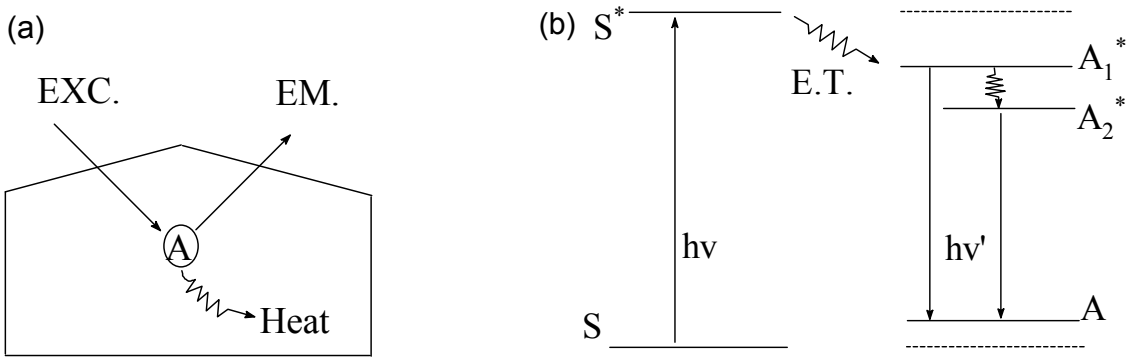

Fig. 1.1. (a) Luminescent ion A in the host lattice, EXC: excitation, EM: emission, Heat: non radiative return to ground state and (b) Schematic energy level diagram of the luminescent ion A in the host lattice.

Figure 1.1 represents a simple luminescence system. In this system, the exciting radiation is absorbed by the activator ion (A), raising it to the excited state (A*). The excited state either returns to the ground state by the emission of the radiation, called luminescence or non-radiative return to the ground state by transferring energy to excite the vibrations of the host lattice, *i.e.* to heat the host lattice. For example, in case of ruby (Al_2O_3:Cr^{3+}), Al_2O_3 is a host, Cr^{3+} is an activator or luminescent center. The excitation energy is absorbed by

Cr^{3+} and excited to $(Cr^{3+})^*$ transient state and it radiate to the red region of the spectrum producing red color in the dark.

In many luminescent materials, the situation is more complicated because the activator either does not absorb the excitation energy itself, or the absorbed energy is transferred to the neighboring luminescent centers as shown below:

$$Eu^{3+} + h\nu \longrightarrow (Eu^{3+})^* \quad (1.1)$$

$$(Eu^{3+})^* + Cr^{3+} \longrightarrow Eu^{3+} + (Cr^{3+})^* \quad (1.2)$$

$$(Cr^{3+})^* \longrightarrow Cr^{3+} + h\nu' \quad (1.3)$$

The equations above indicate absorption, energy transfer and emission, respectively.

1.3. Long Persistent Phosphor

Long persistent phosphors are phosphors that have very long afterglow emission or phosphorescence, in some cases even longer than a whole day. Afterglow is caused by trapped electrons or holes produced during the excitation. Long persistent phosphors are also called long lasting or long afterglow phosphors.

The mechanism of long persistent phosphorescence can be explained in term of three level energy diagrams including a ground state, an excited state and a metastable trapping state for the active electron as simplified in Fig. 1.2. The detail mechanism of long persistent phosphorescence will be discussed later in section 1.3.2.

Phosphorescence life times are usually longer than the life time of excited state and depend on the trap depth and trapping de-trapping rates. Fluorescence, on the other hand, is based on the two level electron transition mechanisms, which includes a ground state and an excited state. The decay time of fluorescence depends on the transition strength between the two states.

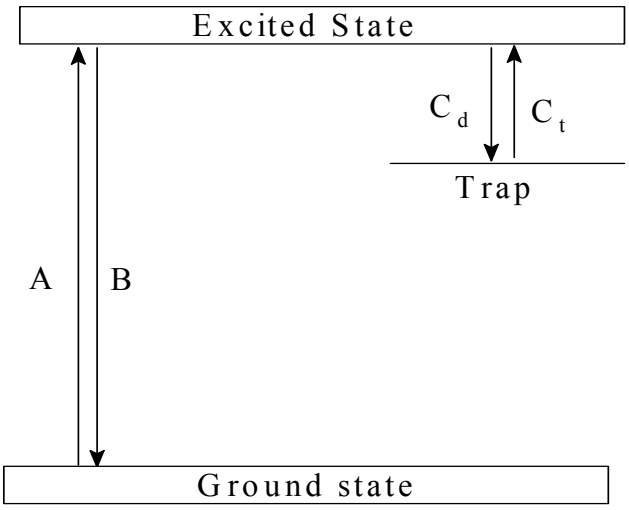

Fig.1.2. Three level model showing the mechanism of long persistent materials. C_t and C_d are the trapping and de-trapping rates, respectively and A and B are the excitation and emission rates, respectively.

Phosphorescence can be classified by its life time as: Very Short Persistent Phosphorescence (VSPP) that has life time of the same order of magnitude as the life time of excited state, *i.e.* in the order of milliseconds, and it is associated with very shallow traps. Some examples are scintillates. Short Persistent Phosphorescence (SPP) that lasts for seconds and generally becomes noticeable to the human eyes. Most phosphor show short persistent phosphorescence after they are exposed to the UV, visible light, plasma beam, electron beam or X-rays. Persistent Phosphorescence (PP) that lasts for minutes and it is due to the deep traps in the materials. These traps hold electrons or holes for some shorts of time and release thermally. Long Persistent Phosphorescence (LPP) that shows life times in the order of tens of minutes or hours. Some example of long persistent phosphors are, $SrAl_2O_4:Eu^{2+}/Dy^{3+}$, $Sr_4Al_{14}O_{25}:Eu^{2+}/Dy^{3+}$, $CaAl_2O_4$: Eu^{2+}/Nd^{3+} *etc.* In this dissertation we are mainly focused on these long persistent phosphors.

1.3.1. History of long persistent phosphors

The first reported instances of light emission from materials entitled persistent phosphorescence, different from radiation stimulated phosphors, was Bolonga Stone (BaS) and appeared in 1609 [4]. More recent development in long persistent phosphors dated to early eras of last century. ZnS based phosphors, such as $ZnS:Cu^+$, were found to have

persistent times as long as 40 minutes [5]. The effect of co-doping were also investigated for example, co-doping ZnS:Cu^{+} with Co^{2+} doubled the persistent time of the phosphor [6].

The next generation of long persistent phosphors compromised the alkali earth sulphides, such as CaS, and SrS. These phosphors, known as Lenard's phosphors [7], activated with various dopants such as Bi^{3+}, Eu^{2+}, Ce^{3+} *etc.* exhibited long persistency over hours. These phosphors can be excited by sunlight showing versatility in applications. However, the applications of these sulphide based phosphors were limited due to chemically unstable and released H_2S when exposed to moisture [8].

In 1990s, Matsuzawa reported a new type of long persistent phosphor, $SrAl_2O_4$:Eu^{2+}/Dy^{3+}, with a strong emission centered at 520 nm (green) [9-10]. The persistent time of this $SrAl_2O_4$:Eu^{2+}/Dy^{3+} phosphor was found to be longer than 16 h. After a short time, a new similar long persistent phosphor $CaAl_2O_4$:Ce^{3+}/Nd^{3+} was reported emitting at 420 nm (dark-blue) [11]. Later, $Sr_4Al_{14}O_{25}$:Eu^{2+}/Dy^{3+} phosphor was developed showing extremely prolonged blue-green (495 nm) phosphorescence that lasts over 20 h [12-13]. These phosphors drew considerable attention because of their ability to persist overnight, chemical stability, wide range of excitation, high quantum yield *etc.* and opened prospect of various applications [14-15].

Recently, the long persistent phosphor research is concentrated in two directions. The first is in the identification of trapping-de-trapping mechanisms of the long persistent phenomena following the improvements on the persistency of the existing phosphors [16-18]. The second is in the development of new long persistent phosphor materials providing coverage through the visible spectrum, the long persistent phosphor with the red color is of particular interest. In the first direction, systematic study on the alkaline earth aluminates doped with Ce^{3+} or Eu^{2+}, for example, have led to the conclusion that trapping-de-trapping mechanisms are closely related to the electrons delocalization processes [19-20]. Many long persistent phosphors have been developed recently such as alkaline earth aluminates doped with Eu^{2+}, Ce^{3+}, Tb^{3+}, Mn^{2+} [21-24], alkaline earth silicates and oxysulphides doped with Eu^{2+}, Er^{3+}, Eu^{3+}, Ti^{4+} and Mg^{2+} [25-27], nitrides and oxy-nitrides [28-29], phosphates [30], halides [31], and so on.

Although many new phosphors have been developed recently, only a few can be excited under natural light like sunlight. The issue of convenient excitation source is very important and actually limits the applications of long persistent phosphors. Many novel methods in the synthesis have been developed to produce persistent materials. These methods mainly includes, preferential co-doping with various ions to create electrons or hole traps, co-doping ions to create defect related electron traps, and introducing sensitizers for persistent energy transfer.

It has been generally accepted that long persistent phosphor results from intrinsic traps or intentionally induced traps or from both. Generally, the traps can be divided into two groups, electron traps that capture electrons below the conduction band and hole traps that capture holes above the valence band. Some traps appear as defect in the host materials, F centers and V (vacancy) centers in crystals are of typical of these types of defects [32-33]. These centers are usually generated by charge compensation requirements to maintain neutrality of a host. For example, in $CaAl_2O_4:Nd^{3+}$ phosphor, Nd^{3+} ions occupy Ca^{2+} sites. Due to the necessity of charge compensations, three Ca^{2+} ions are replaced by two Nd^{3+} ions and results Ca^{2+} vacancy (V^{2+} center). The net negative environment at this site is capable of trapping a hole. Instead, in $CaS:Bi^{3+}$ phosphor, if $2Bi^{3+}$ ions replaces $3Ca^{2+}$ ions (Bi_2S_3-3CaS), then interstitial ions are needed to maintain the neutrality. In this case, the resulting net +2 charge environment will be able to trap electrons. In $CaAl_2O_4:Nd^{3+}$ phosphor, addition of charge compensators like Na^+, Ag^+ *etc.* ions significantly reduce the number of defect centers. When Na^+ ion and Bi^{3+} ion replace two Ca^{2+} site ($NaBiS_2$-2CaS), the like hood of charge related defect centers is reduced so that persistent time is reduced significantly [34].

Another example of defect trapping centers occurs in $SrAl_2O_4:Eu^{2+}$ phosphor. Stoichometric $SrAl_2O_4:Eu^{2+}$ phosphor does not evince any persistent afterglow. If Dy^{3+} is co-doped into $SrAl_2O_4:Eu^{2+}$ phosphor, very long persistent afterglow is observed [21]. The traps may be created intrinsically or by introduction of specific dopants. Defect related traps are easy to be produced in host materials that have complicated crystal structures. Ionic size difference can also produce traps by creating dislocation and other strain related defects.

Another way of producing defect is non stoichometric composition of host or addition of some fluxes [35-36].

In many co-doped trapping centers, with the optical excitation, the dynamics of excited ions can be such as to create meta-stable states which properly belong to dopant ions in modified valance states, for example, $(Dy^{4+})^*$ in $SrAl_2O_4:Eu^{2+}/Dy^{3+}$ and $(Tm^{2+})^*$ in $CaS:Eu^{2+}/Tm^{3+}$ phosphors [10, 37]. These meta-stable states can also acts as trap centers since their electronic structures differs from that of normal dopant ions. The excited electrons or holes do not modify the bonding situation of the dopants, they are just represented by $(Dy^{4+})^*$ or $(Tm^{2+})^*$ where $(Dy^{4+})^* = Dy^{3+} + h^+$ and $(Tm^{2+})^* = Tm^{3+} + e^-$. The electrons and holes created in such a way are loosely bounded and can be easily detached thermally.

Even though the exact nature of meta-stable ionic states of the codopants is not well understood, these states are not simply altered ionic states but are considered more complex ionic entities [38]. The existence of hole and hole trapping model is supported by the observation of holes in the valence band by Photo-Hall effect [38] and unsymmetrical photocurrent experiments [10].

1.3.2. Mechanism of the long persistent phosphorescence

The long persistent phosphorescence mechanism of the inorganic phosphors activated by rare earth ions have been explained by many researchers in their own views supported by some experimental proofs. For a long time, the explanation of the persistent luminescence of rare earth metal activated aluminate phosphors relied on the Matsuzawa model as explained in Fig. 1.3 [10]. In this model, it was proposed that in $SrAl_2O_4:Eu^{2+}/Dy^{3+}$ phosphor, the UV excitation of Eu^{2+} cations from the ground state ($4f^7$) to an excited state ($4f^65d^1$) ($Eu^{2+}\ (4f^7) + hv \rightarrow Eu^{2+*}\ (4f^65d^1)$), generates a hole in the f orbital in the vicinity of the valence band (VB). This transition is followed by an electron capture from the CB leading to the reduction $Eu^{2+*} + e^- \rightarrow Eu^+$. Thus, the hole created in the VB migrates through it and get captured by a Dy^{3+} cation located in suitable depth to form a Dy^{4+} cation, $Dy^{3+} + h^+ \rightarrow Dy^{4+}$. It is supposed that the return to the ground state of Eu^{2+} with light emission is triggered by the thermo-activated promotion of an electron from the

VB to the first unoccupied levels of Dy^{4+}, followed by the migration of trapped hole to a photo-generated Eu^{+} cation. This model was supported by photoconductivity measurements that confirmed the photo carrier is hole [18, 38]. This model was formulated in part to accommodate the hole type photoconductivity of $SrAl_2O_4:Eu^{2+}$ phosphor under the UV illumination founded by Abbruscato [38] and was used to explain the phosphorescence of numerous materials for long period of time. However, recent researcher has pointed out that the model is based on highly improbable assumptions. First, the reduction $Eu^{2+} + e^{-} \rightarrow Eu^{+}$ is highly unlikely (and needs high energy ≥ 4 eV), and so is the oxidation $Dy^{3+} + h^{+} \rightarrow Dy^{4+}$, due to the chemical instabilities of Eu^{+} and Dy^{4+} ions. Second, as recently pointed out by Dorenbos, the proposed VB $\rightarrow Eu^{2+*}$ ($4f^{6+}5d^{1}$) transition leading to the final $4f^{7}5d^{1}$ electronic configuration of Eu^{+} is based on an incorrect concept of a hole state [39]. Electronic band structure calculated for $SrAl_2O_4:Eu^{2+}$ showed that the Eu d-block lie just below the CB bottom and 4f-block of Eu at approximately 3 eV above the VB top [21]. These observations definitely do not support the mechanism of Matsuzawa *et al.*

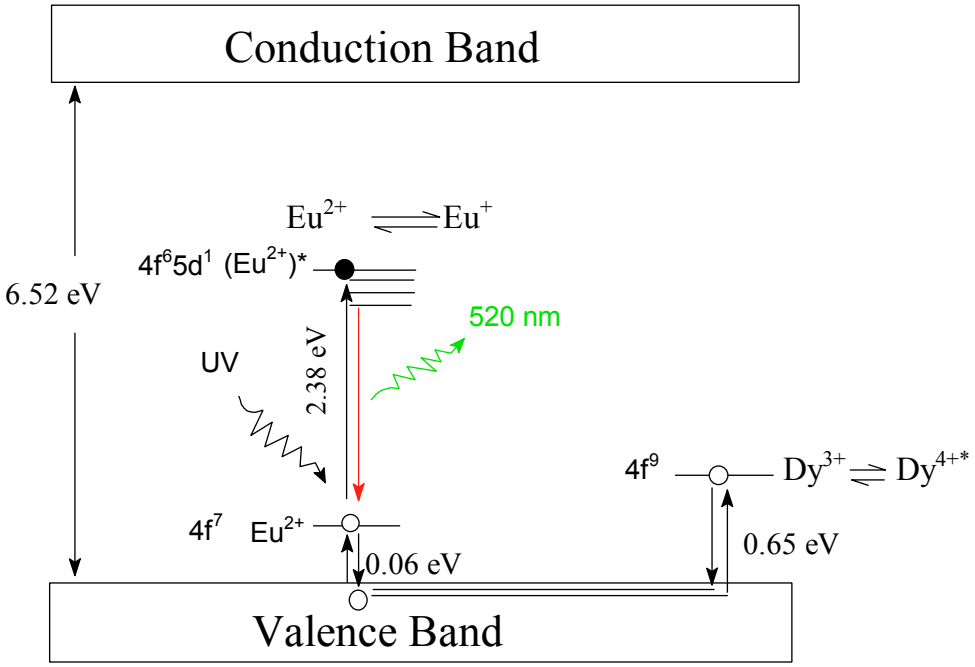

Fig.1.3. Energy level diagram of the $SrAl_2O_4:Eu^{2+}$ phosphor and its co-doped derivatives showing energy traps in Matsuzawa's model.

Due to these drawbacks, the Matsuzawa model of long persistent phosphorescence was modified by Beauger [40] and then by Aitasalo *et al.* [41]. In both modifications, it is assumed that the UV excitation promotes an electron from the VB to a discrete level of unknown origin, while the hole created in the vicinity of VB is trapped by an alkaline earth cation vacancy level V_{Ca}. Then, the thermal energy (kT_{RT}) allows the transfer of the electron from the discrete level of unknown origin to the oxygen vacancy (V_o) located near to it, from which recombination takes place towards the V_{Ca} level. The energy released is then transferred to a Eu^{2+} ion, which is excited and then de-excited instantaneously leading to emission of visible light. The role of co-doped Dy^{3+} is considered to increase the number of cation vacancies and to increase the depth of the existing vacancies. This model is shown in Fig. 1.4.

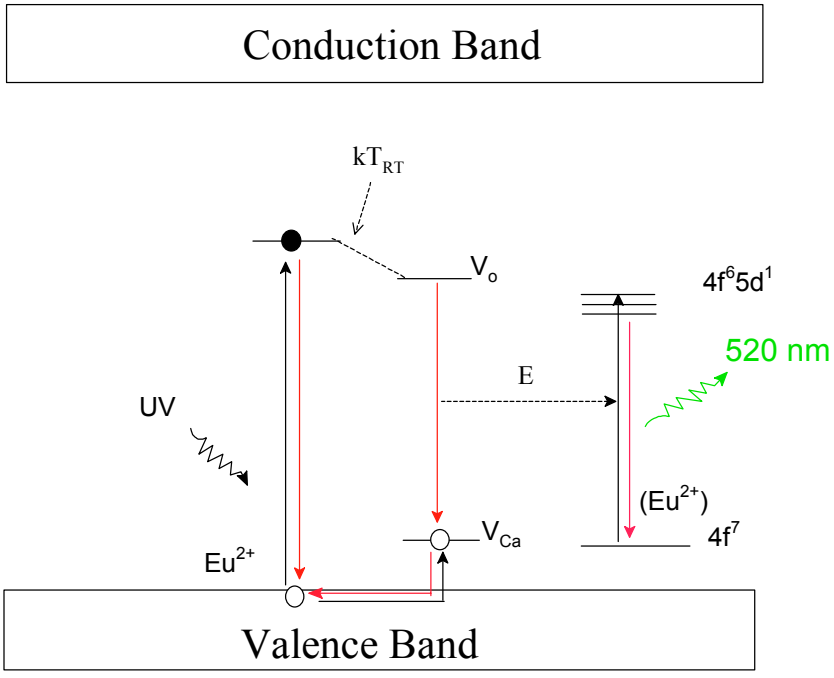

Fig. 1.4. Phosphorescence mechanism of $SrAl_2O_4:Eu^{2+}$ and its codoped derivatives proposed by Aitasalo *et al*. Black and red arrows refer to the trapping and the de-trapping processes, respectively.

Recently, EPR measurements of $SrAl_2O_4:Eu^{2+}/Dy^{3+}$ phosphor shows that the concentration of Eu^{2+} cation decreases under UV irradiation and increases once the irradiation is stopped [42]. This observation does not support the energy transfer process proposed by Beauger and by Aitasalo *et al.* To overcome these defects, F. Clabau *et al.*

proposed a new phosphorescence mechanism [18, 21] which is schematically explained in Fig. 1.5. It relies on the facts that (a) the d-block levels of Eu^{2+} cations partially overlap with the bottom of the conduction band (CB) as suggested from electronic band structure calculations performed for a hypothetical composition $Sr_{0.75}Eu_{0.25}Al_2O_4$, (b) the f^7 ground state of Eu^{2+} lies in the middle of the forbidden band gap as suggested by XPS experiments [43], (c) the Eu^{2+} cations can be oxidized under irradiation because both Eu^{2+} and Eu^{3+} species are stable species in oxides thus the concentration of Eu^{2+} cations could be changed under UV irradiation.

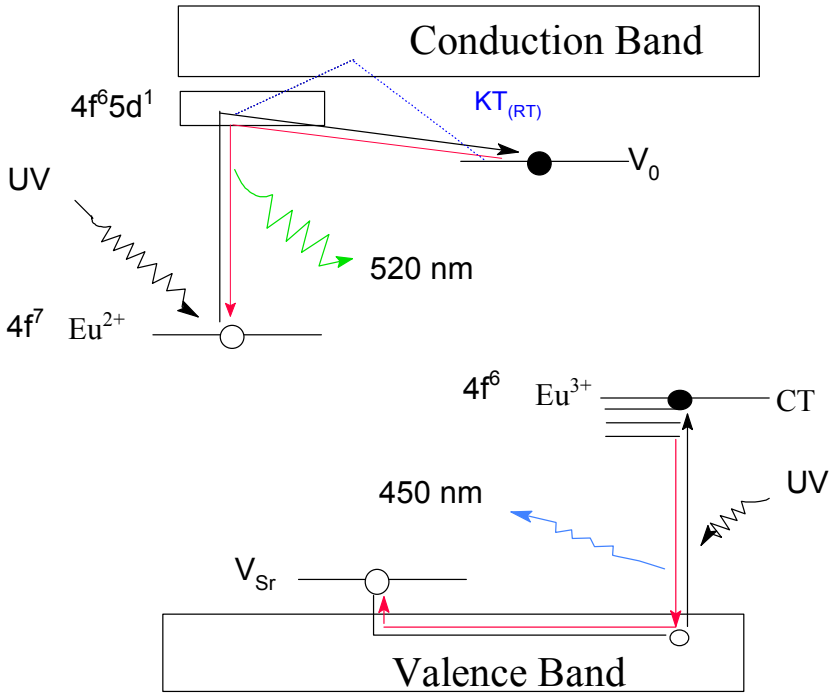

Fig. 1.5. Phosphorescence mechanism of $SrAl_2O_4:Eu^{2+}$ and its codoped derivatives proposed by F. Clabau et al. Black and red arrows refer to the trapping and the de-trapping processes, respectively (CT = charge transfer state).

Under these circumstances, F. Clabau *et al.* assumed the long persistent phosphorescence mechanism for $SrAl_2O_4:Eu^{2+}/Dy^{3+}$ phosphors as follows [21]: under UV irradiation, electrons are promoted from the occupied 4f levels of Eu^{2+} to the empty 5d levels and the CB. Some of these excited electrons are then trapped at the oxygen vacancy levels V_o located in the vicinity of the photo-generated Eu^{3+} cations. Typically, the oxygen vacancy levels in the $SrAl_2O_4$ would correspond to the empty sp^3-orbitals of the Al^{3+} ions

surrounding the oxygen vacancy. The proximity of the activator and its coupled trap is proven by the photoconductivity measurement of the $SrAl_2O_4:Eu^{2+}/Dy^{3+}$ phosphor under UV irradiation [38] which showed an increase from 80 K to 250 K and then a plateau until 300 K. Consequently, even if de-trapping occurs between 250 K and 300 K, no free charge carrier is released. As the thermoluminescence of $SrAl_2O_4:Eu^{2+}/Dy^{3+}$ showed a strong de-trapping at 300 K [43], this suggests that the electron trapping–de-trapping processes do not occur via the CB (or at least, the charge carriers do not migrate far away via the CB). The thermo-activated radiative recombination at Eu sites induces the characteristic green luminescence at 520 nm in $SrAl_2O_4:Eu^{2+}$ and $SrAl_2O_4:Eu^{2+}/Dy^{3+}$ phosphors. They mentioned that in spite of the proximity of the luminescent center with the trap, no direct recombination from the electron trap to the oxidized europium cation takes place owing to the contracted nature of 4f orbital.

Formation of an electron or a hole trap by a defect depends on the energy level position of these ions within the host band gap [39]. These positions may be determined experimentally [11]. As the nature of traps of codopants is not clearly understood, it is difficult to determine the exact nature of the traps [8, 39]. Trapping and detrapping of electrons or holes are understood to be the principal mechanisms responsible for long persistent phosphorescence [22, 41, 44-45].

The electron trapping mechanisms are usually associated with electron excitation and delocalization. Following the excitation of an electron from the ground state to an excited state, the electron is delivered to a trap by some mechanism associated with an electron. Under normal circumstances, in both the ground and excited states, electrons are localized around their parent ions. If sufficient photo-energy is provided to allow the electron to reach the conduction band, it becomes mobile and delocalization of an electron can occur. This process is called as photo-ionization. If the excited state to which an electron is promoted lies just below the host conduction band, phonon-assisted delocalization can occur. At finite temperature, electrons can be thermally excited to the conduction band where delocalization can occur. This mechanism is called thermal ionization and is much weaker than photon ionization. This process will not be strong enough to trap a large number of electrons to produce persistent emission.

In the case of thermal activation, the detrapping rate A is associated with temperature and is given by

$$A = S\, e^{-\frac{\Delta E}{kT}} \tag{1.4}$$

Where, ΔE is the trap depth which is measured from the button of the conduction band, S the electron-phonon interaction frequency factor, k Boltzmann's constant and T is temperature. Excited electrons may at times return to the trap, called trapping process.

Detrapping mechanism becomes complicated if retrapping processes are possible [47]. If the retrapping rate is very low or negligible, the decay of afterglow intensity is exponential function and given by

$$I = \sum_{i=1}^{n} I_i\, e^{-\frac{\Delta E}{kT}} \tag{1.5}$$

Where I is intensity of the afterglow and i refers to the i^{th} trap with trap depth E_i, and n is the number of different types of traps in the material. This model is called first order or mono-molecular reaction mechanism. If the retrapping rate is high, then the decay of afterglow intensity is complicated and explained by 2^{nd} order mechanism as given:

$$I = I_0/(1+\gamma t)^n \tag{1.6}$$

Where I_o is the initial afterglow intensity and n is generally less than 2 which is material dependent. $\gamma = N/An_{t0}$, where N is the density of the trap, n_{t0} the population of the trapped electrons at t = 0, and A the trapping rate.

To study the detrapping mechanisms, afterglow decay curves are usually measured. For, systems, with first- or second- order mechanisms, the decay curves can be analyzed by the above equations.

It has been found that the delocalization rate is in the same order of magnitude as the electron–phonon relaxation rate ($10^{13}s^{-1}$) for a d electron in Ce^{3+} [46]. Delocalization of electrons generally happens in the p and d orbital. Due to better shielding, delocalization from electrons on the f-orbital does not generally occur even though the f-orbital energies

are larger than the d orbital energies. As a result of this, long persistent phosphor with rare-earth ions can be found only when the electrons are excited to the high energy 5d states.

1.3.3. Methods to design Long Persistent Phosphor (LPP)

For the practical applications of long persistent phosphors, persistent time of their afterglow emission is always of most interest. However, many other factors like efficiency, emission color, quenching effects, chemical and physical stability, reproducibility of material preparation and properties, availability of raw materials, environmental aspects, and cost factors have to be considered. So far, many methods have been developed to increase the persistent time by producing more traps in the host and by increasing trapping-detrapping efficiency, some of them are discussed below.

1.3.3.1. Co-doping

Co-doping ions into the host to serve as trapping centers or to produce defect-related trapping centers, is one of the most commonly used method to make long persistent phosphors. The persistent time can be substantially increased with the introduction of proper co-dopants [10, 14, 33]. Introduction of codopants with different valency produces defects because of charge compensation requirements. For example, Cl^- ion is doped into CaS to replace S^{2-}, Y^{3+} and Al^{3+} are doped into CaS to replace Ca^{2+} [34], Mg^{2+} and Ti^{4+} are doped into $Y_2O_2S:Eu^{3+}$ to replace Y^{3+} [46, 48].

Some ions themselves act as trapping centers when they are co-doped into the host. These ions usually trap either electrons or holes and changed to metastable ionic states, that acts as trap. Nd^{3+} in $CaAl_2O_4:Ce^{3+}/Nd^{3+}$ and Gd^{3+} in $BaAl_2O_4:Eu^{2+}/Dy^{3+}/Gd^{3+}$ are typical examples of these types of traps [11].

Ions co-doped into the host not only create extra trapping centers but also enhance trapping efficiency. Ions with stronger transition rates can pump electrons into the host conduction band more efficiently, resulting in larger trap populations. An example is Ce^{3+} doped $MgAl_2O_4$ where electrons pumped into the traps through Ce^{3+} 4f-5d transitions that populate traps 30 times more than those populated through host band gap absorption [49].

1.3.3.2. Persistent energy transfer

The majority of ions in the 4f and 3d series generally do not show persistent phosphorescence so that the color coverage of the emission is limited. A method which exploits inter-ionic interaction leading to optical energy transfer has been proposed to remedy this situation which entails a process known as persistent energy transfer. In persistent energy transfer, the emission center of a known long persistent phosphor is used as a donor and the acceptor is chosen based on its color being pursued. The choice of the acceptor ion depends on the presence of the absorptions at the donor emission frequency to support the emission by the acceptor *i.e.* the energy transfer can only occur if the energy difference between the ground and excited states of donor and acceptor are in resonance condition and also suitable interaction of either exchange or electric or magnetic multi polar interaction should be possible. In simple words, the donor emission spectra should overlap the acceptor absorption spectra. The traps associated with the donor when charged will continuously transfer energy to support the emission by the acceptor. In this way, long persistence of donor is converted into the long persistence of acceptor at the required frequency. This method has been found effective in preparing long persistent phosphors, particularly, in the lower energetic regions of the visible spectrum. Some examples of long energy transfer are $CaAl_2O_4:Ce^{3+}/Tb^{3+}$, $CaAl_2O_4:Ce^{3+}/Mn^{2+}$ where at least 10 h long persistent afterglow of Ce^{3+} has been successfully transferred to yield 10 h green Tb^{3+}, and yellow Mn^{2+} afterglow [24]. Similarly, in $Sr_4Al_{14}O_{25}:Eu^{2+}/Dy^{3+}/Cr^{3+}$, the Eu^{2+} blue-green long persistent afterglow has been transferred into Cr^{3+} red afterglow[50-51].

1.3.3.3. Multiple Center Doped Materials

Another way to obtain long persistent phosphor at desired colors is to mix two or more persistent phosphors. However, it can result time dependent emission color changes because of the difference of persistence times for each of the components. To overcome this difficulty, multiple emission centers can be doped into the same host in the hope that the decay times are equalized by the same detrapping mechanism. An example of material produced by this method is Eu^{2+} and Bi^{3+} doped CaS. A purple color was obtained by mixing Eu^{2+} (red) and Bi^{3+} (blue) long persistent afterglow emissions. The afterglow color is very stable because they have the same afterglow decay mechanism [52].

Another method for this purpose is mixing the host component within the single dopant. For example, addition of Ca to replace Sr in the $SrAl_2O_4:Eu^{2+}/Dy^{3+}$ produce blue green afterglow due to mixing of $CaAl_2O_4:Eu^{2+}$/Dy (Blue) and $SrAl_2O_4:Eu^{2+}/Dy^{3+}$ (Green) [53], and substitution of Ba by Sr cause the blue shift in the $BaAl_2O_4:Eu^{2+}/Dy^{3+}$ phosphor [54].

1.3.4. Experimental Techniques of Measuring in Long Persistent Phosphors

To study the persistent mechanism, absorption, excitation and emission spectra, thermoluminescence, photoconductivity, and thermal conductivity measurements are employed.

1.3.4.1. Excitation and absorption spectra

Excitation and absorption spectra measurement for long persistent phosphors in ceramics or powder form requires extra care because the trapping and detrapping processes are considerably longer than the excitation measurement time. When a large number of electrons are being trapped and detrapped during the excitation process, the excitation spectrum measured can be distorted. There are two ways to compensate for the trapping effect and to obtain correct excitation spectra. One is to use weak excitation source followed by deconvolution of the trapping effects. The other is to use a strong excitation source to saturate the trapping effects [1-3]. The later is easier and commonly used method.

1.3.4.2. Thermoluminescence (TL)

TL measurements provide important information on the nature of the traps in the long persistent phosphors. TL records glow intensity as a function of temperature, providing information regarding trapping energies and detrapping mechanisms [46]. Generally, considering single type of trap, the glow intensity (I) at temperature T is given by:

$$I(T) \propto n_{t0} s e^{-\frac{\Delta E}{kT}} \; e^{-\int s e^{-\frac{\Delta E}{kT}} dT/\beta} \qquad (1.7)$$

Where, n_o is the number of electrons in the trap at beginning, β the heating rate, s the frequency factor, and E, the depth of the trap. For rising part of the TL glow curve at low

temperature, the number of electrons in the trap remains almost constant, and hence the glow intensity is given by:

$$I(T) \propto n_0 s e^{-\frac{\Delta E}{kT}} \tag{1.8}$$

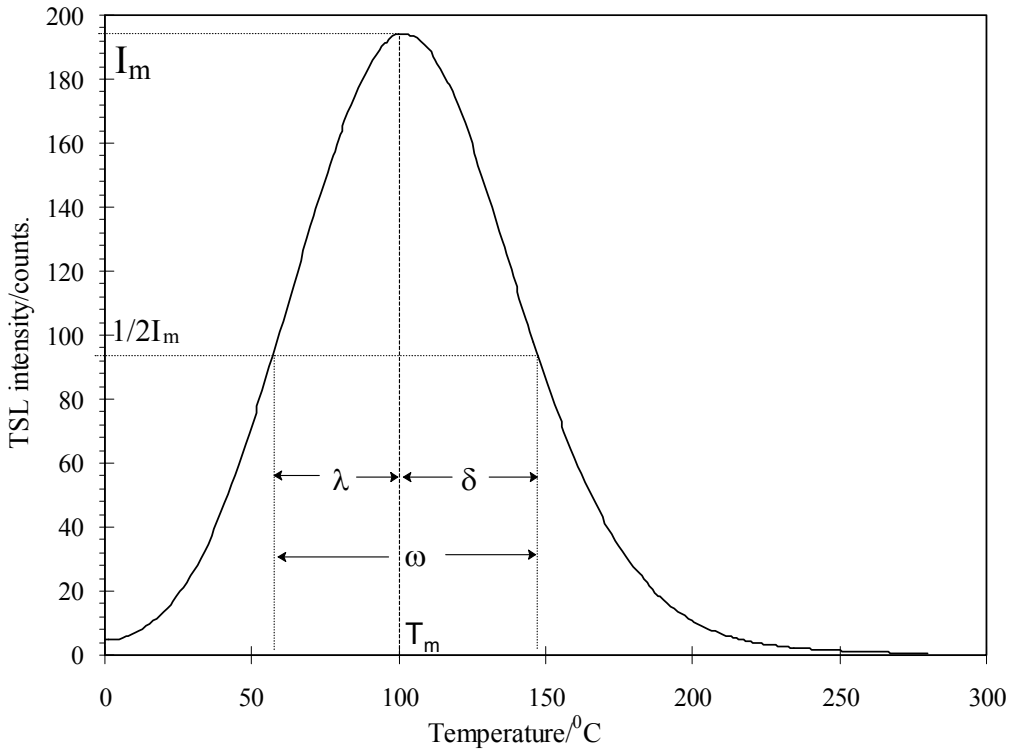

Fig. 1.6. A typical thermoluminescent glow curve of strontium aluminate phosphor showing various parameters.

It is difficult to determine the depth of an electron trap for rise time of a signal, so the trap depth of an electron calculated by this method is not accurate. Thus, the trap depth is generally calculated using T_m, the peak temperature of the TL glow curves as explained in equations below and Fig 1.6:

$$\frac{\beta \Delta E}{kT_m^2} = s e^{-\frac{\Delta E}{kT_m}} \tag{1.9}$$

If frequency factor 's' is calculated by other methods, the trap depth can be estimated as:

$$\Delta E = \left(T_m - T_0\left(\frac{\beta}{s}\right)\right) / K\left(\frac{\beta}{s}\right) \quad (1.10)$$

More generally, trap depth and its concentrations can be determined by a general kinetics method as [55]:

$$\Delta E = \left[2.52 + 10.52\left(\mu_g - 0.42\right)\right]K_B T_m^2/\omega - 2kT_m \quad (1.11)$$

$$n_0 = \frac{\omega I_m}{\beta\left[2.52+10.2\left(\mu_g-0.42\right)\right]} \quad (1.12)$$

Where, ω is sum of high temperature (δ) and low temperature (τ) half widths and $\mu_g = \delta/\omega$.

Experimentally, the TL spectrum is obtained by first populating the traps at low temperatures. The temperature is then increased at constant speed β, and the glow intensity is monitored at selected wave length using a filter or a monochromator. TL peaks in the persistent phosphor are only observed when they are exposed to higher energy excitation. This is evidence that the trapping mechanism is related to the ionization process of the emission centers.

1.3.5. Methods of Preparation of Long Persistent Phosphors

1.3.5.1. Solid State Method

In general, almost all phosphors are synthesized by solid state reaction between raw materials at high temperatures. First the high purity materials of host crystals, activator and fluxes are mixed and blended to get homogeneous mixture. Then the mixture was fired at high temperature in a container. The fired product is then crushed, milled and then sorted to remove coarse and excessively crushed particles. The schematic process is summarized in Fig. 1.7.

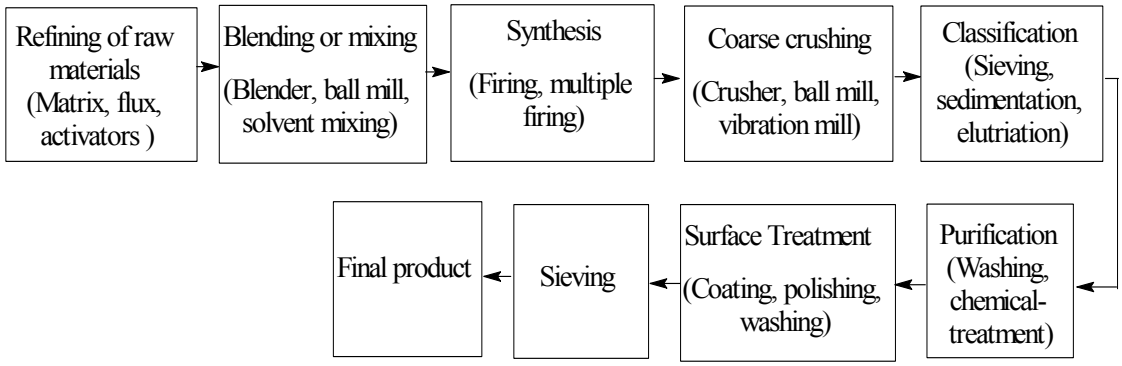

Fig. 1.7. Schematic synthetic process of phosphors by solid state reaction method

There are two different kinds of reactions in phosphor synthesis. In the first method, the activator ion is introduced into the existing host materials (ZnS-based phosphors are prepared by this technique, where following the particle growth of ZnS host crystal, diffusions of the activators into the host takes place). In the second scheme, host material synthesis and activator incorporation proceed simultaneously during the calcinations process. For example, in the preparation of $SrAl_2O_4:Eu^{2+}/Dy^{3+}$ phosphor, $Sr(CO_3)_2$, Al_2O_3, Eu_2O_3 and Dy_2O_3 along with some B_2O_3 flux is mixed together and blended to get homogeneous mixture. Then it is fired at a suitable temperature of 1300-1500^oC in slightly reducing environment. $SrAl_2O_4$ is formed and Eu^{2+} and Dy^{3+} ions are incorporated simultaneously into the formed host lattice by replacing one of the host ion.

During the solid state reaction process, some of the elementary process taking place can be investigated by means of differential thermal analysis (DTA), thermogravimetric analysis (TGA), crystal structure analysis by X-ray diffraction, microscopic observations and chemical analysis. For example, manganese activated zinc silicate phosphor is synthesized from ZnO, SiO_2 and $MnCO_3$. The DTA studies of the raw materials mixture show the ZnO and SiO_2 starts reacting at 770^oC [58] where the reaction proceed by diffusion of ZnO into the SiO_2 lattice. The Mn ion is incorporated into the lattice in proportion to the amount of synthesized Zn_2SiO_4.

In the solid state reactions high temperature firing is indispensable. However, the purpose of firing is not only to cause solid state reactions but also to form well crystallized particles with an appropriate average diameter. The substance added to the raw material

mixture to help crystal growth is called a flux. Fluxes are usually alkali and alkaline earth compounds (*e.g.* LiF, NaCl, KI, $MgCl_2$, $BaCl_2$, $CaCl_2$) or some others like NH_4F, NH_4Cl, NH_4I, B_2O_3 *etc.* having low melting points [2]. When the fluxes melt, the surface tension of the liquid helps particles coagulate. The melt also makes easier for particles to slide and rotate providing chance to particle-particle contacts and promotes the particles growth that highly lowers the formation temperatures [59]. Not only this, the melt flux helps the added activators to penetrate deep inside the matrix and forms homogeneous distribution in the matrix. Another important role of the flux is that it acts itself as a source of co-activator or trapping centers of electrons or holes. In case of $ZnS:Ag^+/Cl^-$, the Cl^- co-activator is supplied by the flux NaCl [2] and Dy-borates acts as hole traps in the case of $SrAl_2O_4:Eu^{2+}/Dy^{3+}$ prepared with the aid of B_2O_3 [10, 60].

1.3.5.2. Sol-Gel Method

Phosphors used for most of the display devices are in the powder form, whose quality mainly determines the quality of the display. Fine and uniform powders with excellent crystallinity are generally preferred which is possible only by wet chemical methods, especially, sol-gel technique. In general, the sol-gel method is a wet chemical technique that uses metal alkoxides for the synthesis of ceramics through a series of chemical processes including hydrolysis, gelation, drying, and thermal treatment. The metal alkoxides are subjected to the hydrolysis. A mixture of water, alcohol and hydrochloric acid are added into the precursor metal alkoxides mixture by drop wise. The hydrolysis reaction of metal alkoxides with water in the presence of HCl catalyst takes place that produce hydroxide of precursors. The reaction can be expressed as follows:

$$(OR)_3\text{-Si-OR} + H_2O \longrightarrow (OR)_3\text{-Si-OH} + ROH \qquad (1.13)$$

Where, R stands for alkyl group, C_nH_{2n+1}. During the hydrolysis process, the activators and co-activators are also added and blended together.

A sol is defined as a colloidal of solid particles suspended in liquid. A gel, on the other hand, is a composite substance consisting of continuous solid skeletal structure, which results from the gelation of the sol. The gel obtained is mixed with appropriate amount of

flux if needed and grinded to form fine powder. The mixture powder is then subjected to thermal treatment at various temperatures according to need of the final phosphor product.

The sol-gel method owes following overcomes above the solid state method and have been using extensively in phosphor research,

1. Higher homogeneity of the chemical composition in the material product.
2. High uniformity of doping ions distribution, no local concentration quenching will occur because of impurity clustering.
3. Processing temperature can be very low. This allows the doping of fragile organic and biological molecules into porous inorganic materials and fabrication of organic-inorganic hybrid materials.
4. The controlled microstructure (pores and particles distributions). High density materials can be produced at high annealing temperature.
5. By spinning or dipping method, thin films and multi layered coating can be obtained.
6. Fine, uniform particles can be obtained that reduced the crystal destruction by milling and crushing as in solid state methods.

However, some disadvantages of this method also exist:

1. For transparent samples, the annealing process should be slow and deliberate, otherwise, cracks and striations will appear in the samples.
2. To remove organic groups completely, high temperature heating above $1000^{o}C$ is required, that may produces undesirable side products.
3. It is well suited for micro-scale production, but very expensive and unsuitable for mass production.

For the macro-scale production, a salted sol-gel technique (Pechini method) is employed, where solutions of various inorganic salts and metal alkoxides are used in

combination. In this method of preparation of aluminate phosphor (*e.g.* $SrAl_2O_4:Eu^{2+}/Dy^{3+}$), aluminum and strontium nitrates or acetates solutions are mixed slowly together with doping metal ions. A small amount of flux (B_2O_3) is added and stirred vigorously at elevated temperature of 80^oC till it becomes viscous sol. It was dried to get gel and fired at 500 - 800^oC to remove organics completely. Then the organics free powder is annealed at suitable temperature to get final phosphor product.

1.3.5.3. Chemical Combustion method

Phosphor of smaller particles and regular morphologies can be prepared by a more efficient and energy saving combustion method, one of the liquid phase synthesis method. The combustion method of preparing oxides, aluminates and silicates phosphor powders is a facile and an efficient method, that takes hardly few minutes and have been extensively used for the mass production recently. Further, the combustion method being a liquid phase synthesis method, each component of the host and activators can be accurately controlled and uniformly mixed to get the homogeneous product. In this method, all the precursors used are salts such as nitrates or acetates. A proper amount of organic fuel like urea, glycine, ethylene glycol *etc.* is added to the aqueous solution of the salts. The heat released during the exothermic redox reaction between metal nitrates precursors (oxidant) and organic fuel (reductant) makes the reaction feasible at relatively lower temperatures in a very short interval of time (hardly few minutes). The whole scheme of redox reaction can be expressed as:

$$3M(NO_3)_2 + 5NH_2CONH_2 \xrightarrow{300–500^oC} 3MO + 5CO_2 + 10H_2O + 5N_2 \quad (1.14)$$

$$6Al(NO_3)_3 + 15NH_2CONH_2 \xrightarrow{300–500^oC} 3Al_2O_3 + 15CO_2 + 30H_2O + 24N_2 \quad (1.15)$$

$$6Eu(NO_3)_3 + 6Dy(NO_3)_3 + 30NH_2CONH_2 \longrightarrow 3Eu_2O_3+3Dy_2O_3+30CO_2+60H_2O + 48N_2 \quad (1.16)$$

$$MO + Al_2O_3 \xrightarrow{500^oC/B_2O_3} MAl_2O_4 \quad (1.17)$$

$$MAl_2O_4 + 5Al_2O_3 \xrightarrow{500^oC/B_2O_3} MAl_{12}O_{19} \quad (1.18)$$

$$17MAl_2O_4 + 3SrAl_{12}O_{19} \xrightarrow{1200^oC/B_2O_3} 5M_4Al_{14}O_{25} \quad (1.\ 19)$$

In general, the stoichometric amounts of corresponding metal nitrates and organic fuel along with dopant and co-dopants are heated nearly at 80^{o}C for few hours till it becomes viscous sol. Then the mixture is inserted into the furnace pre-heated at 300 – 500^{o}C. The exothermic combustion reaction between metal nitrates and fuel occurs vigorously. Initially, the sol boils, fourths, foams and catches fire. Then the fire propagates to its own leading to the completion of the reaction in less than ten minutes.

1.4. Long Persistent Phosphor: A collection from the past

So far, more than 100 different kinds of long persistent phosphors are existed, most of them, listed below (Table 1), were developed during the past two decades. Most of the phosphor consists rare earth metal ions, for example, Eu^{2+}, Eu^{3+}, Ce^{3+}, Tb^{3+}, Sm^{3+} , Pr^{3+}, Dy^{3+}, Er^{3+}, Tm^{3+} as an activator ion. Upon UV and visible light excitation, the trivalent rare earth ions exhibits persistent afterglow because the 5d electronic state of these ions is energetically close to the conduction band of the host, making delocalization and trapping of electrons possible. Among various rare earth ions as an emission center in most of the phosphor, Eu^{2+} is a most common emission center in persistent materials. It can often be pumped by the sunlight and its emission wavelength from $4f^{6}5d^{1}$ to $4f^{7}$ varies greatly from host to host and can give good coverage of the spectrum. Other long persistent phosphors used transition metal ions with 3d electrons, such as V^{3+}, Cu^{+}, Mn^{2+}, Ti^{4+}, Sn^{2+}, Co^{3+} *etc.* and some other ns^{2} type centers such as Bi^{3+}, Pb^{2+} *etc*.

Host materials are of critical importance for long persistent phosphors. Early host materials used for long persistence were of the ZnS type. Due to low band gap energy of 2.16 eV (hence afterglow is no longer than an hour) and its chemical instability, many other suitable host have been developed in last few decades. Some of them are Lenard's host Ca/Sr/BaS, alkali earth aluminates like $SrAl_2O_4$, $Sr_4Al_{14}O_{25}$, $CaAl_4O_7$, $BaAl_2O_4$ *etc.*, silicates like $SrSiO_3$, $CaMgSi_2O_6$, $Sr_3Al_{10}SiO_{20}$, $Na_4CaSi_7O_{17}$ *etc.*, oxides like SrO, Y_2O_3, and oxy-sulphide like Y_2O_2S, Gd_2O_2S etc. Among them alkali earth aluminates host have attracted much attentions due to their wide band gap of approximately 6 eV, suitable for very long persistent phosphorescence over night, chemical stability, high quantum yield of greater than 90% and wide range of excitation.

Table 1.1. Wavelength and persistent time of various long persistent phosphor listed by emission centers

Emission center	Co-dopant/s	Host material	Emission wavelength/nm	Persistent Time/h
Eu^{2+}	-	$CaAl_2B_2O_7$ [61]	510	8
Eu^{2+}	-	$SrAl_{1.7}B_{0.3}O_4$ [62]	520	2
Eu^{2+}	-	$SrAl_2SiO_6$ [63]	510	24
Eu^{2+}	-	$CaMg_2SiO_6$ [64]	438	>4
Eu^{2+}	Dy^{3+}	$SrAl_2O_4$ [10]	530	>10
Eu^{2+}	Dy^{3+}	$BaAl_2O_4$ [54]	520	>10
Eu^{2+}	Dy^{3+}	$CaAl_2O_4$ [65]	500	>10
Eu^{2+}	Dy^{3+}	$MgAl_2O_4$ [66]	480	<1 min
Eu^{2+}	Dy^{3+}	$SrAl_4O_7$ [67,68]	480	<1 min
Eu^{2+}	Dy^{3+}	$SrAl_{12}O_{19}$ [68]	475	-
Eu^{2+}	Dy^{3+}	$Sr_4Al_{14}O_{25}$ [10,69]	424, 486	>20
Eu^{2+}	Dy^{3+}	$Sr_4Al_{14}BO_{25}$ [70]	490	>1
Eu^{2+}	Dy^{3+}	$Sr_3Al_2O_6$ [71]	618	>1
Eu^{2+}	Dy^{3+}	$Sr_2MgSi_2O_7$ [72]	466	5
Eu^{2+}	Dy^{3+}	CaS/SrS [73]	616	> 1min
Eu^{2+}	Dy^{3+}	$Sr_2Al_2SiO_7$ [74]	484	> 1min
Eu^{2+}	Dy^{3+}	$Sr_2ZnSi_2O_7$ [75]	457	-
Eu^{2+}	Dy^{3+}	$Sr_3MgSi_2O_8$ [76]	475	5
Eu^{2+}	Dy^{3+}	$Sr_3Al_{10}SiO_{20}$ [77]	466	6
Eu^{2+}	Dy^{3+}	$Ca_2MgSi_2O_7$ [72]	447,516	5
Eu^{2+}	Dy^{3+}	$CaAl_2Si_2O_8$ [78]	440	-
Eu^{2+}	Dy^{3+}	$Ba_2MgSi_2O_7$ [72]	505	5
Eu^{2+}	Dy^{3+}	$(Sr,Ca)MgSi_2O_7$[79]	490	20
Eu^{2+}	Dy^{3+}	Sr_2SiO_4 [80]	479,493,560	>5 min
Eu^{2+}	Dy^{3+}/Cr^{3+}	$Sr_4Al_{14}O_{25}$ [51]	490, 695	>5
Eu^{2+}	Nd^{3+}/Cr^{3+}	$CaAl_2O_4$[81,82]	440	10
Eu^{2+}	Nd^{3+}	$(Sr,Ca)Al_2O_4$ [83]	440-517	>10
Eu^{2+}	Nd^{3+}	$Ca_{12}Al_{14}O_{33}$ [84]	440	1

Continued…

Emission center	Co-dopant/s	Host material	Emission wavelength/nm	Persistent Time/h
Eu^{2+}	-/ Nd^{3+}	$CaMgSi_2O_6$ [85]	338,447	>4
Eu^{2+}	Nd^{3+}	$Ba_2ZnSi_2O_7$ [86]	505	-
Eu^{2+}	-	CaO [87]	626	1
Eu^{2+}	-	SrO [87]	626	1
Eu^{2+}	-	BaO [87]	626	1
Eu^{3+}	-	$CaWO_4$ [88]	614	-
Eu^{3+}	Ti^{4+}/Mg^{2+}	Y_2O_3 [89]	612	1.5
Eu^{3+}	Ti^{4+}/Mg^{2+}	Y_2O_2S [48]	612	1
Ce^{3+}	Nd^{3+}	$SrAl_2O_4$ [46]	627	>12
Ce^{3+}	Nd^{3+}	$CaAl_2O_4$ [46]	385,427	>12
Ce^{3+}	-	$BaAl_2O_4$ [90]	413	>12
Ce^{3+}	-	$Sr_4Al_{14}O_{25}$ [22]	450,412	-
Ce^{3+}	-	$Sr_2Al_2SiO_7$ [91]	400	-
Ce^{3+}	-	$Ca_2Al_2SiO_7$ [24]	414,482,588	>10
Ce^{3+}	-	CaS [92]	417	0.2
Ce^{3+}	-	$CaAl_2O_4$ [93]	507	1
Tb^{3+}	-	CaO [94]	543	>1
Tb^{3+}	-	SrO [94]	543	>1
Tb^{3+}	-	$CaSnO_3$ [95]	543	4
Tb^{3+}	-	$YTaO_4$ [96]	492,543,624	2
Tb^{3+}	Ce^{3+}	$CaAl_2O_4$ [97]	543	10
Tb^{3+}	Ce^{3+}	$CaAl_4O_7$ [98]	543	10
Pr^{3+}	-/Zn^{2+}	$CaTiO_3$ [99]	612	0.1
Pr^{3+}	-	$CdSiO_3$ [100]	402,602	~1
Pr^{3+}	Li^{+}	$CaZrO_3$ [101]	494	3
Dy^{3+}	-	$CdSiO_3$ [102]	White	5
Dy^{3+}	-	$SrSiO_3$ [103]	White	1

Continued…

Emission center	Co-dopant/s	Host material	Emission wavelength/nm	Persistent Time/h
Dy^{3+}	-	Sr_2SiO_4 [104]	White	1
Sm^{3+}	-	$CdSiO_3$ [105]	Orange-red	1
Sm^{3+}	-/Mg^{2+},Ti^{4+}	Y_2O_2S [106]	Orange-red	1
Sm^{3+}	-	$CaAl_2O_4$ [107]	Orange-red	-
Sm^{3+}	-/Ti^{4+}	Gd_2O_2S [108]	Red	-
Tm^{3+}	-	Y_2O_2S [109]	Orange-yellow	>1
Ho^{3+}	-	$CaGaS_4$ [110]	560	>1
Mn^{2+}	-	$CdSiO_3$ [111]	Orange	>1
Mn^{2+}	-	Mg_2GeO_3 [112]	Red	>1
Mn^{2+}	Sn^{2+}	$BaMg_2Si_2O_7$ [113]	400,660	>1
Mn^{2+}	Ga^{3+}	B-$Zn_3(PO_4)_3$ [114]	Red	0.6
Cu^{2+}	Sn^{2+}	$Na_4CaSi_7O_{17}$ [115]	510	1.5
Cu^{+}	-	ZnS [2]	530	0.6
Cu^{+}	Co^{2+}	ZnS [2]	530	1.5
Bi^{3+}	-	CaS [116]	447	2
Bi^{3+}	Tm^{3+}	$Ca_xSr_{1-x}S$ [34]	453	5
Pb^{2+}	-	$CdSiO_3$ [117]	498	10
Ti^{4+}	-/Mg^{2+}	Y_2O_2S [117]	594	5
V^{3+}	-/Ce^{3+}	$MgAl_2O_4$ [49]	520	1

1.5. Objectives of the present study

When Matsuzawa reported long persistent $SrAl_2O_4:Eu^{2+}/Dy^{3+}$ phosphor [10], great efforts have been done to develop the persistent phosphors over the visible spectrum. As a result, blue, green and red persistent phosphors have been developed in last decade but their brightness and persistent time are not enough to apply in the practical applications. At the same time, BMJ Smets [13] introduced the $Sr_4Al_{14}O_{25}:Eu^{2+}$ phosphor with high quantum yield, bright phosphorescence and very long persistent time if doped with Dy^{3+} ion. However, there are very few reports on the systematic study of the $Sr_4Al_{14}O_{25}$ phosphor. Thus, I have selected it and performed detailed study. The short term objectives of the present study are:

1. To explore the scope of phosphor materials, especially, long persistent phosphor.
2. To explore the existing mechanisms of long persistent phosphorescence and find out the improved one to satisfy all the characteristics observed for a long persistent phosphor.
3. To prepare and characterize the strontium aluminate phosphor *viz.* $Sr_4Al_{14}O_{25}:Eu^{2+}/Dy^{3+}$.
4. To find out the effects of various parameters like use of flux, synthetic conditions (calcinations temperature, time, atmosphere *etc.*), additives (emission centers, co-dopants, charge compensators), substitution by similar cations (Ca and Ba), use of proper raw powders (*e. g.* alumina type and its size) for the better phosphorescence properties.
5. To develop a white afterglow phosphor by Sr/Ca substrate control in the $Sr_4Al_{14}O_{25}:Eu^{2+}/Dy^{3+}$ phosphor.
6. To synthesize the $Sr_4Al_{14}O_{25}:Eu^{2+}/Dy^{3+}$ phosphor particles by sol-gel, combustion, solid state methods and compare its surface morphology and photoluminescence characteristics to find the better method of preparation.
7. To search the possibility of red phosphorescence in $Sr_4Al_{14}O_{25}$ phosphor by co-doping various metal ions.

The long term objectives of the study are:

1. To develop the long persistent phosphor materials that can persist over night and can be used in night vision applications.
2. To establish the fabrication process of similar ‘rare metal doped aluminates phosphors’.

3. To contribute to a sustainable society through the alternative source of energy (phosphor materials), by the use of sunlight as a source.

References

[1] G. Blasse, B.C. Grabmailer, Luminescent Materials, Springer-Verlag, 1994.

[2] W.M. Yen, S. Shionoya, H. Yamamoto, Phosphor Hand Book, CRC press, 1995.

[3] R. C. Ropp, Luminescent and the Solid State, Elsevier, 2004.

[4] W.M. Yen, M.J. Weber, Inorganic Phosphors, compositions, preparations and optical properties, CRC press, Boca Raton, FL, 2004.

[5] W. de Groot, Physica **6** (1939) 275.

[6] F.A. Kroger, Some Aspects of Luminescence of Solids, Elsevier, Amsterdam, 1948.

[7] W. Lehmann, J. Lumin. **5** (1972) 87.

[8] G.F.J. Garlick, D.E. Mason, J. Electrochem. Soc. **96** (1949) 90.

[9] Y. Murayama, N. Takeuchi, Y. Aoki, T. Matsuzawa, US Patent No. 5, **424** (1995) 006.

[10] T. Matsuzawa, Y. Aoki, N. Takeuchi, Y. Murayama, J. Electrochem. Soc. **143** (1996) 2670.

[11] H. Yamamoto, T. Matsuzawa, J. Lumin. **72** (1997) 287.

[12] J.T.C van Kemendo, G.P.F. Hoeka, Electrochem. Soc. Spring Meeting Abstract, San Francisco, 1983, Abstract No. 607.

[13] BMJ Smets, Mater. Chem. Phys. **16** (1987) 283.

[14] E. Nakazawa, T. Mochida, J. Lumin. **72-74** (1997) 236.

[15] T. Katsumata, T. Nabae, K. Sasajima, S. komuro, T. Morikawa, J. Electrochem. Soc. **144** (1997) L243.

[16] C.W. Thiels, H. Cruguel, Y. Sun, J. Lumin. **94-95** (2001) 1.

[17] E. Nakazawa, Y. Murazaki, S. Saito, J. Appl. Phys. **100** (2006) 113113.

[18] F. Clabau, X. Rocquefelte, S. Jobic, P. Denieard, M.H. Whangbo, A. Garcia, T. Mercier, Solid State Sci. **9** (2007) 608.

[19] D. Jia, W.M. Yen, J. Electrochem. Soc. **150** (2003) H61.

[20] F. Clabau, X. Rocquefelte, T. Le Mercier, P. Deniard, S. Jobic, M.H. Whangbo, Chem. Mater. **18** (2006) 3212.

[21] F. Clabau, X. Rocquefelte, S. Jobic, P. Deniard, M.H. Whangbo, A. Garcia, T.L. Mercier, Chem. Mater. **17** (2005) 3904.

[22] S.H. Han , Y.J. Kim, Opt. Mater. **28** (2006) 626.

[23] D. Jia, X.J. Wang, W.M. Yen, Chem. Phys. Lett. **363** (2002) 241.

[24] X.J. Wang, D.D. Jia, W.M. Yen, J. Lumin. **102-103** (2003) 34.

[25] G. Blasse, W.L. Wanmaker, J.W. Vrugt, A. Bril, Philips Res. Rep. **23** (1968) 189.

[26] T.L. Barry, J. Electrochem. Soc. **117** (1970) 381.

[27] Y. Lin, Z. Tang, Z. Zhang, J. Zhang, Mater. Sci. Eng. B **86** (2001) 79.

[28] H. A. Höppe, H. Lutz, P. Morys, W. Schnick, A. Seilmeier, J.Phys. Chem. Solids, 61, **12** (2000) 2001.

[29] Y. H. Liu, R. Liu, Rare Earths **25** (2007) 392.

[30] R. Pang, C. Li, L. Jiang, Q. Su, J. Alloys. Compd. **471**(1-2) (2009) 364.

[31] W. J. Schipper, Z.A.E.P. Vroon, G. Blasse, T. Schleid, G. Meyer, Chem. Mater. ***4*** (3) (1992**)** 688.

[32] H. Hosono, T. Kinoshita, H. Kawazoe, M. Yamazaki, Y. Yamamoto, N. Sawanobori, J. Phys. C **10** (1998) 9541.

[33] X. Lu, W. Shu, Rare Metals, **26** (4) (2007) 305.

[34] D. Jia, J. Zhu, B. Wu, J. Electrochem. Soc. **147** (2000) 386.

[35] N. Suriyamurthy, B.S. Panigrahi, J. Lumin. **128** (11) (2008) 1809.

[36] A. Nag, T.R.N. Kutty, J. Alloys Compd. **354** (2003) 221.

[37] D. Jia, W. Jia, D.R. Evans, W.M. Dennis, H. Liu, J. Appl. Phys. **88** (2000) 3402.

[38] V. Abbruscato, J.Electrochem.Soc.**118** (1971) 930.

[39] P. Dorenbos, J. Electrochem. Soc. **152** (2005) H107.

[40] C. Beauger, Thesis, Universite de Nice, France, 1999.

[41] T. Aitasalo, P. Deren, J. Hölsa, H. Jungner, J. Krupa, M. Lastusaari, J. Legendziewicz, J. Niittykoski, W. Strek, J. Solid State Chem. **171** (2003) 114.

[42] Rhodia Electronics and Catalysis, Private Communication, 2001.

[43] F. Clabau, thesis, University of Nantes, France, 2005.

[44] Y.H. Lin, Z.L. Tang, Z.T. Zhang, J. Euro. Ceram. Soc. **23** (2003) 175.

[45] E. Nakazawa, H. Yamamoto, J. Lumin. **128**(3) (2008) 494.

[46] D. Jia, X.J. Wang, W.M. Yen, Phys. Rev. B **69** (2004) 235113.

[47] S.W.S. Mc Keever, Thermoluminescence of solids, Cambridge University Press, Cambridge, 1985.

[48] X. Wang, Z. Zhang, Z. Tang, Y. Lin, Mater. Chem. Phys. **80** (2003) 1.

[49] D. Jia, W.M. Yen, J. Lumin. **101** (2003) 115.

[50] D. Jia, X.J. Wang, W. Jia, W.M. Yen, J. Appl. Phys. **93** (2003) 148.

[51] Z. Ruixia, Z. Jiahua, S. Lu, W. Xiao-jun, Appl. Phys. Lett. **88** (2006) 201916.

[52] D. Jia, B. Wu, J. Zhu, Acta Phys. Sin. **90** (2000) 30.

[53] A. K. Prodjosantoso, B. J. Kennedy, Mater. Res. Bull. **38 (1)** (2003) 79.

[54] H. Ryu, B.K. Singh, K.S. Bartwal, Physica B **403** (2008) 126.

[55] C. Chang, Z. Yuan, D. Mao, J. Alloys Compd. **415** (2006) 220.

[56] W. Hoogenstraaten, Philips Res. Rep. **13** (1958) 515.

[57] S. Basun, G.F. Imbusch, D.D. Jia, W.M. Yen, J. Lumin. **104** (2003) 283.

[58] K. Takagi, J. Chem. Soc. Japan, Ind. Chem. Soc. **65** (1962) 847.

[59] G.F.J. Garlick, Luminescent Materials, Oxford University Press, UK, 1949.

[60] A. Nag, T.R.N. Kutty, J. Alloys Compd. **354** (2003) 221.

[61] J. Que, K. Hirao, Solid State Commun. **106** (1998) 795.

[62] J. Sanchez-Benitez, A. de Andres, M. Marchal, E. Cordoncillo, M. Vallet Regi, P. Escribano, J. Solid State Chem. **171** (2003) 273.

[63] J. Que *et al.* J. Phys. Chem. Solids **59** (1998) 1521.

[64] L. Jiang, C. Chnag, D. Mao, C. Feng, J. Alloy. Compd. **377** (2004) 211.

[65] H. Ryu, K.S. Bartwal, J. Alloys Compd. **476** (2009) 379.

[66] A.S. Maia, R. Stefani, C.A. Kodira, M. C.F.C. Felinto, E.E.S. Teotonio, H.F. Brito, Opt. Mater. **31** (2008) 440.

[67] C. Chang, D. Mao, J. Shen, C. Feng, J. Alloys Compd. **348** (2003) 224.

[68] T. Katzumata, T. Tanabe, K. Sasajima, S. Komuro, T. Morikawa, J. Electrochem. Soc. **144** (1997) L243.

[69] Y.H. Lin, Z.L. Tang, Z.T. Zhang, Mater. Lett. **51** (2001) 14.

[70] A. Nag, T.R.N. Kutty, Mater. Res. Bull. **39** (2004) 331.

[71] P. Huang, C. Cui, S. Wang, Opt. Mater. **32** (2009) 184.

[72] Y.H. Lin, C.W. Nan, X.S. Zhou, J.B. Wu, H.F. Wang, D.P. Chen, S.M. Xu, Mater. Chem. Phys. **82** (2003) 860.

[73] X. Duan, S. Huang, F. You, K. Kang, J. Rare Earths **27** (2009) 43.

[74] Y. Ding, Y. Zhang, Z. Wang, W. Li, D. Mao, H. Han, C. Chang, J. Lumin. **129** (2009) 294.

[75] L. Jiang, C. Chang, D. Mao, B. Zhang, Mater. Lett. **58** (2004) 1825.

[76] A.A.S. Alvani, F. Moztarzadeh, A.A. Sarabi, J. Lumin. **114** (2005) 131.

[77] Y.J. Kuang, Y. Liu, J. Zhang, L. Huang, J. Rong, D. Yuan, Solid State Commun. **136** (2005) 6.

[78] C. Zhang, J. Yang, C. Lin, C. Li, J. Lin, J. Solid State Chem. **182** (2009) 1673.

[79] Y. Chen, B. Liu, M. Kirm, Z. Qi, C. Shi, M. True, S. Vielhauer, G. Zimmerer, J. Lumin. **118** (2006) 70.

[80] N. Lakshminarasimhan, U.V. Varadaraju, Mater. Res. Bulletin **43** (2008) 2946.

[81] Y. Lin, Z. Tang, Z. Zhang, C. Nan, J. Europ. Cer. Soc. **23** (2003) 175.

[82] H. Ryu, K.S. Bartwal, J. Alloys Compd. **464** (2008) 317.

[83] C. Liu, Y. Wang, Y. Hu, R. Chen, F. Liao, J. Alloys Compd. **470** (2009) 473.

[84] J. Zhang, Z. Zhang, T. Wang, W. Hao, Mater. Lett. **57** (2003) 4315.

[85] T. Kida, M.M. Rahman, M. Nagano, J. Electrochem. Soc. **153 (4)** (2006) 82.

[86] S. Yao, Y. Li, L. Xue, Y. Yan, J. Alloys. Compd. **490** (2010) 200.

[87] J. Fu, Electrochem. Solid State Lett. **3** (2000) 350.

[88] X. Lou, D. Chen, Mater. Lett. **62** (2008) 1681.

[89] Y. Lin, C.W. Nan, N. Cai, X. Zhou, H. Wang, D. Chen, J. Alloy. Compd. **361** (2003) 92.

[90] D. Jia *et al.,* Opt. Commun. **204** (2002) 247.

[91] W. Pan, G. Ning, Y. Lin, X. Yang, J. Rare Earths **26** (2008) 207.

[92] D. Jia, R. S. Meltzer, W. M. Yen, J. Lumin. **99** (2002) 1.

[93] D. Jia, X.J. Wang, W.M. Yen, Chem. Phys. Lett. **363** (2002) 241.

[94] J.Y. Kuang *et al.,* Chin. J. Inorg. Chem. **21** (2005) 1383.

[95] Z. Liu, Y. Liu, Mater. Chem. Phys. **93** (2005) 129.

[96] T. Takayama, T. Katsumato, S. Komuro, T. Morikawa, J. Crystal Growth, **275** (2005) e2013.

[97] D. Jia, R.S. Meltzer, W.M. Yen, W. Jia, X. Wang, Appl. Phys. Lett. **80** (2002) 1535.

[98] D. Jia, J. Zhu, B. Wu, J. Lumin. **93** (2001) 107.

[99] X. Yuan, X. Shi, M. Shen, W. Wang, L. Fang, F. Zhang, X. Wu, J. Alloys Compd. **485** (2009) 831.

[100] J. Kuang, Y. Liu, Chem. Phys. Lett. **424** (2006) 58.

[101] H. Liu, Y. Wang, Q. Chang, W. Jiao, Y. Song, Opt. Commun. **251** (2005) 388.

[102] Y. Liu, B. Lei, C. Shi, Chem. Mater. **17** (2005) 2113.

[103] J. Kuang, Y. Liu, J. Solid State Chem. **179** (2006) 266.

[104] J. Kuang, Y. Liu, Chem. Lett. **34** (2005) 598.

[105] B. Lie, Y. Liu, J. Liu, Z. Ye, C. Shi, J. Solid State Chem. **177** (2004) 1333.

[106] B. Lie, Y. Liu, J. Liu, G. Tang, Z. Ye, C. Shi, Mater. Chem. Phys. **87** (2004) 227.

[107] V. Singh, T.K.G. Rao, D.K. Kim, Rad. Measurements **43** (2008) 1198.

[108] C. Song, X. Wang, Y. Liu *et al.*, Chemistry **5** (2004) 273.

[109] B. Lie, Y. Liu, J. Liu, G. Tang, Z. Ye, C. Shi, Chem. J. Chin. Univ. **24** (2003) 782.

[110] C. Guo, C. Zhang, Y. Lu, Q. Tang, Q. Su, Phys. State Sol. (a) **201** (2004) 1588.

[111] B. Lie, Y. Liu, J. Liu, Z. Ye, C. Shi, J. Lumin. **109** (2004) 215.

[112] M. Iwasaki, D.N. Kim, K. Tanaka, T. Murata, K. Morinaga, Sci. Technol. Adv. Mater. **4** (2003) 137.

[113] L. Jiang, D. Jia, W. Yen, J. Lumin. **102** (2003) 34.

[114] C.Q. Yao, H. Lin, L. Zhang, G.X. Lu, M.L. Gong, M.Z. Su, J. Mater. Chem. **8** (1998) 585.

[115] J. Qui, A. Makisima, Sci. Technol. Adv. Mater. **4** (2003) 35.

[116] D. Jia, J. Zhu, B. Wu, J. Lumin. **91** (2000) 59.

[117] J. Kuang, Y. Liu, J. Electrochem. Soc. **153** (2006) G245.

Chapter II

Systematic study on the synthesis of $Sr_4Al_{14}O_{25}:Eu^{2+}/Dy^{3+}$ phosphor and its photoluminescence characteristics

2.1. Introduction

Phosphor materials with long afterglow is a kind of energy storing materials that can absorb UV or visible light from sun light, and gradually release the absorbed energy in the darkness at a certain wavelengths, in the form of visible light [1].

Among the various phosphors ZnS-based materials doped with Cu or Mn ions were first prepared and applied for the various fields [2]. However the luminescent intensity of these phosphors was not bright enough and the afterglow time was short. Therefore, some radio-active elements such as tritium (^{3}H), radium (^{225}Ra) and promethium (^{147}Pr) had to be co-doped into the ZnS based phosphors to prolong the afterglow time. Due to the hazardous radio-active radiations, the uses of such radio-active isotope doped ZnS type phosphors were limited.

As far as the development of phosphor is concerned, Eu^{2+} ion was frequently used as an activator ion in various host lattices. Due to the shielding effect of the outer shells, the 5d electrons split easily by the crystal field around it. Thus the peak position of Eu^{2+} emission strongly depends on the Eu^{2+} ions surrounding, consequently, Eu^{2+} ions can emit from near UV to red region of the spectrum. For example, Eu^{2+} ions give blue (440 nm) luminescence in $CaAl_2O_4$ or CsBr phosphors [3-4], blue-green (495 nm) in $Sr_4Al_{14}O_{25}$ or γ-AlON phosphor [5-6], green (520 nm) in $SrAl_2O_4$ phosphor [5, 7], yellow (558 nm) in $CaSi_2O_2N_2$ phosphor [8] and orange (610 nm) in $Sr_3Al_2O_5Cl_2$ phosphor [9]. Further, it can often be pumped by the sunlight or other natural light source. Therefore, as a new phosphor, alkaline earth aluminate phosphors doped with divalent europium ion (Eu^{2+}) have been investigated as an efficient phosphor that has high quantum efficiency and good stability, indicating good practical prospects [10-15]. These phosphors have decay time ranging from nanosecond to

tens of seconds and were used as important constituents of light emitting devices, fluorescent lamps, plasma display panels and lamp for medical applications [16]. However, for specific dark vision applications involving signage, blackouts, emergency rescue guidance systems and luminous watches, the developed phosphor with appreciable brightness, high stability and long persistent time of more than 5 h is fundamental requisites [17].

In 1996, Matsuzawa *et al.* reported a new type of aluminate based phosphor, $SrAl_2O_4:Eu^{2+}/Dy^{3+}$, with a strong emission centered at 520 nm (green) [7]. The persistent life time of this $SrAl_2O_4:Eu^{2+}/Dy^{3+}$ phosphor was found to be longer than 16 h. After a short time, a new similar long persistent phosphor $CaAl_2O_4:Ce^{3+}/Nd^{3+}$ was reported that showed persistent emission at 420 nm (blue) [18]. Though, Smets *et al.* reported blue-green emitting $Sr_4Al_{14}O_{25}:Eu^{2+}$ phosphor, he did not observed the long afterglow [5]. Later, $Sr_4Al_{14}O_{25}:Eu^{2+}/Dy^{3+}$ phosphor was developed showing extremely prolonged blue-green (495 nm) phosphorescence [19-20]. These phosphors drew considerable attention because of their ability to persist overnight, chemical stability, wide range of excitation, high quantum yield *etc.* opening prospect of various applications [21-22].

During the last decade, the research on the development of new persistent phosphors and improvement of persistent life time of existing phosphor has been done enormously. Study on the mechanism of persistency of the afterglow revealed that electron and hole traps are responsible for the long persistent time of these phosphors, which in turn depends on the doped auxiliary ions or the defects in the crystal lattice. Various rare metals (Dy^{3+}, Nd^{3+}, Gd^{3+}, Sm^{3+} *etc.*) have been studied to trap the electrons and holes to prolong the afterglow durations [23-25] and it is concluded that in the strontium aluminate doped with Eu^{2+} (SAE) type phosphors, Dy^{3+} is the most effective co-activator to prolong the afterglow life time.

Thus, in order to improve the phosphorescence characteristics, Dy^{3+} ion has been added to SAE phosphors and fabrication conditions have been examined [16-25]. For specific dark vision applications, the existing brightness and persistent phosphorescence have been improved but are not enough and needed more improvements. Fascinated by the techno-commercial applications, many researchers started exploring the dependence of various physico-chemical parameters such as thermal parameters [14], addition of fluxes

[15-17, 24-28], and effect of composition [22, 27-29] on the luminescence and long persistence behavior of these phosphors.

The $Sr_4Al_{14}O_{25}:Eu^{2+}/Dy^{3+}$ phosphor showed bright luminescence, extremely long persistent time and very high quantum yield (>90%) and can be applied in various display applications, especially, for overnight display purposes. Thus, I have selected $Sr_4Al_{14}O_{25}$ phosphor for the detail study. In this chapter the systematic examination of rare earth ions (Eu^{2+}, Dy^{3+}, and other lanthanides), monovalent to hexavalent charge compensators (Li, Na, Ag, Mg, Ca, Ba, B, Si, W), flux (H_3BO_3), substitution effect of Ca or Ba in the Sr site, effect of starting alumina powder type and its particle size, preheating and reduction temperatures and time, and the reduction atmosphere for the improvement of morphology and photoluminescence characteristics of the $Sr_4Al_{14}O_{25}$ phosphor has been explained in detail. I will discuss the origin of white afterglow in the $Sr_4Al_{14}O_{25}$ matrix by substitution with Ca ions.

2.2. Experimental

Strontium aluminate phosphor doped with Eu^{2+} and Dy^{3+} ($Sr_4Al_{14}O_{25}:Eu^{2+}/Dy^{3+}$) were prepared by the reaction between strontium carbonate ($SrCO_3$; Aldrich, 99.9+ %), aluminum oxide (Al_2O_3; Baikalox, ultrapure, 0.05, 0.1 and 1.0 μ powder), europium oxide (Eu_2O_3; Aldrich, 99.9+ %) and dysprosium oxide (Dy_2O_3; Aldrich, 99.9+ %). Small amount of boric acid (H_3BO_3; AR) was used as a flux. The raw powder was mixed according to the nominal composition of $4SrCO_3 + 7Al_2O_3$ + (0.00, 1.75, 3.50 and 8.75) mol% H_3BO_3 + x at% Eu^{3+} and y at% Dy^{3+}. However, the proportion of aluminium and strontium were varied from its ratio (Al/Sr) 3.4 to 4.0 to prepare various non-stoichometric phosphor samples. In case of Ca/Ba substituted samples 0 to 1 mol fraction of Sr is substituted by Ca or Ba. Some monovalent to hexavalent ions (Li^+, Na^+, Ag^+, Mg^{2+}, Ca^{2+}, Ba^{2+}, B^{3+}, Si^{4+}, W^{6+}) were added to the starting mixture to compensate the charge neutrality. Then, an appropriate amounts of the starting material according to the above mentioned composition was mixed thoroughly in mortal and pestle with the help of little ethanol. Pellets (ϕ 13 mm × 3 mm) were prepared and preheated in air atmosphere at 900°C -1100°C for 4 h and then pulverized to get fine powder. Again pellets (ϕ 13 mm × 3 mm) were prepared and then heated at 1100°C - 1400°C for 5 h in a reducing atmosphere of 10% H_2 and 90% N_2 by flowing 20 ml/min H_2 and 180

ml/min N_2. The phosphor product obtained was gritty solid that was grinded to get fine powder, washed with boiling acetic acid followed by distilled water to get rid from some glassy phases. Then, the dried powder was used for characterizations and evaluations. The complete preparation scheme is shown in Fig. 2.1.

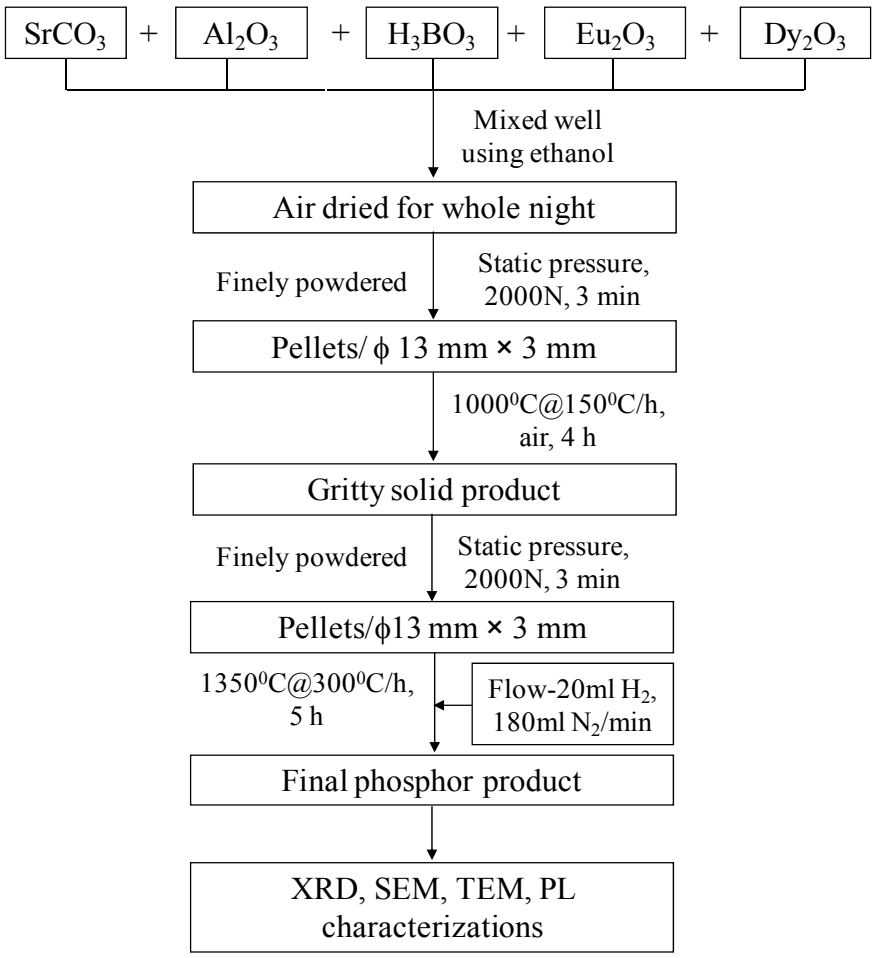

Fig. 2.1. Flow chart for the preparation of $Sr_4Al_{14}O_{25}:Eu^{2+}/Dy^{3+}$ phosphor by solid state reaction method.

Phase identifications were carried out using a Shimadzu XRD-630D instrument with Cu-Kα radiation. Thermo-gravimetric (TG) and differential thermal (DTA) analyses were carried out using a SEIKO TG/DTA 6300 instrument. Scanning Electron Microscopy (SEM) observations were carried out using a Hitachi S-3000N SEM instrument. Elemental mapping images were recorded using EDX coupled with SEM. Before SEM-EDX measurements phosphor particles were coated (about 5 nm thickness) with Pt-Pd using ion sputter. Surface elemental analyses were carried out using Rayny107 energy dispersive X-ray fluorescence

meter. TEM images were obtained by a Hitachi H-800MU microscope. Photoluminescence spectra (absorption, excitation and emission) were recorded using USB 4000-UV-VIS fiber optic spectrometer (Ocean optics). The afterglow intensity and decay curves were obtained at room temperature using a brightness meter (Konica Minolta LS-100). Before decay curves measurement, each sample was exposed to standard 15W xenon lamp for 20 minutes. Thermoluminescence glow peaks were recorded from 0 to 300^{o}C using a self assembled instrument.

2.3. Results and Discussion

2.3.1. Effect of Flux

To understand the thermal behavior of the raw mixture and the effect of flux on the formation of target product during raising temperature, it is necessary to observe TG and DTA results. The TG and DTA measurements were carried out for representative samples containing different amount of boric acid as a flux as $4SrO.7Al_2O_3.B_0$ (without Boric acid), $4SrO.7Al_2O_3.B_{0.2}$ (1.75 mol% Boric acid) and $4SrO.7Al_2O_3.B_{0.4}$ (3.5 mol% Boric acid) with 4 at% europium and 8 at% dysprosium. Fig. 2.2 depicts the TG and DTA results of various raw mixtures containing different amount of flux. The weight loss below 300^{o}C indicates the dehydration of boric acid and γ-alumina used as raw powder (since γ-alumina contained small amount of $Al(OH)_3$). For $4SrO.7Al_2O_3.B_0$ mixture nearly 3 wt% loss was due to dehydration of γ-alumina. The weight loss of $4SrO.7Al_2O_3.B_{0.2}$ and $4SrO.7Al_2O_3.B_{0.4}$ mixtures below 300^{o}C were 3.4 and 3.8 wt%, respectively, that came from the weight loss by γ-alumina (3 wt%) as well as that of the boric acid used. The total weight loss of 16.2 wt%, 16.8 wt% and 17.3 wt%, is analogous to the theoretical values of, 17.1 wt%, 17.4 wt% and 17.7 wt% for the $4SrO.7Al_2O_3.B_0$, $4SrO.7Al_2O_3.B_{0.2}$ and $4SrO.7Al_2O_3.B_{0.4}$, respectively. The sharp weight loss and endothermic peak on the TG and DTA at 700 to 900^{o}C indicates the decomposition of $SrCO_3$ to form SrO. From Fig. 2.2 it is seen that $SrCO_3$ decomposed at relatively lower temperatures in case of boric acid rich mixture than that of boric acid free mixture. Further, boric acid flux greatly promotes the $Sr_4Al_{14}O_{25}$ phase formation and reduced its formation temperature [30]. Thus, it can be concluded that the boric acid flux decreases the decomposition temperature of $SrCO_3$ and greatly reduces the phase formation temperature in strontium aluminate systems.

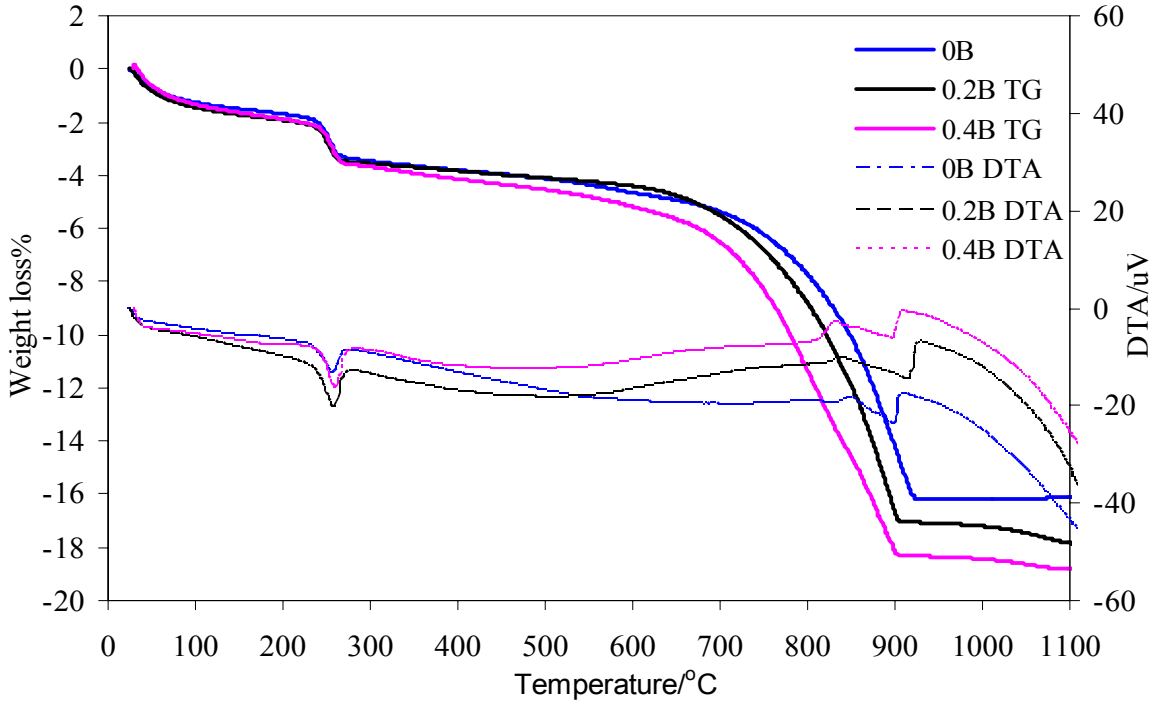

Fig. 2.2. TG- DTA curves of precursor mixtures with or without H_3BO_3 showing the reaction process aided by the flux (H_3BO_3) during calcinations.

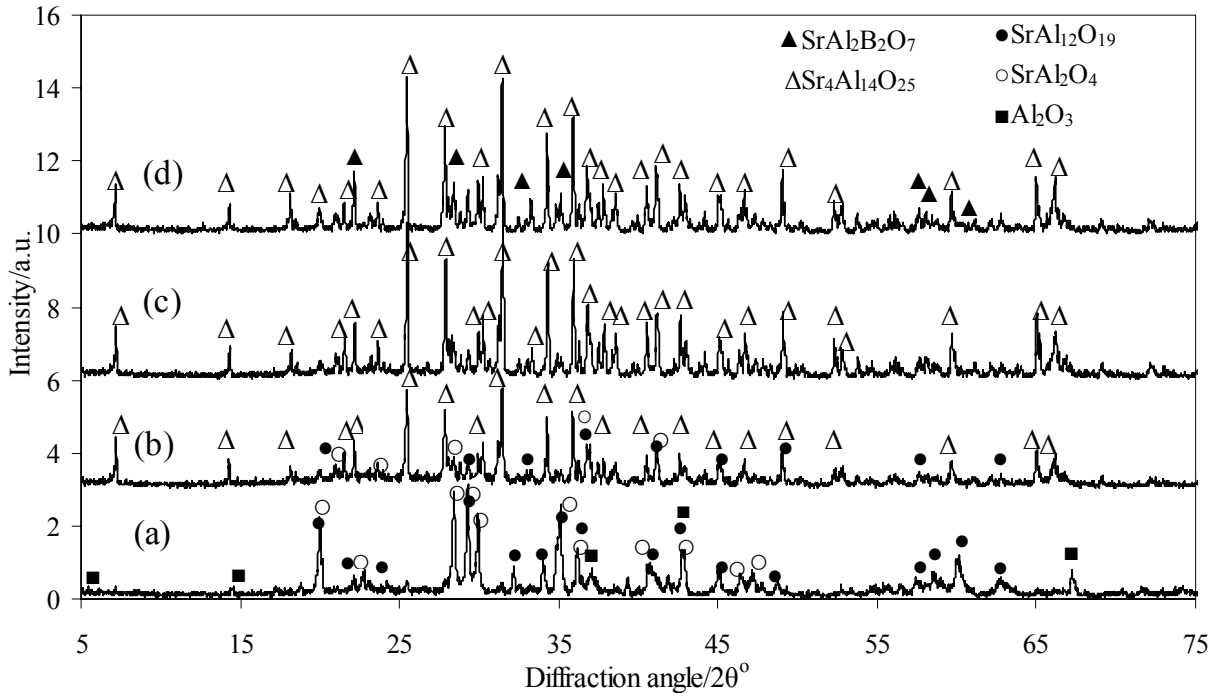

Fig. 2.3. XRD patterns of strontium aluminate system for the samples (a) $4SrO.7Al_2O_3.B_0$, (b) $4SrO.7Al_2O_3.B_{0.2}$ (c) $4SrO.7Al_2O_3.B_{0.4}$ and (d) $4SrO.7Al_2O_3.B_{1.0}$.

Figure 2.3 (a-d) show the XRD patterns of SAED phosphor samples prepared adding 0.00, 1.75, 3.50 and 8.75 mol% H_3BO_3, respectively, heated at 1300°C for 5 h. In the $S_4A_7B_0$ phosphor sample, $SrAl_2O_4$ (JCPDS; 34-0379) and $SrAl_{12}O_{19}$ (JCPDS; 26-0976) phases were observed as main phases along with some residual alumina (JCPDS; 46-1212). On increasing boric acid concentration to 1.75 mol% ($S_4A_7B_{0.2}$), these $SrAl_2O_4$ and $SrAl_{12}O_{19}$ phases decreased and a new phase ($Sr_4Al_{14}O_{25}$) was appeared. Further increasing boric acid concentration to 3.50 mol% ($S_4A_7B_{0.4}$), highly crystalline, pure $Sr_4Al_{14}O_{25}$ phase was observed. The $Sr_4Al_{14}O_{25}$ phase was refined to be the orthorhombic crystal structure with *Pmma* space group. The unit cell lattice parameters calculated from XRD results were a = 24.78*Å*, b = 8.48*Å* and c = 4.86*Å*. These values are in well agreement with that in the JCPDS card data (52-1876) and the values reported in other articles [16, 17, 31]. It is suggested that the metastable $Sr_4Al_{14}O_{25}$ phase was formed by the reaction between $SrAl_{12}O_{19}$ and $SrAl_2O_4$ intermediate phases in the presence of boron oxide flux that accelerates the $Sr_4Al_{14}O_{25}$ phase formation acting as high temperature solvent [31]. However, if boric acid concentration was increased to 8.75 mol% ($S_4A_7B_{1.0}$), there appeared much glasses and some crystalline aluminoborate phase, $SrAl_2B_2O_7$ (JCPDS; 47-0182) along with the $Sr_4Al_{14}O_{25}$ phase. Thus, at higher concentration, boric oxide not only acts as high temperature solvent, but actively participates in chemical reaction with the aluminates to form alumino-borate as seen in Fig. 2.3 (d). Therefore, synthesis of $Sr_4Al_{14}O_{25}$ phase involves complex reaction processes, in which $SrAl_2O_4$ and $SrAl_{12}O_{19}$ are formed as intermediate phases [31]. Formations of these intermediate phases were further confirmed by the XRD results of the phosphor samples prepared at 900°C and 1000°C (Fig. 2.9). At those temperatures, only $SrAl_2O_4$ and $SrAl_{12}O_{19}$ phases were formed. Thus, the synthesis of $Sr_4Al_{14}O_{25}$ phosphor can be expressed by the following chemical reactions:

$$2H_3BO_3 \xrightarrow{<300\ ^oC} B_2O_3 + 3H_2O \qquad (2.1)$$

$$2Al(OH)_3 \text{ (From } \gamma\text{-}Al_2O_3) \xrightarrow{<300\ ^oC} Al_2O_3 + 3H_2O \qquad (2.2)$$

$$SrCO_3 \xrightarrow{700\text{-}900\ ^oC} SrO + CO_2 \qquad (2.3)$$

$$SrO + Al_2O_3 \xrightarrow{1200\ ^oC} SrAl_2O_4 \qquad (2.4)$$

$$SrAl_2O_4 + 5Al_2O_3 \xrightarrow{>1200\ ^oC} SrAl_{12}O_{19} \quad (2.5)$$

$$17SrAl_2O_4 + 3SrAl_{12}O_{19} \xrightarrow[B_2O_3]{\sim 1300\ ^oC} 5Sr_4Al_{14}O_{25} \quad (2.6)$$

$$Sr_4Al_{14}O_{25} + B_2O_3\ (\text{Excess}) \xrightarrow{\geq 1400^oC} SrAl_2B_2O_7 + SrB_4O_7 \quad (2.7)$$

Change in the grain morphology of the phosphor was studied by SEM observations. Figures 2.4 (a-d) represent the SEM micrograph of SAED phosphor samples $4SrO.7Al_2O_3.B_0$, $4SrO.7Al_2O_3.B_{0.2}$, $4SrO.7Al_2O_3.B_{0.4}$ and $4SrO.7Al_2O_3.B_{1.0}$, respectively, after treated with an acetic acid solution. In the phosphor sample $4SrO.7Al_2O_3.B_0$, prepared in absence of H_3BO_3, irregular particles (almost spherical) were formed. The particle size was very small in the range of 0.2 to 0.5 μm (Fig. 2.4 (a)). These particles get connected with each other creating numerous pores on the surface whose average diameter was about 1μm. On adding 1.75 mol% boric acid, the growth of phosphor particles was accelerated producing bigger particles with high angularity and sharp corners. The particle size distribution increased drastically and form angular particles of nearly 1.5 μm long and 1 μm wide (Fig. 2.4 (b)). In between these angular particles there appeared some spherical to irregular particles. Appearance of angular particles and disappearance of spherical particles at the same time suggests that the spherical particles were gradually transformed to the angular particles. From the XRD results (Fig. 2.3) it was found that the spherical particles were that of $SrAl_2O_4$ crystals while that of angular particles were $Sr_4Al_{14}O_{25}$ crystals. Therefore, it is suggested that addition of small amount of boric acid help to transform $SrAl_2O_4$ phase to $Sr_4Al_{14}O_{25}$. A similar result has been presented by A. Nag *et.al.* in the preparation of $SrAl_2O_4$ phosphor [27]. If the boric acid concentration was further increased to 3.5 mol%, further particles growth occurred and there appeared particles with very sharp corners, fixed boundary and angular to hexagonal shape. The average particles size was 2 μm long and 1 μm wide as shown in Fig. 2.4(c). However, as in Fig. 2.4(b), there was no any spherical to irregular particles observed. It suggests that growth of $Sr_4Al_{14}O_{25}$ phase was completed.

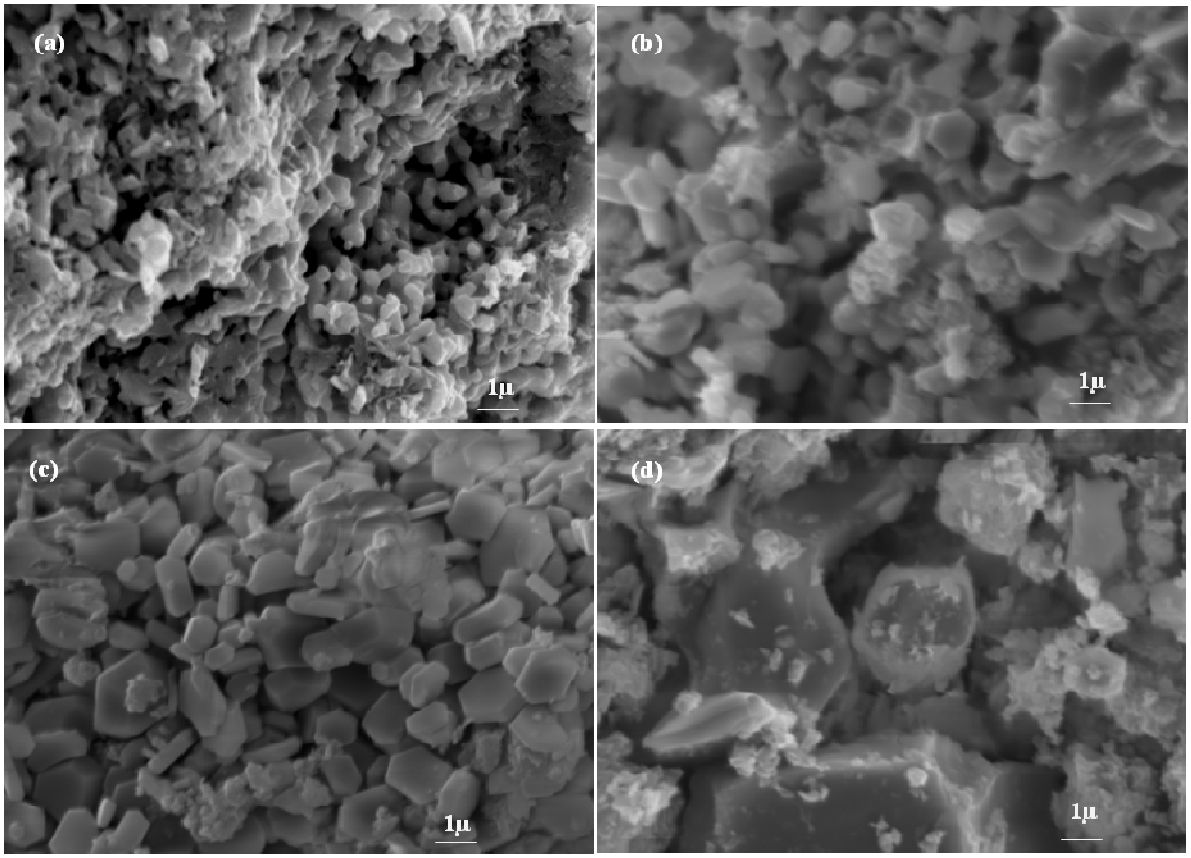

Fig. 2.4. SEM microstructures of the SAED phosphors prepared with different H_3BO_3 contents: (a) 0.00 mol% ($4SrO.7Al_2O_3.B_0$), (b) 1.75 mol% ($4SrO.7Al_2O_3.B_{0.2}$), (c) 3.5 mol% ($4SrO.7Al_2O_3.B_{0.4}$) and (d) 8.75 mol% ($4SrO.7Al_2O_3.B_{1.0}$).

However, as boric acid concentration was increased to 8.75 mol%, the particles growth increased drastically showing very wide particle size distribution ranging between 5 to 10 μm (Fig. 2.4(d)). However, in these particles the fixed geometry had been destroyed and the corner was with smooth surface. These particles were covered randomly by minute particles that were found to be $SrAl_2B_2O_7$ phase as confirmed by the XRD analysis. As we know, boric acid is a good glass former at higher concentration and high temperature, it forms undesired strontium alumino borate and other glassy phases that cover the surface of the phosphor. The glassy phase was washed away by hot acetic acid treatment and hence not observed clearly in the SEM micrographs, however, strontium alumino borate was clearly observed. Therefore, it is concluded that boric acid flux promotes the $Sr_4Al_{14}O_{25}$ phase formation at optimum concentration but at higher concentration undesired product like glass is possible.

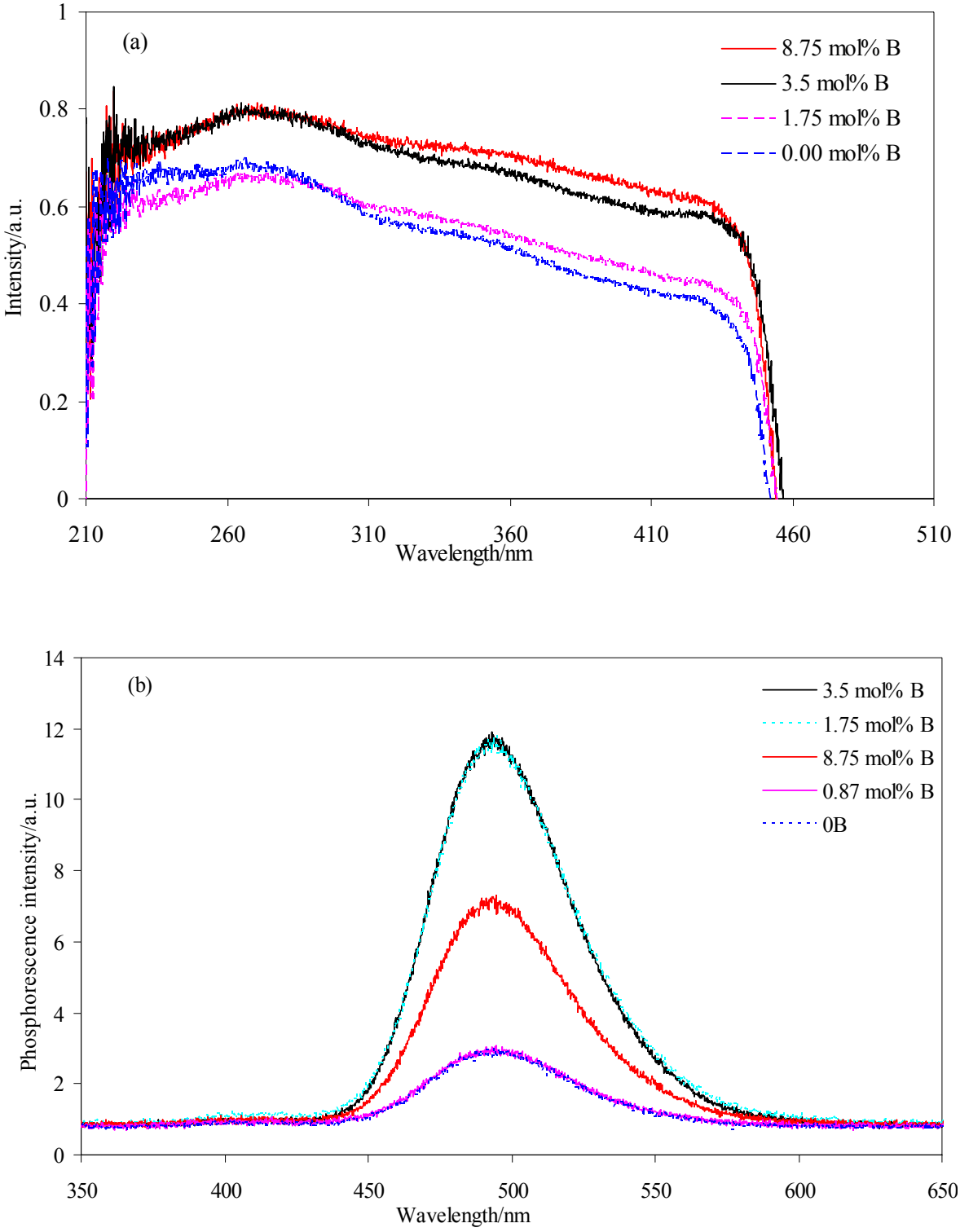

Fig. 2.5. SAED phosphors prepared with the aid of various amount of boric acid, (a) absorption spectra and (b) phosphorescence spectra.

Figure 2.5 (a) and (b) shows the absorption and emission spectra of $Sr_4Al_{14}O_{25}:Eu^{2+}/Dy^{3+}$ phosphor, respectively. The room temperature absorption spectra of SAED phosphors consist of strong absorption plateau with step edges at nearly 210 and 450 nm. Thus, these SAED phosphors can be efficiently excited by the UV radiation of sunshine and thus does not require any artificial excitation source. All these SAED phosphor samples emitted blue-green light centered at 497 nm (the most appropriate region of human sensation) but its intensity varied significantly with boric acid concentrations. On increasing boric acid concentrations, the phosphorescence intensity also increased and reached maximum when added boric acid concentration was 3.5 mol% and above that it decreased again, as in the inserted graph in Fig. 2.6.

It may be explained as: in case of boric acid free phosphor samples, $SrAl_2O_4$ and $SrAl_{12}O_{19}$ mixed phases were existed, the later shows very low afterglow intensity [10]. On increasing boric acid concentration (1.75 mol %), the $SrAl_{12}O_{19}$ phase disappeared and there appeared $Sr_4Al_{14}O_{25}$ phase. Both the $SrAl_2O_4:Eu^{2+}/Dy^{3+}$ and $Sr_4Al_{14}O_{25}:Eu^{2+}/Dy^{3+}$ phosphors show high brightness and long afterglow, hence the afterglow intensity and persistent time sharply increased. Further increasing boric acid concentration to 3.5 mol%, highly crystalline, single phase $Sr_4Al_{14}O_{25}$ phosphor was formed that produced very high phosphorescence intensity and afterglow duration. However, as boric acid concentration was increased above 3.5 mol%, the afterglow intensity sharply decreased. It has been reported that boric acid flux can properly facilitate the entry of activator ions into the crystal lattice and aids in the formation of luminescent centers [32]. Due to liquid boron oxide as high temperature flux, distribution of the rare metal ions becomes random and deep throughout the lattice. Further, the flux enforce the Eu^{2+} and Dy^{3+} ions to replace the Sr^{2+} site in the lattice [32]. This increases the Eu^{2+} and Dy^{3+} ions concentration in the $Sr_4Al_{14}O_{25}$ lattice and causes steep increase in the photoluminescence properties. To prove the increment of activator ions in the strontium aluminates phosphor, EDX experiments of samples prepared adding 0.00, 1.75 mol%, 3.50 mol% and 8.75 mol% boric acid in the starting mixture were carried out keeping the constant amount of europium (4 at%) and dysprosium (8 at%) and the result are presented in Table 2.1. Although the added amount of europium and dysprosium in the raw mixture was constant (4 at% and 8 at%, respectively), actual incorporated amount of Eu^{2+} and Dy^{3+} in the $Sr_4Al_{14}O_{25}$ lattice (after acetic acid treatment)

increased with the increase of the boric acid concentration. Even though the incorporated amount of Eu^{2+} and Dy^{3+} ions into the $Sr_4Al_{14}O_{25}$ lattice was higher in the sample prepared adding 8.75 mol% boric acid, the emission intensity was decreased in that sample. The decrease in the emission intensity with higher flux concentration might be due to formation of non emitting phase $SrAl_2B_2O_7$ as observed in XRD and some of the glasses that covered the phosphor surface and protect the surface from emission or it disperse the emitted light to undesired directions.

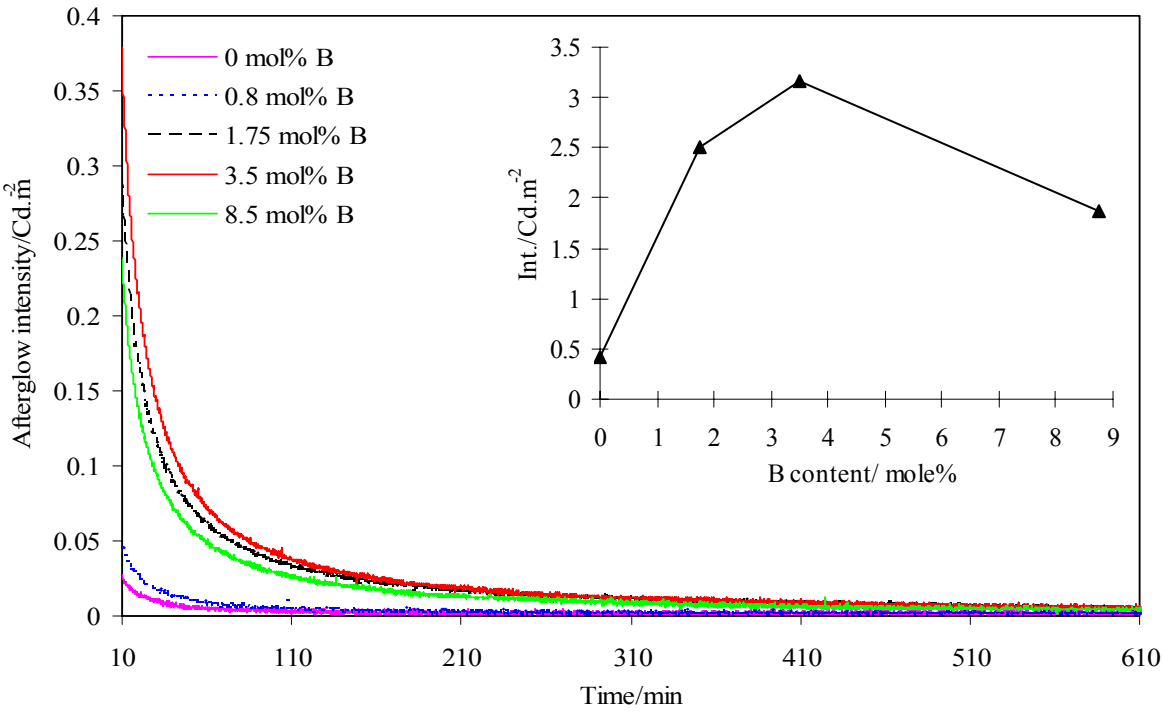

Fig. 2.6. Variation of afterglow intensity and its decay speed of strontium aluminate phosphors prepared adding various concentration of boric acid. The inset figure shows the variation of afterglow intensity with boric acid concentration.

Table 2.1. List of samples with various boric acid contents, Eu^{2+} and Dy^{3+} concentrations obtained from EDX studies correlated with afterglow emission intensities values.

Samples name	Phases observed	Amount Eu^{2+}	Amount Dy^{3+}	Afterglow intensity ($Cd.m^{-2}$)	Afterglow time(h)
0B (boron free)	$SrAl_2O_4$	0.125%	0.5%	0.18	< 2
0.2B (1.75 mol% B)	$SrAl_2O_4$, $Sr_4Al_{14}O_{25}$	0.144%	0.79%	2.514	>15
0.4B (3.5 mol% B)	$Sr_4Al_{14}O_{25}$	0.146%	0.89%	3.17	>20
1.0B (8.75 mol% B)	$Sr_4Al_{14}O_{25}$, $SrAl_2B_2O_7$	0.156%	0.92%	1.815	<10

Figure 2.6 depicts the persistent afterglow curves of the various phosphor samples prepared adding 0.00, 0.85, 1.75, 3.50 and 8.75 mol% boric acid under the condition of 4 at% Eu^{2+} and 8 at% Dy^{3+}. We found that the persistence time from boric acid free phosphor was the least, almost non emissive. As the added amount of boric acid was increased to 3.5 mol%, the phosphorescence intensity was increased dramatically and same was the persistent life time that persisted over 20 h. The liquid phase sintering aided by flux facilitates the grain growth of the strontium aluminates and increases the penetration of trap centers in these phosphors. As explained in mechanism of long persistency of phosphorescence in chapter 1.3.2, increased amount of Dy^{3+} ions in the host increased the hole trapping capacity that enhances the phosphorescence intensity and its depth or the release rate of trapped holes control the afterglow duration [33]. Further, the dissolved B^{3+} ions substitute Al^{3+} ions at tetrahedral positions [34]. This substitution results in the shrinkage of $Sr_4Al_{14}O_{25}$ lattice and enhance the hole trapping ability of Dy^{3+} ions that further increases the afterglow intensity [27]. The decrease of afterglow intensity and persistent time on further increasing the boric acid concentration above 4 mol% may be due to formation of glass and other impurity phases that obviously reduced the phosphorescence intensity and afterglow duration.

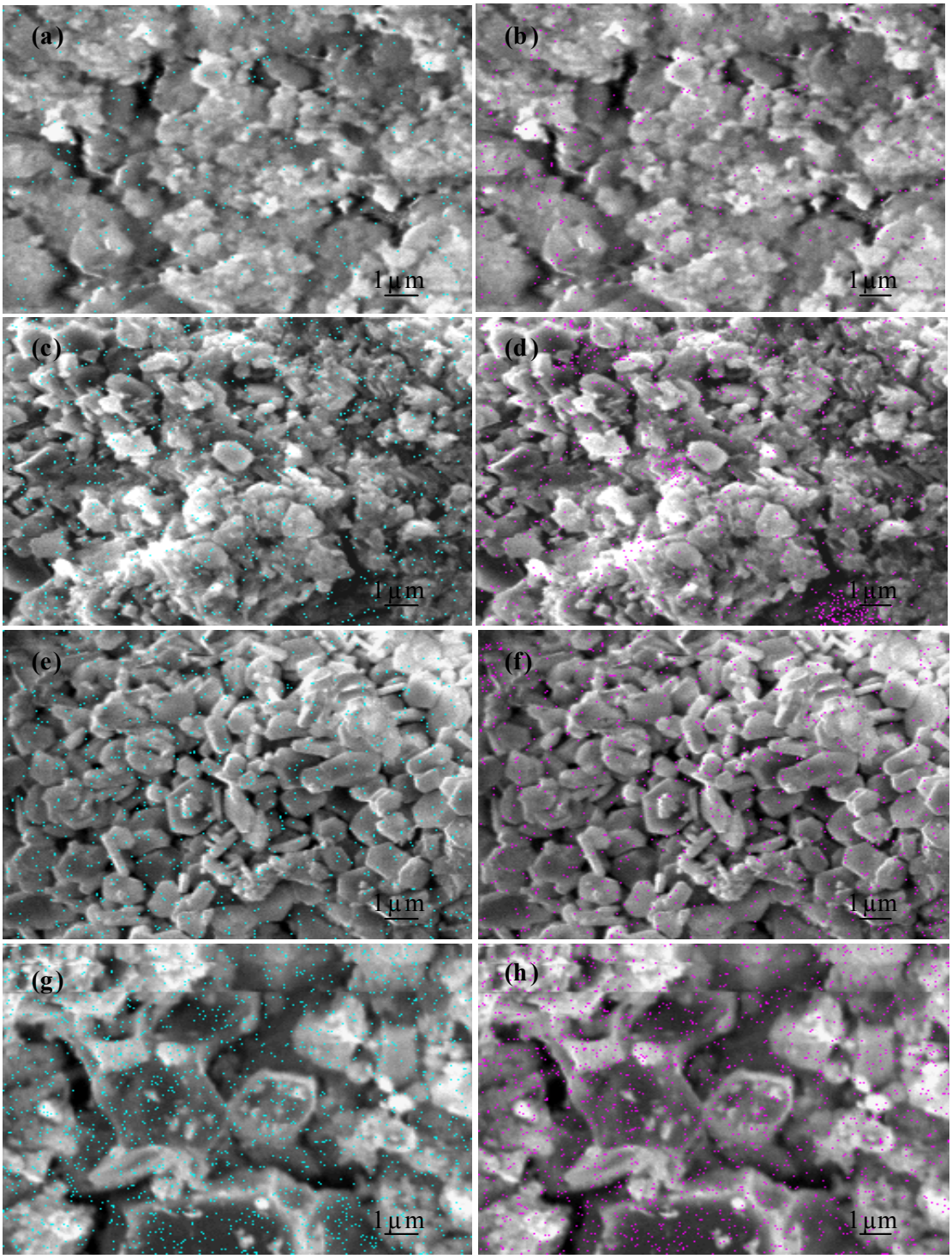

Fig. 2.7. EDX mapping in SAED phosphors: europium (a, c, e & g) and dysprosium (b, d, f & h) prepared with different H_3BO_3 concentration: (a, b) 0 mol%, (c, d) 1.75 mol%, (e, f) 3.5 mol% and (g, h) 8.75 mol%.

2.3.2. Effect of Heating Environment

Figure 2.8 depicts the variation of afterglow intensity as a function of preheating temperatures for the synthesis of SAED phosphors. The phosphorescence intensity and long persistent time increased on increasing the preheating temperature from 800°C to 1000°C above that remained almost constant as shown in Fig. 2.8. When the mixture was preheated at 800°C to 900°C, there appeared some peaks of alumina, $SrAl_2O_4$ and $SrAl_{12}O_{19}$ phases, as shown in XRD results in Fig. 2.9. As the preheating temperature was increased to 1000°C, alumina peaks completely disappeared and that of $SrAl_{12}O_{19}$ peaks increased. As described above in equation 2.6, $SrAl_{12}O_{19}$ and $SrAl_2O_4$ phases reacts with each other in the presence of boron oxide flux to generate $Sr_4Al_{14}O_{25}$ phase. Thus, preheating at suitable temperature (1000°C) generates proper precursor powders that enhance the final phase formation. According to F. Clabau *et.al.* [35], preheating in air condition at optimum temperature increase the phosphorescence properties. It is because heating in air environment increases the oxygen vacancies around the Europium ions. These oxygen vacancies are found to enhance the phosphorescence properties. Therefore, the raw mixture should be preheated in air atmosphere at around 1000°C to get the better photoluminescence properties.

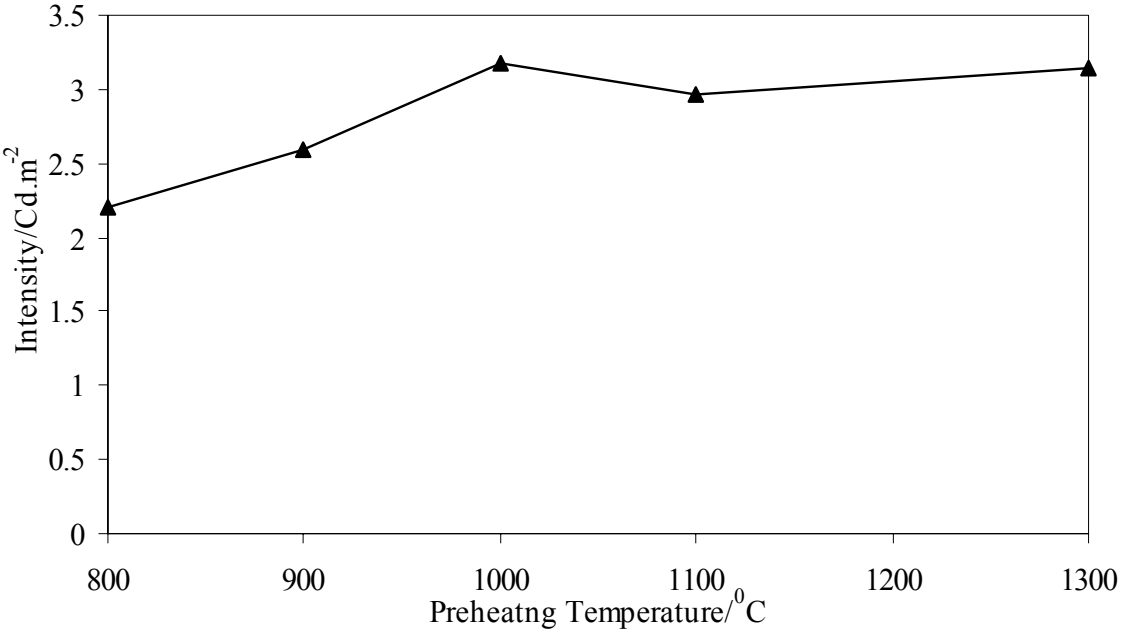

Fig. 2.8. Variation of phosphorescence intensity for strontium aluminate phosphors preheated at various temperatures and then reduced at 1300°C for 5 h.

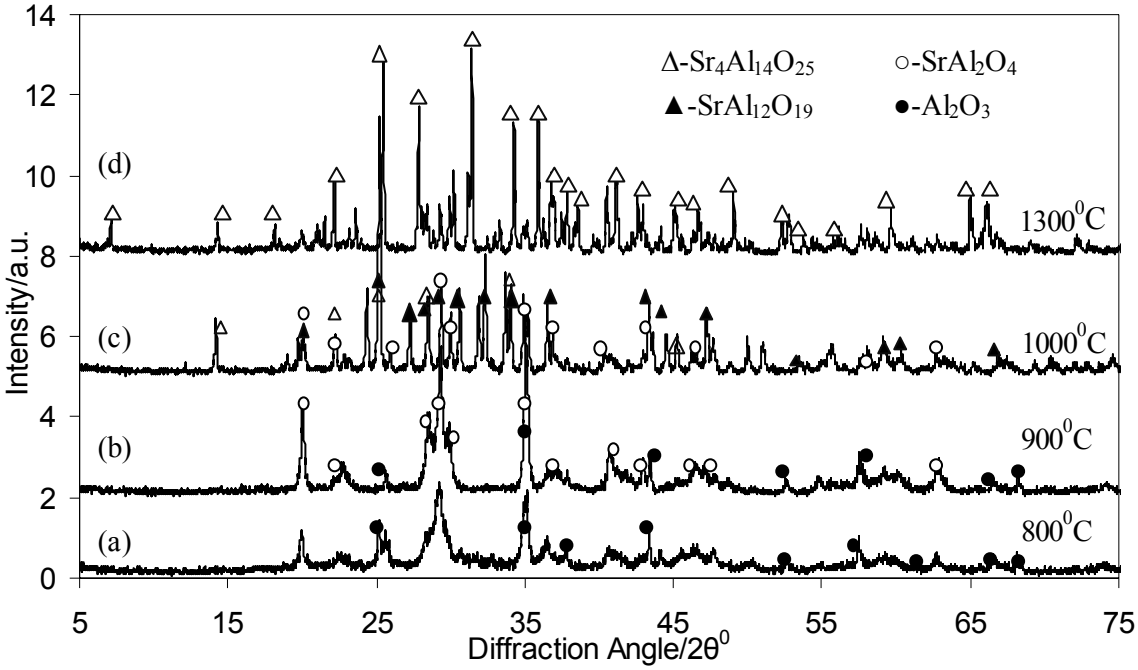

Fig. 2.9. Effect of preheating temperatures for the phase formation of SAED phosphors.

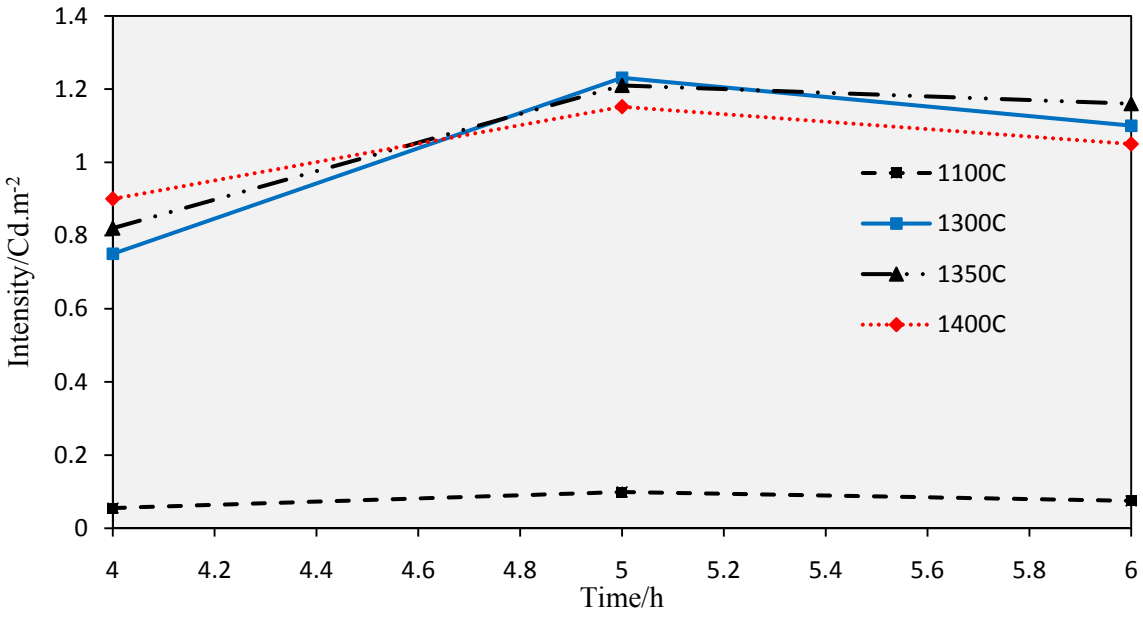

Fig. 2.10. Variation of afterglow intensities of the SAED phosphors as a function of reduction temperatures and time.

Figure 2.10 shows the variation of afterglow intensity as a function of heating temperature and time. It was observed that the phosphor prepared at 1300°C–1350°C sintered for 5 h in reducing atmosphere has higher phosphorescence intensity and longer persistent time. Increase in phosphorescence intensity and persistent time of the phosphor prepared above 1350°C was incremental, indicating 1350°C heating for 5 h is the sufficient temperature and enough time to get excellent photoluminescence properties. The phosphor should be prepared under slightly reducing atmosphere so that the Eu^{3+} ions can be reduced to Eu^{2+} ions because the emission center is Eu^{2+} ions in this phosphor. When the phosphor was prepared in air atmosphere, the phosphorescence intensity was very dim, almost non emissive. The negligible emission was due to self reduction of Eu^{3+} ions to Eu^{2+} ions in the $Sr_4Al_{14}O_{25}$ host [36]. Calcinations of the $Sr_4Al_{14}O_{25}$ phosphor at higher temperatures revealed that it was stable up to 1700°C and above that temperatures, it breaks down into $SrAl_4O_7$ and $SrAl_2O_4$ phases.

2.3.3. Effect of activator and co-activator concentrations

The $Sr_4Al_{14}O_{25}$ phosphor consists of three dimensional networks composed of the octahedral anion groups (AlO_6) separated by double layers of tetrahedral anion groups (AlO_4) as shown in Fig. 2.11. The ionic radius of Sr^{2+} ($r_{Sr^{2+}}$= 118 pm) is very similar to the ionic radius of Eu^{2+} ($r_{Eu^{2+}}$= 117 pm). Due to the very similar ionic radius and isovalency, the doped Eu^{2+} ions are supposed to substitute the Sr^{2+} ions site in the $Sr_4Al_{14}O_{25}$ phosphor [2, 29]. Two types of Sr^{2+} site are present in this phosphor, one surrounded all around by AlO_4 tetrahedra and another at least one side by AlO_6 octahedra. As a consequence, there exist two types of Eu^{2+} ions in the $Sr_4Al_{14}O_{25}$ phosphor, hereafter called Eu1 and Eu2. The concentration of Eu1 and Eu2 ions were found to be almost similar [2]. The emission spectra of $Sr_{4-x-y}Al_{14}O_{25}$:xEu^{2+}/yDy^{3+} (x varies from 0.005 to 0.1 and y=0.08) are presented in Fig. 2.12. In the emission spectra of $Sr_4Al_{14}O_{25}$:Eu^{2+}/Dy^{3+} phosphor, when europium concentration was increased from 0.5 at% to 1 at%, two distinct emission bands at 405 and 500 nm were observed. With the increase of Eu^{2+} ions concentration, the emission intensity at 405 nm (high energy band) decreased gradually and at the same time, the emission intensity at 500 nm (low energy band) increased. When Eu^{2+} ions concentration increased to 4 at% (0.04), only the emission band at 500 nm was observed. Thus, at low Eu^{2+} ions

concentration, these two emission centers (Eu1 & Eu2) emit light and forms two respective emission bands at 405 and 500 nm. However, at higher europium ions concentration, these two emission bands merge and emits at 500 nm. This fact implies that the Eu1 emission center located at 405 nm is quenched at higher concentrations.

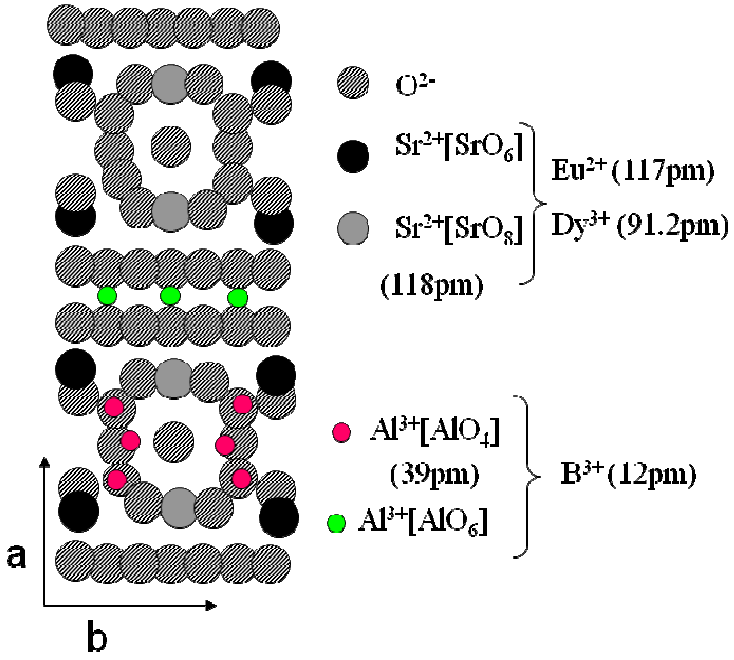

Fig. 2.11. Crystal structure of $Sr_4Al_{14}O_{25}:Eu^{2+}/Dy^{3+}$ phosphor projecting the unit cell along the [001] direction.

Further increasing the Eu^{2+} ions concentration beyond 5 at%, the emission intensity decreased gradually and it became almost non emissive when Eu^{2+} ions concentration reached 50 at%. It indicates that both Eu1 and Eu2 emission centers are quenched at higher concentrations. Thus concentration quenching process of $Sr_4Al_{14}O_{25}:Eu^{2+}/Dy^{3+}$ phosphor includes two different quenching processes *viz.* Eu1 emission quenching at first followed by Eu2 emission quenching process. It is well documented that the distance between Eu1-Eu2 is shorter than the distance between Eu1-Eu1 and Eu2-Eu2 in such type of host lattice [29]. Thus, the interaction between Eu1-Eu2 is stronger than those of Eu1-Eu1 and Eu2-Eu2. It is inferred by taking the specific concentration quenching process stated above that accompanying with Eu^{2+} concentration increasing from low to high, the emission from Eu1 center is quenched first by transferring excitation energy to nearby Eu2 centers and secondly, the emission from Eu2 center that is quenched by transferring the excitation energy from

Eu2 center via adjacent Eu2 center and finally to the non luminescent centers. The critical quenching concentration at which the emission of Eu^{2+} in $Sr_4Al_{14}O_{25}:Eu^{2+}/Dy^{3+}$ begins to decrease is nearly 4 at% and the quenching mechanism is dipole-dipole interaction [37].

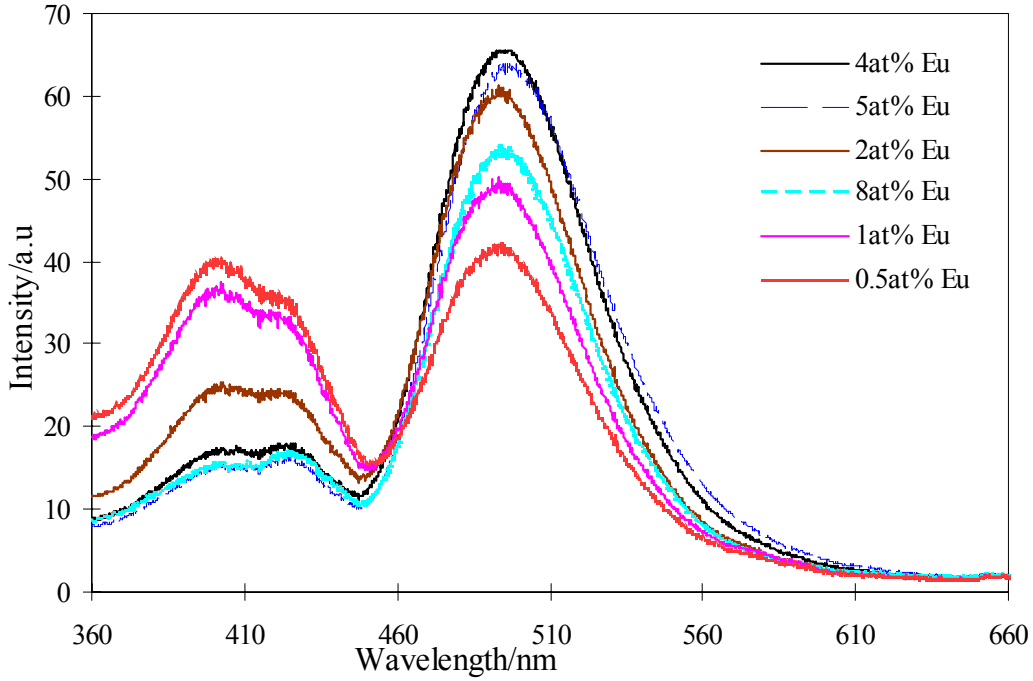

Fig. 2.12. Variation of emission intensity of $Sr_4Al_{14}O_{25}:Eu^{2+}/Dy^{3+}$ phosphor at various Eu^{2+} concentrations when Dy^{3+} concentration was fixed to 8 at%.

Further, very small red shift of the emission maxima was observed on increasing the Eu^{2+} ion concentrations. When the Eu^{2+} concentration was increased, the probability of an energy transfer from one Eu^{2+} ion to another nearby Eu^{2+} ion is increased because the distance between Eu^{2+} ions is decreased. In the 4f → 5d transition of the Eu^{2+} ion in this case, the energy transfer is non radiative. This leads to decrease the energy of the excited state of Eu^{2+} ion and results in the red shift of the emission peak [38-39].

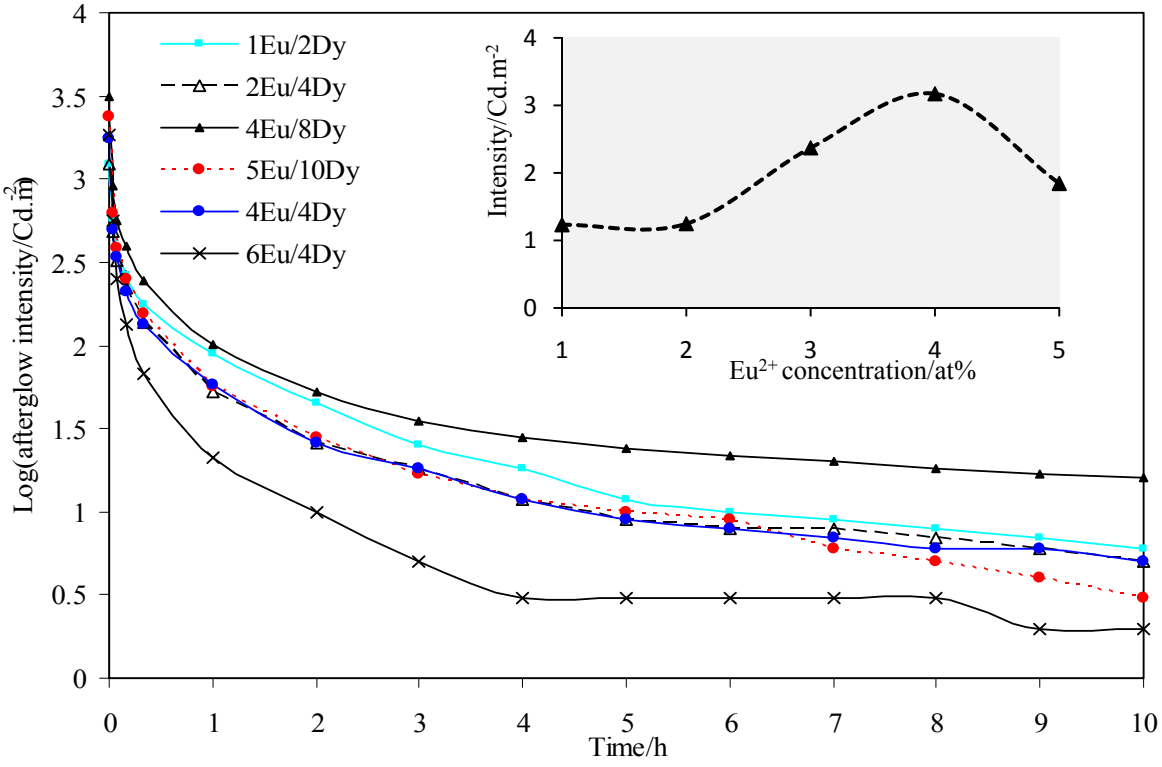

Fig. 2.13. Variation of phosphorescence intensity and afterglow decay speed of $Sr_4Al_{14}O_{25}:Eu^{2+}/Dy^{3+}$ phosphor doped with different concentrations of Eu^{2+} and Dy^{3+}. Inserted figure shows the effect of Eu^{2+} at% on the afterglow intensity.

The phosphorescence intensity and afterglow decay curves of $Sr_4Al_{14}O_{25}:Eu^{2+}/Dy^{3+}$ phosphor doped with various amount of Eu^{2+} ions are presented in Fig. 2.13. On increasing Eu^{2+} ions concentration from 0.5 at% to 4 at%, the phosphorescence intensity increased, attained maximum when the doped amount of Eu^{2+} ions was 4 at% and then on further increasing, it decreased as shown in the inset in Fig. 2.13. It is obvious that higher the concentration of emission center in the host lattice, higher is the phosphorescence intensity. However, as stated above, the critical quenching concentration of Eu^{2+} in this phosphor is 4 at%, above that concentration quenching process occurs and decrease the phosphorescence intensity [29].

The phosphorescence intensity and afterglow decay speed of the europium doped strontium aluminate phosphors can be strongly increased by co-doping with trivalent rare earth metal ions (RE^{3+}) [28]. According to Matsuzawa *et.al.* [3, 7], RE^{3+} ions ($r_{RE^{3+}}$= 87 pm to 105 pm) replace Sr^{2+} ($r_{Sr^{2+}}$= 118 pm) sites due to similar ionic radii in the $Sr_4Al_{14}O_{25}$

crystal. These RE^{3+} ions in coordination with boron forms RE^{3+}-borate complex and acts as trap centers [2, 28]. These trap centers trap the holes generated during the exposure of phosphor to excitation source. For phosphorescent phosphors to exhibit long phosphorescence at room temperature, it is crucial to have trapping level at a suitable depth in relation to the thermal release rate at the room temperature. In particular, if the depth of trapping level is too shallow in this relation, the phosphor would show fast decay speed that does not last for long time. Contrarily, if it is too deep, the phosphor no longer shows phosphorescence at room temperature. Thus, the suitable energy of activation of the hole trapped by these rare earth ions monitor the afterglow life time and the densities of these trapped holes and its release rate determine the intensity of the phosphorescence. According to Nakazawa *et.al* [24], the energy of traps (E_{trap}) observed from thermoluminescence glow peak measurements are in the order:

$$Yb^{3+} >> Sm^{3+} >> \mathbf{Dy^{3+}} > Pr^{3+} > Nd^{3+} > Er^{3+} > Ce^{3+} > Gd^{3+} > La^{3+}$$

The trap depths of Sm^{3+} and Yb^{3+} are very deep greater than 2 eV. Further, these ions can be easily reduced to divalent state under a slightly reducing synthetic condition and can fill the cation vacancy involved in the persistent luminescence process [11]. So, the phosphors doped with these ions have lowest persistency. The other rare earth ions co-doping prolonged the phosphorescence intensity according to the trap depths as observed by Nakazawa *et.al.* [24].

Further F. Clabau *et.al.* [40] reported that variation of phosphorescence intensity according to the ionization potentials (IPs) of the ions in the $SrAl_2O_4:Eu^{2+}$ phosphor. According to this model, the phosphorescence intensity and its decay time by co-doping with RE^{3+} ions results from the stabilization of the pre-existing traps. The relative extent of traps stabilization can be roughly estimated by the difference between IPs of substituting and substituted ions, the lower the IP of the co-doped ions relative to the IP of Sr^{2+} ion, the more strongly the traps attracted and larger would be the trap depth becomes [40]. This is what they have observed the phosphorescence intensity and its decay time in the $SrAl_2O_4:Eu^{2+}$ phosphor in the decreasing order $Dy^{3+} \sim Nd^{3+} > Ho^{3+} > Er^{3+} >$ undoped $> Gd^{3+} > Y^{3+}$ and the IPs of cations in the increasing order $Dy^{3+} \sim Nd^{3+} < Ho^{3+} < Er^{3+} < Sr^{2+} < Gd^{3+} < Y^{3+}$.

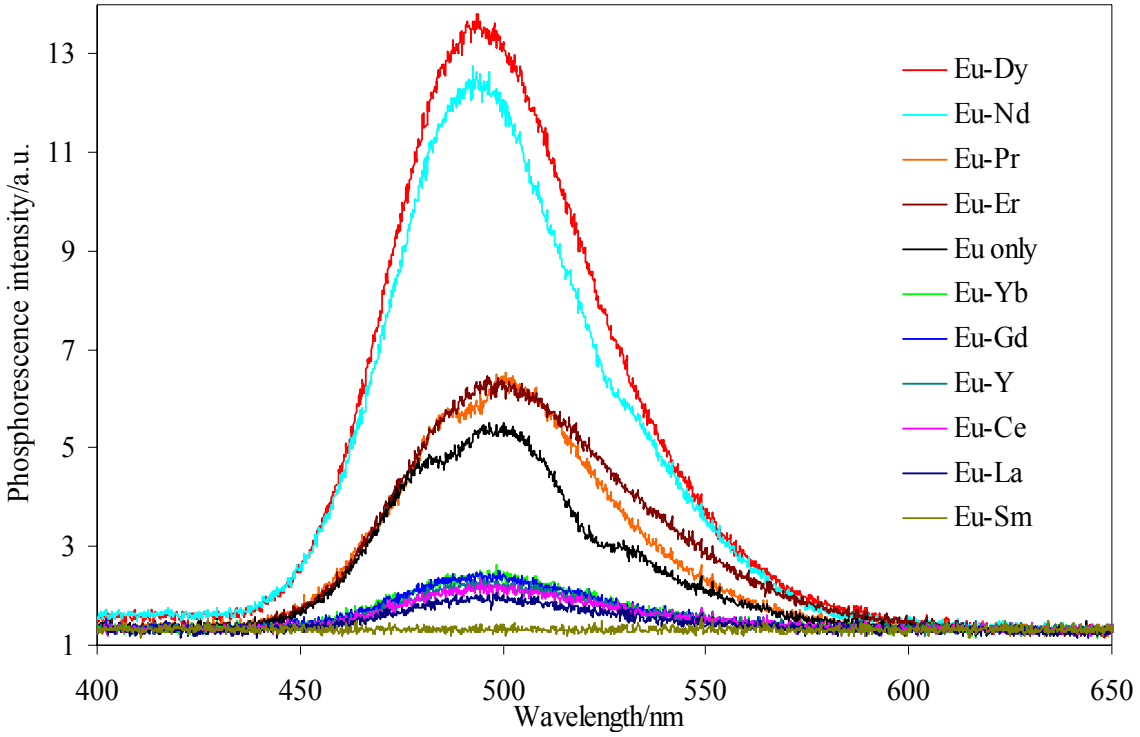

Fig. 2.14. Variation of phosphorescence intensity of $Sr_4Al_{14}O_{25}$: Eu^{2+}/RE^{3+} phosphor with some of the lanthanide additives, each additives being 8 at%.

Best on these observations, we tried to correlate the phosphorescence variation of $Sr_4Al_{14}O_{25}:Eu^{2+}$ phosphor according to the doped RE^{3+} ions. We have prepared various samples by doping 4 at% Eu^{2+} ion and 8 at% RE^{3+} ions (La^{3+}, Ce^{3+}, Pr^{3+}, Nd^{3+}, Sm^{3+}, Gd^{3+}, Dy^{3+}, Er^{3+}, Yb^{3+} and Y^{3+}) and the results are presented in Fig. 2.14. It was found that the phosphorescence intensity (recorded 10 s after the excitation source was off) varied in the following order:

$$Dy^{3+} > Nd^{3+} >> Pr^{3+} > Er^{3+} >> Gd^{3+} \sim Yb^{3+} > Ce^{3+} > La^{3+} >> Sm^{3+}$$

This trend is in accordance with the trap depths they form in the $Sr_4Al_{14}O_{25}:Eu^{2+}$ phosphors as observed by E. Nakazawa *et.al.* in the same $Sr_4Al_{14}O_{25}:Eu^{2+}$ phosphor [24].

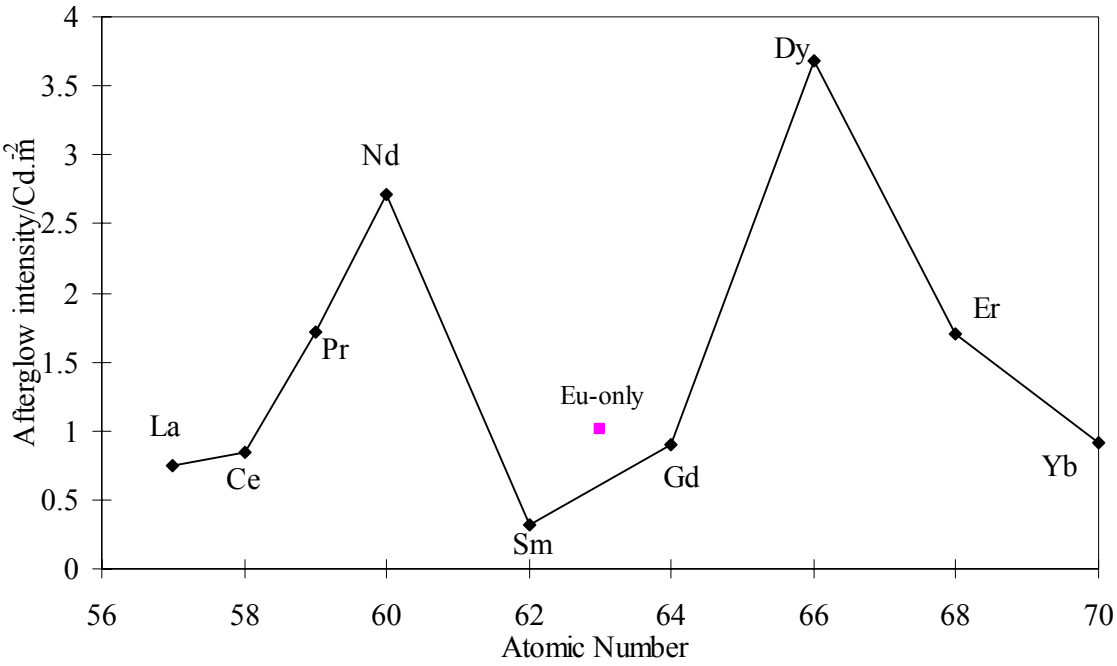

Fig. 2.15. Variation of afterglow intensity of $Sr_4Al_{14}O_{25}:Eu^{2+}$ phosphor with some of the lanthanide additives, each additives being 8 at%.

As mentioned already the phosphorescence intensity depends on the densities of traps located at suitable depths that can be released easily at room temperatures and combine with the excited Eu^{2+} ions to exhibit the phosphorescence. Thus, higher the RE^{3+} ions in the host, higher is the traps expected and higher the phosphorescence intensity. For the $Sr_4Al_{14}O_{25}:Eu^{2+}$ phosphor, Dy^{3+} was found to be suitable co-dopant due to formation of suitable trap. Thus, the detailed experiments regarding the effect of its concentration on the phosphorescence intensity and long afterglow duration was carried out. I found that as increasing Dy^{3+} ions concentration from 1 at% to 8 at%, the phosphorescence intensity increased gradually, attained maximum when it was 8 at% and then, on further increasing, it decreased as shown in inset Fig. 2.14. It can be assumed that small amount of Dy^{3+} is insufficient to form enough trap defects in the strontium aluminate matrix to capture sufficient holes. However, if the amount of doped Dy^{3+} is greater than 8 at%, the interaction between the nearby hole traps would be possible there by releasing these trapped holes easily at room temperature and fade the afterglow intensity and persistency rapidly.

Thus, in the $Sr_4Al_{14}O_{25}:Eu^{2+}$ phosphor, the optimum concentration of Eu^{2+} is 4 at% and that of Dy^{3+} is 8 at%. Under these doped concentrations the maximum phosphorescence intensity (3.17 $Cd.m^{-2}$) and longest afterglow persistent time (longer 20 h over the value of 5 $mCd.m^{-2}$) was observed.

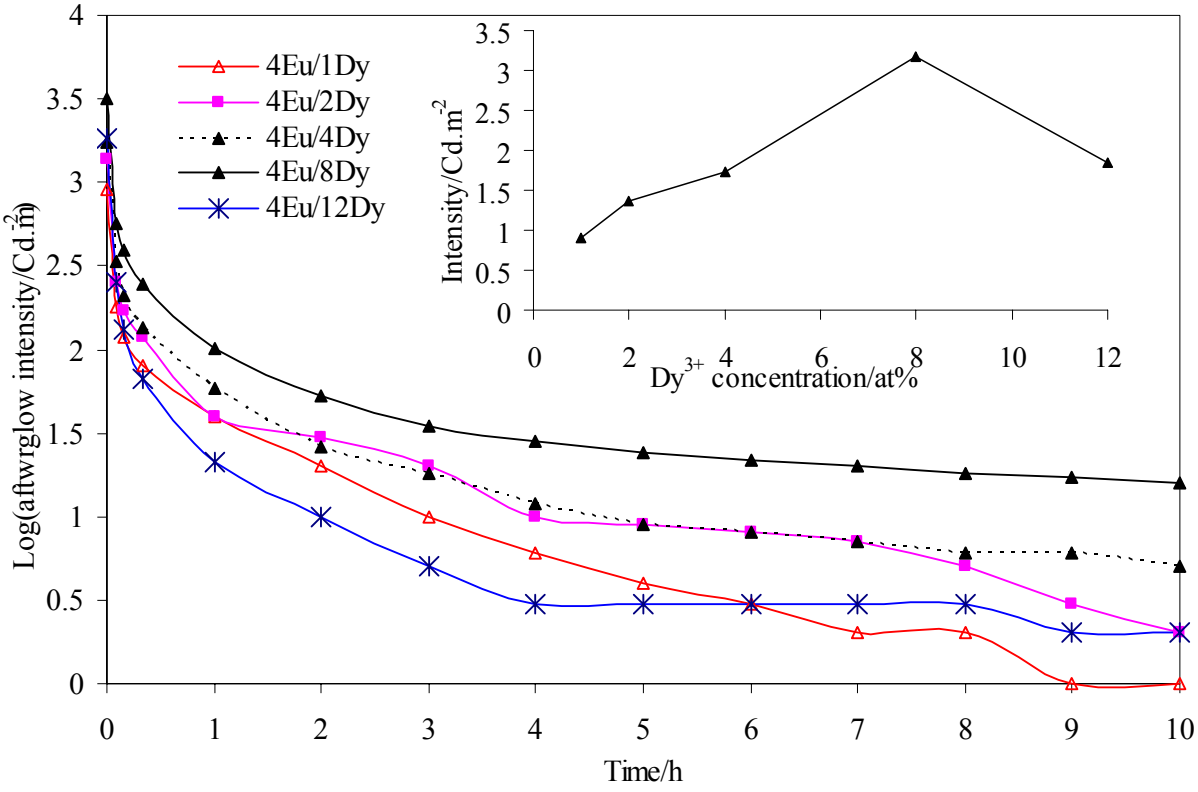

Fig. 2.16. Variation of afterglow decay speed of $Sr_4Al_{14}O_{25}:Eu^{2+}/Dy^{3+}$ phosphor according to the Dy^{3+} ions concentration. Inset figure shows the effect of Dy^{3+} concentration on the phosphorescence intensity.

Figure 2.16 shows the effect of Eu^{2+}/Dy^{3+} ratio and dysprosium concentrations on the afterglow decay speed of the $Sr_4Al_{14}O_{25}:Eu^{2+}/Dy^{3+}$ phosphor. It is clear that the afterglow decay speed is slower when the Eu^{2+}/Dy^{3+} ratio was ½, *i.e.* 4 at % Eu^{2+} and 8 at% Dy^{3+} which is in consistent with the results of A. Nag *et al.* [41]. If the Dy^{3+} concentration is small, the traps holes are negligible and it would empty in short time exhibiting shorter afterglow time. However, if the Dy^{3+} concentration is much high, it would trap much of the holes generated that lead to decrease the distance between trap holes and interaction between them would be increased. Thus, it would be possible to transfer trapped holes form

one Dy^{3+} ion to another and easily release it to the valence band. This process would also empty the trapped holes rapidly and quench the persistent phosphorescence.

2.3.4. Effect of Composition

It is well known that stoichometry of the component ions of a phosphor significantly affects the photoluminescence properties of a phosphor [17, 22, 26]. A non stoichometric composition may results either enhancement or quenching of the luminescence of the phosphor. T. Katsumata *et.al.* [22] reported that in the $SrAl_2O_4:Eu^{2+}/Dy^{3+}$ phosphor, the persistence time of phosphorescence vary dramatically with composition. Z.X. Yuan *et.al.* [17] reported that the deficit and stoichometric amount of strontium has equally strong luminescence intensity in the strontium aluminate phosphors. However, the luminescence of phosphor with excess of strontium is very weak compared to the other two. The reason has been explained on the basis of creation of some alternative relaxation paths through which the excitation energy may be lost. Also, the persistent luminescence intensity of these phosphors with strontium deficit phosphor is superior to those of others. It may be due to the formation of cation/anion vacancies that involved in the persistence luminescence.

In the present study, I have prepared five different samples of $Sr_4Al_{14}O_{25}:Eu^{2+}/Dy^{3+}$ phosphor varying Al to Sr ratio (R=Al/Sr) from 3.4 to 4.0. The sample with R value 3.5 is stoichometric, those less than 3.5 are Sr excess and greater than 3.5 are Sr deficit samples. From the Fig. 2.17, it is clear that the peak position of the phosphorescence spectra did not vary much with the composition range of R from 3.4 to 4.0. It implies that the same phase was formed irrespective of very small change in Sr to Al compositions. To confirm that the XRD patterns of these five samples with R value 3.4, 3.5, 3.6, 3.7 and 4.0 were analyzed. All these samples exhibited the same $Sr_4Al_{14}O_{25}$ phase. Further, the crystal field which affects the 5d electron state of Eu^{2+} ions that can shift the peak position of the phosphor is not expected to change much by the Al to Sr composition variation of the $Sr_4Al_{14}O_{25}:Eu^{2+}/Dy^{3+}$ phosphor due to the existence of same Eu^{2+} surrounding. However, the phosphorescence intensity was found to vary drastically with the variation of R value as shown in Fig. 2.17. The increased afterglow intensity in case of Al rich phosphor might be due to creation of large number of traps that plays important roles in the afterglow properties. Keeping the trap depth constant, the phosphorescence intensity is proportional to the

densities of the traps and its release rate [22]. In the Al excess samples the defects related to traps are expected to be higher exhibiting intense afterglow [1, 17]. Whereas in the phosphor samples with excess strontium, lack of cation vacancies may be dominantly responsible for the quenching of the persistent luminescence [17, 22].

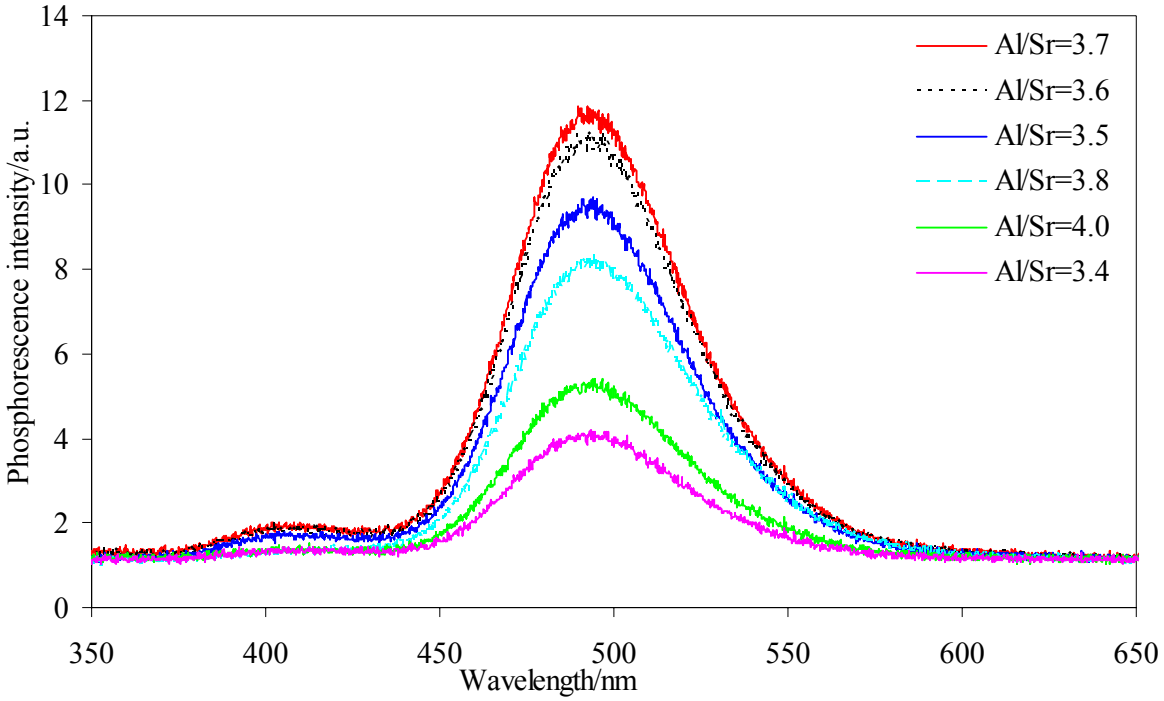

Fig. 2.17. Variation of phosphorescence intensity according to the molar ratio of aluminum to strontium (Al/Sr=R) in the starting mixture.

Figure 2.18 shows the variation of afterglow decay speed of the phosphor samples having various R values. These specimens were irradiated for 20 min by 15W xenon lamp before recording the afterglow decay curves. All these samples showed a rapid decay speed at first and subsequently long lasting phosphorescence. While increasing the concentration of Al with R value 3.4 to 4.0, the afterglow intensity and long persistent time duration of these phosphors first increased and then decreased when R value was over 3.7, *i.e.* the phosphorescence intensity and afterglow duration was higher for Al rich phosphors than that of Sr rich and stoichometric phosphors.

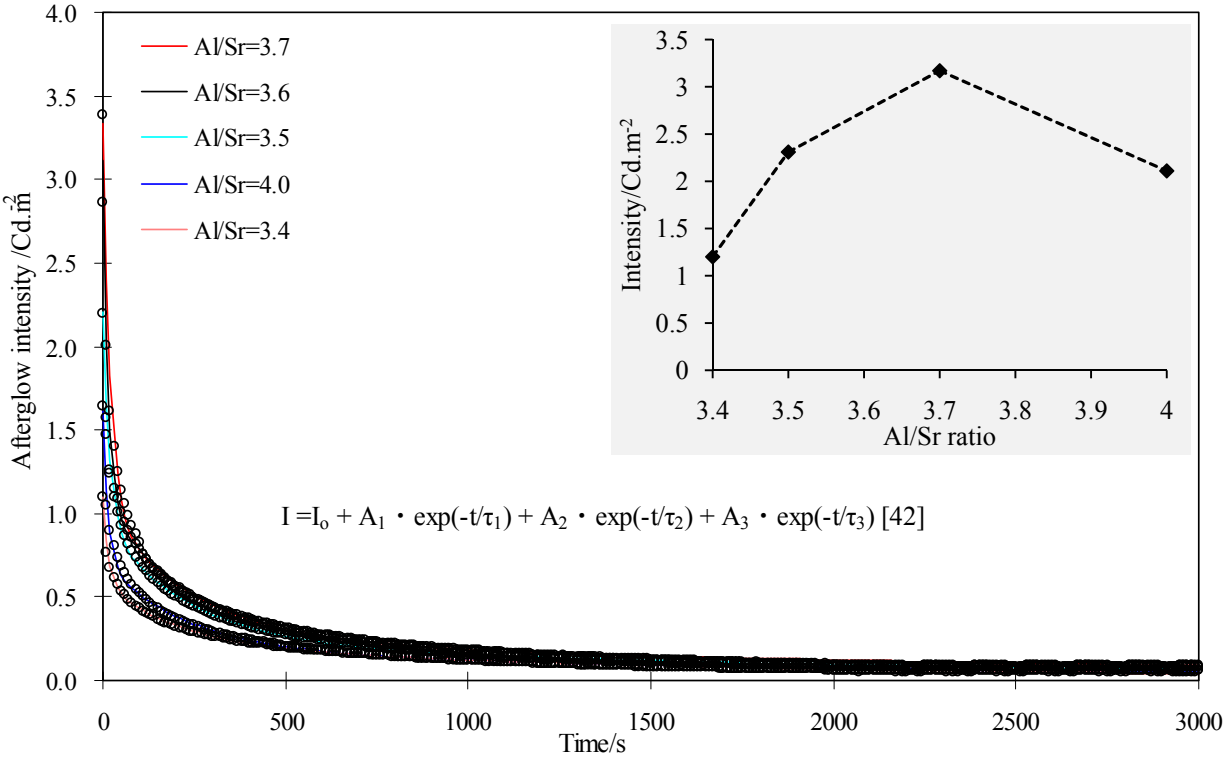

Fig. 2.18. Variation of afterglow decay speed of $Sr_4Al_{14}O_{25}:Eu^{2+}/Dy^{3+}$ phosphor with the stoichometry of the starting materials (dots and solid lines are observed and fitted curves, respectively). Inset figure shows the effect of Al/Sr ratio on the afterglow intensity.

The afterglow decay behavior of these phosphor samples can be analyzed by curve fitting method using the following multiple exponential equations [42]:

$$I = I_o + A_1 \exp(t/\tau_1) + A_2 \exp(t/\tau_2) + A_3 \exp(t/\tau_3) \qquad 2.8$$

Where, I represents the phosphorescence intensity, A_1, A_2, A_3 are constants, t is time and τ_1, τ_2, τ_3 are the exponential components, respectively. Using the fitting functions, these parameters τ_1, τ_2 and τ_3 can be calculated and the results are shown in Table 2.2. From the fitting curves results, the decay times τ_1, τ_2 and τ_3 for the phosphor with R= 3.4 is the shortest. With the increase of R value from 3.4 to 3.7, the decay time of the phosphor also increased. However, when R value continues to increase over 3.7, the value of decay time became smaller. It has been normalized that the life time τ of trapped charge carrier is inversely proportional to the trapping probability, and depends exponentially on the ratio of trap depth to the thermal energy, $^{E_T}/_{K_BT}$. Consequently, the life time τ, and thus the

luminescence is longer when the detrapping requires a higher energy [1, 17, 22, 33]. In simple words, higher the value of τ, the deeper was the trap depth becomes and hence the longer the persistent afterglow time duration of the phosphors.

Table 2.2, Decay parameters calculated from decay curve fitting method for $Sr_4Al_{14}O_{25}:Eu^{2+}/Dy^{3+}$ phosphor with different composition of strontium and aluminium (Al/Sr=R) in the starting mixture.

Composition (R = Al/Sr)	Decay parameters A and τ (s)					
	A_1	τ_1	A_2	τ_2	A_3	τ_3
3.4	0.51	15.0	0.38	207.0	0.200	1850
3.5	1.28	19.0	0.71	241.1	0.215	2350
3.6	2.05	19.3	0.79	243.7	0.225	2550
3.7	2.3	20.1	0.80	249.0	0.235	3051
4.0	0.9	14.1	0.53	223.0	0.180	2300

2.3.5. Effect of Charge compensators

Co-doping rare metal ion (*e.g.* Dy^{3+}) into the strontium aluminate phosphor by substituting Sr^{2+} sites generates lattice defects associated with the interstitial oxygen [26, 33, 43]. These defects are known to be phosphorescence killers [44]. Co-doping various charge compensating ions like Li^+, Na^+, Ag^+, Mg^{2+}, Ca^{2+} *etc.* replaces part of Sr^{2+} or Al^{3+} by eliminating these oxygen related defects and improves the brightness of these $SrAl_2O_4:Eu^{2+}/Dy^{3+}$ phosphors [44]. Further, ionic radii of charge compensator ions were found to monitor the emission intensity of the phosphor. For example, co-doping the $SrAl_2O_4:Eu^{2+}/Dy^{3+}$ phosphor with Li^+ (92 pm), Na^+ (118 pm), and K^+ (138 pm) ions, the possibility of entering and charge balancing capacity of Li^+ will be higher due to smaller ionic radii of it compared to Sr^{2+} (118 pm) and subsequently increase the brightness of the phosphor [45].

Thus, in this research I have investigated the luminescence of $Sr_4Al_{14}O_{25}:Eu^{2+}/Dy^{3+}$ phosphor by substituting either strontium or aluminum by various ions like monovalent (Li^+, Na^+, Ag^+), divalent (Mg^{2+}, Ca^{2+}, Ba^{2+}), trivalent (B^{3+}), tetravalent (Si^{4+}), hexavalent (W^{6+})

etc. Except B^{3+}, most of the substituting ions have ionic radii comparable to Sr^{2+} ion and they are expected to occupy the Sr^{2+} sites in the $Sr_4Al_{14}O_{25}$ host lattice. In case of divalent ions, they occupy strontium sites without charge imbalance due to isovalency. However, other ions substitution creates charge related defects that might be helpful to compensate the defects that already exist during the rare metal ions doping and may improve or deteriorate the phosphorescence intensity.

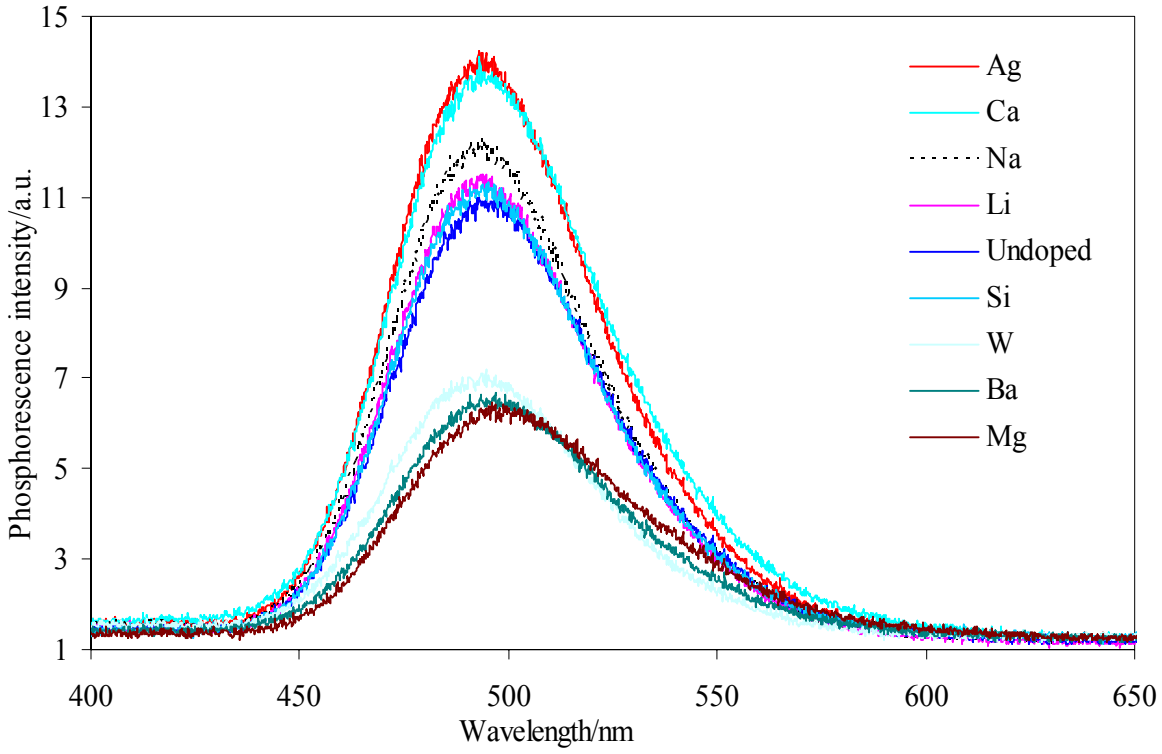

Fig. 2.19. Variation of phosphorescence intensity of $Sr_4Al_{14}O_{25}:Eu^{2+}/Dy^{3+}$phosphor with some of the charge compensating ions, each additives being 4 at%.

Figure 2.19 shows the variation of phosphorescence intensity by co-doping with various charge compensating ions in the $Sr_4Al_{14}O_{25}:Eu^{2+}/Dy^{3+}$ phosphor. It is found that Li^+, Na^+, Ca^{2+} and Ag^+ ions co-doping enhanced the afterglow intensity in the increasing order. The optimum concentrations of monovalent (Ag^+) and divalent (Ca^{2+}) ions were found to be 3 mol% and 10 mol%, respectively, for the $Sr_4Al_{14}O_{25}:Eu^{2+}/Dy^{3+}$ phosphor to yield highest afterglow emission. Variation of phosphorescence intensity with Ag^+ ions concentration in $Sr_4Al_{14}O_{25}:Eu^{2+}/Dy^{3+}$ phosphor samples were shown in Fig. 2.20. It is clear that Ag^+ ions addition gradually increased the phosphorescence intensity. Interestingly, 3 mol% Ag^+ doped

$Sr_4Al_{14}O_{25}:Eu^{2+}/Dy^{3+}$ phosphor sample exhibited almost 1.5 times increased phosphorescence intensity. However, beyond 3 at% Ag^+ addition, the phosphorescence intensity decreased that might be due to concentration quenching process. No significant increase was observed co-doping with Li^+ and Na^+ ions. However, Si^{4+}, W^{6+}, Ba^{2+} and Mg^{2+} co-doping decreased the afterglow intensity of this phosphor in the increasing order. The reason for the enhancement of the afterglow intensity by doping with suitable charge compensating ions in optimum concentration is believed to be due to removal of the defects sites originated in the Sr^{2+} sites during the doping of RE^{3+} ions. Further, it is reported that suitable charge compensating ions increase the solubility of Eu^{2+} and Dy^{3+} ions in the host lattice and leads to increase the emission intensity [46].

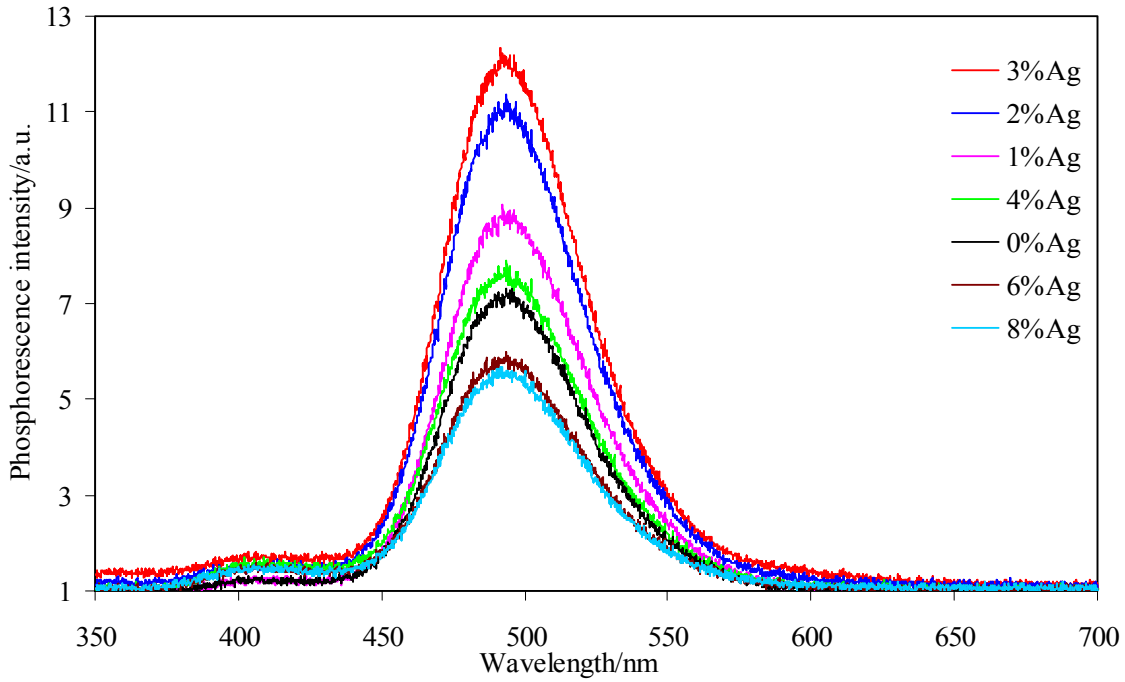

Fig. 2.20. Variation of phosphorescence intensity of $Sr_4Al_{14}O_{25}:Eu^{2+}/Dy^{3+}$/x at% Ag^+ phosphor with Ag^+ ions concentration.

2.3.6. Effect of substitution with Ca^{2+} or Ba^{2+} ions

It is agreed that the luminescence of Eu^{2+} ion in the strontium aluminate phosphor is due to the transition between the ground state and the excited state configuration of the Eu^{2+} ions. Even though, the 4f electrons are inert to environment of crystal field, the 5d electrons can be easily split by the crystal field. Thus the peak position of emission spectra strongly

depends on the Eu^{2+} surrounding. Consequently, the Eu^{2+} ion can emit visible light of various colors under different crystal fields [47]. Host lattices with a high degree of covalency and/or large crystal field splitting at the site in which Eu^{2+} substitute can lead to efficient visible emission by absorbing light in the near UV to visible range of the electromagnetic spectrum. For example Eu^{2+} ion emits blue in $CaAl_2O_4:Eu^{2+}/Nd^{3+}$ phosphor [18], blue-green in $Sr_4Al_{14}O_{25}:Eu^{2+}/Dy^{3+}$ phosphor [2] and green in $SrAl_2O_4:Eu^{2+}/Dy^{3+}$ phosphor [7].

Thus, substitution of Sr^{2+} ions in $Sr_4Al_{14}O_{25}:Eu^{2+}/Dy^{3+}$ phosphor by similar cations with smaller or bigger ionic radius is expected to change the crystal field around the Eu^{2+} ions and hence the optical properties. Replacement of part of Sr^{2+} ion with Ca^{2+} (smaller) or Ba^{2+} (bigger) is expected to shift the Eu^{2+} emission band in the $Sr_4Al_{14}O_{25}:Eu^{2+}/Dy^{3+}$ phosphor because of the 5d electron crystal field changes that gives rise to shift in the emission peak position. In particular, the simultaneous presence of two different cations (Ca^{2+} and Sr^{2+} or Sr^{2+} and Ba^{2+}) in a single crystal lattice enable and hence can control a gradual change of crystal field and covalence regime of the Eu^{2+} ion in the host crystal. This leads to gradual shift in the emission peak positions. C. Lui and J.L. Pascal *et.al.* [47, 48] have studied the influence of partial replacement of Sr^{2+} ions by other alkaline earth ions (*e.g.* Ca^{2+} or Ba^{2+}) in $SrAl_2O_4:Eu^{2+}$ phosphor. They found the substantial change in emission wavelength of Eu^{2+} ions in the phosphor. Therefore, I aim to investigate the change in crystal field structures of $Sr_4Al_{14}O_{25}:Eu^{2+}/Dy^{3+}$ phosphor by partial or complete substitution of Sr^{2+} by Ca^{2+} or Ba^{2+} ions and its influence on the photoluminescence emission and afterglow properties.

The phase purity and end compositions of $Sr_4Al_{14}O_{25}:Eu^{2+}/Dy^{3+}$, $CaAl_4O_7$ or $CaAl_2O_4:Eu^{2+}/Dy^3$ and $BaAl_4O_7$ or $BaAl_2O_4:Eu^{2+}/Dy^{3+}$ phosphors were analyzed by X-ray powder diffraction analysis. Figure 2.21 and 2.26 show the XRD patterns of $Sr_{4-y}Ca_yAl_{14}O_{25}:Eu^{2+}/Dy^{3+}$ and $Sr_{4-z}Ba_zAl_{14}O_{25}:Eu^{2+}/Dy^{3+}$ (y = z = 0, 0.2, 0.4, 0.6, 0.8, 2.0, 3.2 and 4.0) phosphor samples, respectively. The Eu^{2+} and Dy^{3+} concentrations were optimized independently [in chapter 2.3.3], and kept at 4 at% and 8 at%, respectively, in the present study. The XRD patterns were compared with JCPDS standard values of the possible phases and marked with different symbols. For the $Sr_4Al_{14}O_{25}$, $CaAl_4O_7$ and $BaAl_4O_7$

compositions, precise structure analyses have been already published [40, 49-50]. The diffraction peaks in Fig. 2.21 (a) can be indexed to the orthorhombic phase structure of $Sr_4Al_{14}O_{25}$ (JCPDS card no. 52-1876), and no peaks of other phases were detected. With the increase of Ca content to y = 0.2 ($Sr_{3.8}Ca_{0.2}Al_{14}O_{25}$), 0.4 ($Sr_{3.6}Ca_{0.4}Al_{14}O_{25}$) and 0.6 ($Sr_{3.4}Ca_{0.6}Al_{14}O_{25}$), the same $Sr_4Al_{14}O_{25}$ phase was observed. It suggests that no new phase was formed. However, with increase of Ca content to y = 0.8 ($Sr_{3.2}Ca_{0.8}Al_{14}O_{25}$) and 2.0 ($Sr_2Ca_2Al_{14}O_{25}$), a new phase ($CaAl_4O_7$) was appeared as shown in Fig 2.21(f, g) along with the major phase $Sr_4Al_{14}O_{25}$. However, if the calcium content was increased to y = 3.2 ($Sr_{0.8}Ca_{3.2}Al_{14}O_{25}$) and 1.0 ($Sr_0Ca_4Al_{14}O_{25}$), the $Sr_4Al_{14}O_{25}$ phase was completely vanished and $CaAl_4O_7$ phase was observed as major phase ($CaAl_2O_4$ phase appeared as minor phase) as shown in Fig 2.21 (h and i). From the foregoing XRD analysis, it is concluded that the single phase region in $Sr_{4-y}Ca_yAl_{14}O_{25}$ was in between y = 0 to y = 0.6 (X_{Ca} = 0.00 to 0.15). In other words, $Sr_4Al_{14}O_{25}$ phase remains a single phase in the $Sr_4Ca_0Al_{14}O_{25}$, $Sr_{3.8}Ca_{0.2}Al_{14}O_{25}$, $Sr_{3.6}Ca_{0.4}Al_{14}O_{25}$ and $Sr_{3.4}Ca_{0.6}Al_{14}O_{25}$ compositions while only calcium aluminate phases in $Sr_{0.8}Ca_{3.2}Al_{14}O_{25}$ and $Sr_0Ca_4Al_{14}O_{25}$ compositions. This indicates that solid solution of calcium was formed in strontium aluminate system up to 0.15 mol fraction of calcium and solid solution of strontium was formed in calcium aluminate system only up to 0.05 mole fraction of strontium, i.e. solid solubility of calcium is higher in strontium aluminate system than the solid solubility of strontium in calcium aluminate system. This might be due to size effect. Smaller the size of substituting cations easier is the substitution and higher would be the solid solubility.

The interesting phenomenon is that the major diffraction peaks, *e.g.* (801) of $Sr_4Al_{14}O_{25}$ phase shifted towards the higher diffraction angles with the increase of Ca mole fraction. The results were shown in Table 2.1. The 2θ values of the diffraction peak (801) shifted from 34.3^o to 34.4^o when the mole fraction of Ca increased from 0.0 ($Sr_4Ca_0Al_{14}O_{25}$) to 0.2 ($Sr_{3.2}Ca_{0.8}Al_{14}O_{25}$). The value of d (801) has been calculated by Bragg equation, $2d \sin\theta = \lambda$ (λ=0.15418 nm). In Fig. 2.22, the value of the d (801) is plotted against mole fraction of Ca for $Sr_{4-y}Ca_yAl_{14}O_{25}:Eu^{2+}/Dy^{3+}$ phosphor samples. The shift of the diffraction peaks to larger angles is consistent with a contraction of $Sr_4Al_{14}O_{25}$ crystal lattice parameters, which is ascribed to the substitution of much bigger Sr^{2+} ions (118 pm) by smaller Ca^{2+} ions (104 pm).

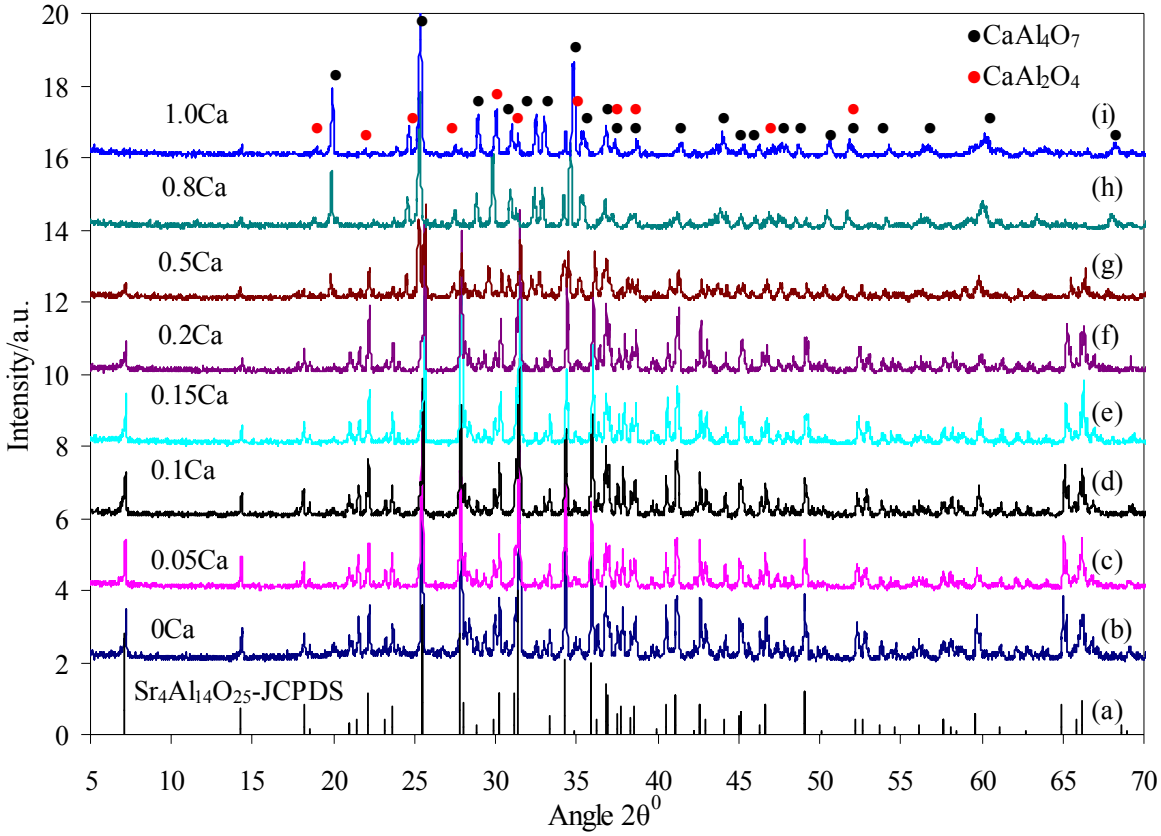

Fig. 2.21. XRD patterns of various mole fraction of calcium substituted $Sr_{4-y}Ca_yAl_{14}O_{25}:Eu^{2+}/Dy^{3+}$ phosphors ($0<y\leq4$).

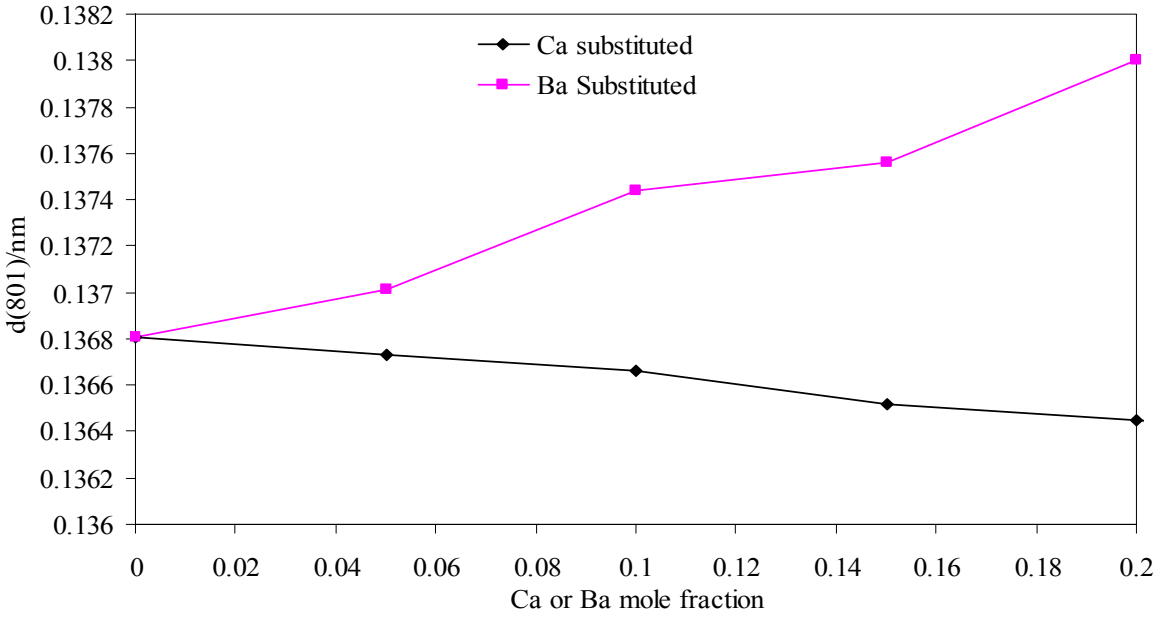

Fig. 2.22. Variation of value of d against mole fractions of Ca and Ba in the $Sr_{4-y}Ca_yAl_{14}O_{25}:Eu^{2+}/Dy^{3+}$ and $Sr_{4-z}Ba_zAl_{14}O_{25}$: Eu^{2+}/Dy^{3+} phosphor samples.

A similar study was carried out by substituting strontium by barium. The mole fraction of barium ($X_{Ba} = {}^{Ba}/_{Ba+Sr}$) was varied from 0.0 to 1.0. In the lower concentration of barium substitution (X_{Ba} = 0.05 to 0.2), $SrAl_2O_4$ and $BaAl_2O_4$ phases were observed in addition to $Sr_4Al_{14}O_{25}$ major phase (Fig. 2.23). For the X_{Ba} = 0.5 and higher barium mole fractions, instead of $Sr_4Al_{14}O_{25}$ phase, only $SrAl_2O_4$, $BaAl_2O_4$ and $BaAl_4O_7$ phases were observed. It is clear that on increasing barium content, strontium aluminates phase decreased and $BaAl_4O_7$ phase increased gradually. As in calcium substitution, substitution of strontium by barium decreased the diffraction angle (*e.g.* in the 801 plane) to lower value as shown in Fig. 2.22. The shift of the diffraction peaks to smaller angles is consistent with the expansion of $Sr_4Al_{14}O_{25}$ crystal lattice parameters that is due to the substitution of smaller Sr^{2+} site (118 pm) by much bigger Ba^{2+} sites (134 pm) in the lattice.

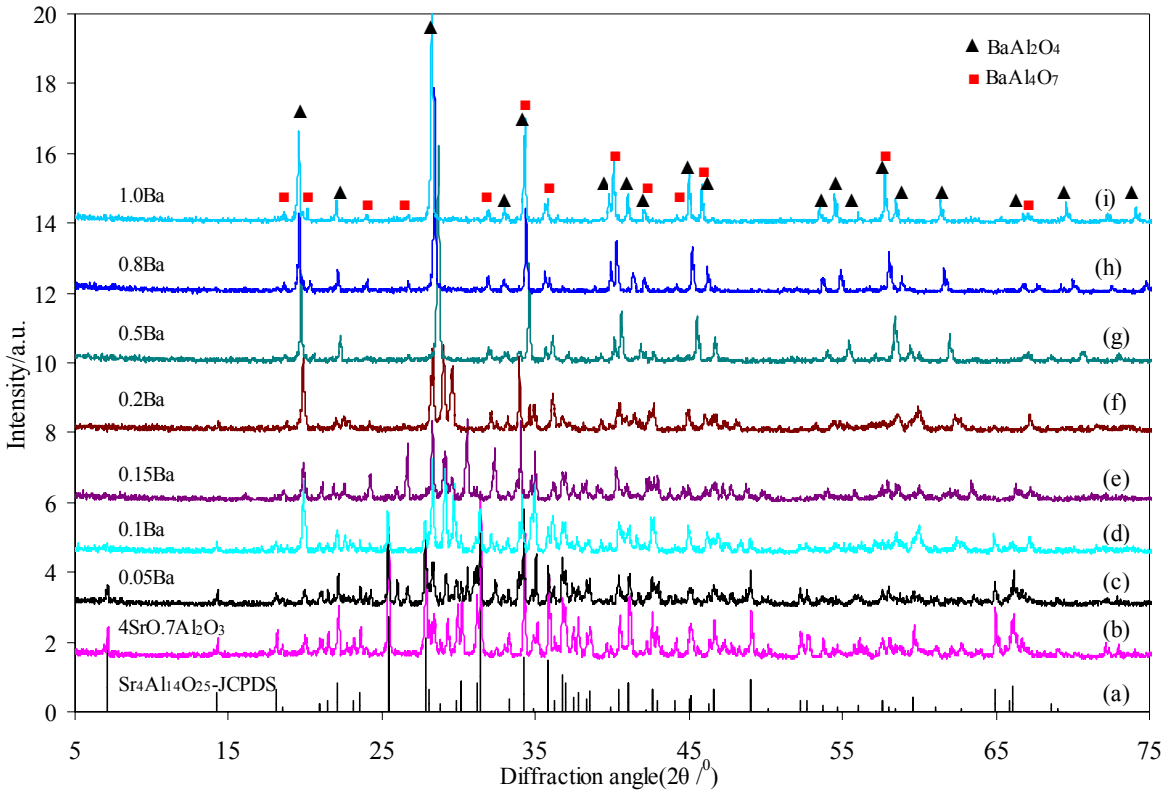

Fig 2.23 XRD patterns of various mole fraction of Ba substituted $Sr_{4-z}Ba_zAl_{14}O_{25}:Eu^{2+}/Dy^{3+}$ phosphor ($0<z\leq4$).

To understand the partial replacement of Sr^{2+} ions by the other alkaline earth ions (Ca^{2+} and Ba^{2+}), it is good to compare the luminescence spectra of Eu^{2+} ions in the pure host lattices for all these three alkaline ion *i.e.* $4SrO.7Al_2O_3$, $4CaO.7Al_2O_3$ and $4BaO.7Al_2O_3$. Figure 2.24 shows the absorption and emission spectra of these three extreme compositions *i.e.* $4CaO.7Al_2O_3$ ($CaAl_4O_7$), $4SrO.7Al_2O_3$ ($Sr_4Al_{14}O_{25}$) and $4BaO.7Al_2O_3$ ($BaAl_4O_7$ and $BaAl_2O_4$), each doped with 4 at% Eu^{2+} and 8 at % Dy^{3+} (measured at room temperature). The emission maxima are at 445 nm, 497 nm and 505 nm for Ca, Sr and Ba compounds, respectively. The onset of the $4f^65d^1$ band in the emission spectra shift from higher energy to lower energy band on going from Ca to Sr to Ba and the band shift is wider on going from Sr to Ca than from Sr to Ba. The shift to higher energy of the $4f^65d^1$ emission from Ba to Sr to Ca is due to two effects. First, the crystal field splitting of the d-manifold is smaller in the larger cation sites ($BaAl_2O_4$ or $BaAl_4O_7$). As a result the position of the lowest 5d level shifts to the higher energy site from Ca^{2+} to Sr^{2+} to Ba^{2+} host lattices. A second origin for the wider shift of the emission to higher energy from Ba to Sr to Ca is the strokes shift. The strokes shift is the largest for the Eu^{2+} emission in the Ca compound and smallest in the Ba compound. There is increasing evident that the equilibrium distance in the f to d excited states of the rare earth ions can be smaller than for the ground states [47]. Calculations and experimental results for Eu^{2+} and Ce^{3+} showed the bonding in $4f^65d^1$ excited state is stronger than in ground state. As a result, the change in equilibrium distance in the $4f^65d^1$ excited state results in largest relaxation and shift of the parabolas in the configuration coordinate diagram. On the other hand, when Eu^{2+} replaces larger cation (Ba^{2+}), reduction of the distance between Eu^{2+} and the coordinating anions will be unfavorable, since the site is already large for Eu^{2+} ($Eu^{2+}<Sr^{2+}<<Ba^{2+}$). The small relaxation will result in a small shift in the configuration coordinate parabola. This is reflected in the emission spectra by small stroke shift and narrow band width.

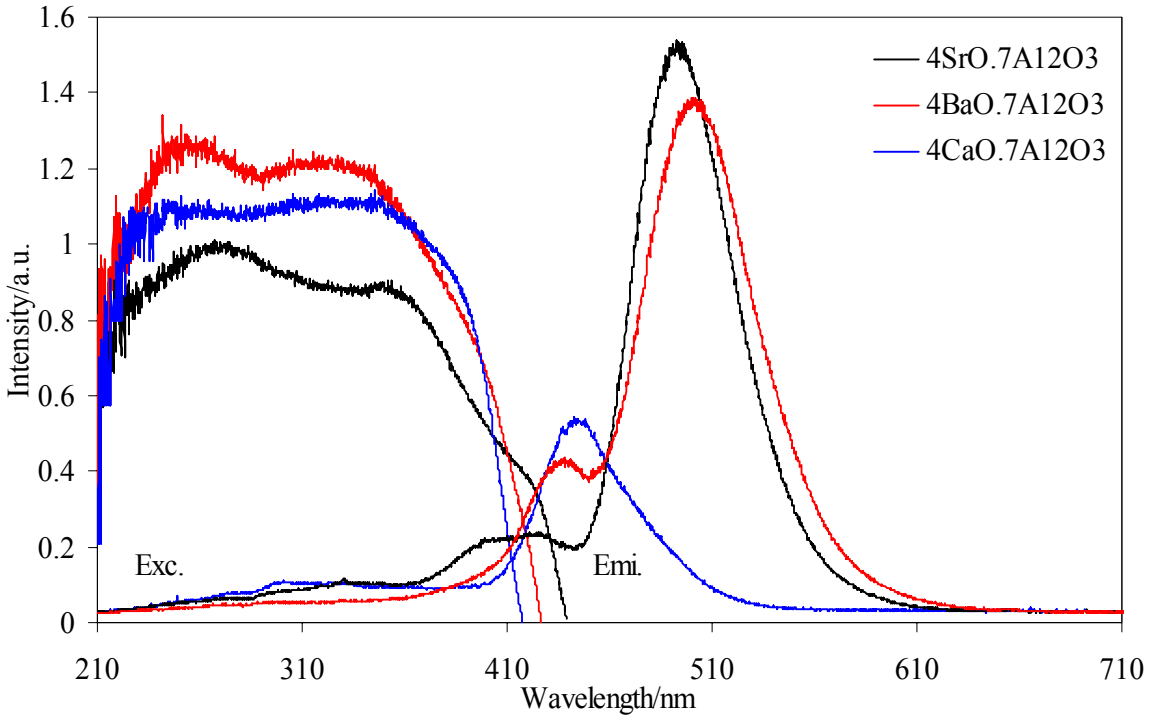

Fig. 2.24. Absorption and fluorescence spectra of three extreme compositions of Ca, Sr and Ba, *viz*. $4CaO.7Al_2O_3$, $4SrO.7\ Al_2O_3$ and $4BaO.7Al_2O_3$ phosphors doped with 4 at% Eu^{2+} and 8 at% Dy^{3+}.

The emission spectra of the $Sr_{4-y}Ca_yAl_4O_{25}:Eu^{2+}/Dy^{3+}$ ($0<y\leq4$) phosphor samples doped with 4 at% Eu^{2+} and 8 at% Dy^{3+} are shown in Fig. 2.25. As seen in the spectra, the peak wavelength of the fluorescence spectra varies with the change of calcium concentrations. Only one emission band was observed from the emission spectra of $Sr_{4-y}Ca_yAl_4O_{25}:Eu^{2+}/Dy^{3+}$ phosphor when y ranges from 0 to 0.8 (up to 0.2 mole fraction). However, the emission maxima gradually shift to higher energy site (blue shift) on increasing Ca concentration from 0 to 0.8. As seen from the XRD profile, no other new phases were observed till that concentration. It suggests that the substitution of Sr^{2+} ions by smaller Ca^{2+} ions in the $Sr_4Al_{14}O_{25}$ lattice increases the covalency of Eu-O bond. This led to decrease in the energy splitting between the 5d levels of Eu^{2+} ions. Thus, the lowest 5d energy state would be at higher energy level and led to emission in higher energy side of the spectrum *i.e.* the blue shift in the emission was observed [15]. As the Ca concentration was increased to 2.0, there appeared two emission maxima, one nearly at 490 nm and the other at 438 nm. As seen in XRD profiles (Fig. 1.21), two phases $Sr_4Al_{14}O_{25}$ and $CaAl_4O_7$ were

appeared at that composition *i.e.* the solid solubility Sr and Ca components exceeded the limit and two separate phases were appeared. It is reported that $CaAl_4O_7$ emits at 440 nm [49]. Thus the peaks at 440 and 590 nm were due to emission of Eu^{2+} ions in the $CaAl_4O_7$ and $Sr_4Al_{14}O_{25}$ host, respectively. However, as the concentration of Ca was increased to 3.2, there appeared $CaAl_4O_7$ phase as a major phase with $CaAl_2O_4$ as a minor phase as seen in XRD profiles. At this concentration the solid solution of Sr in calcium aluminate compound was formed and the Eu^{2+} emission was observed only in $CaAl_4O_7$ host. As explained above, substitution of small Ca^{2+} ions in $CaAl_4O_7$ host by larger Sr^{2+} ions, the covalency of Eu-O bond decreases [51]. This lead to increase the difference between 5d levels of Eu^{2+} electrons and causes small red shift in the emission maxima from 440 nm to 443 nm when the concentration of Sr was changed from 0.0 to 0.2 in the $CaAl_4O_7$ mixture.

Table 2.3 Summary of Ca substitution effects on the phase changes, lattice parameters, and photoluminescence emission and afterglow properties of $Sr_{4-y}Ca_yAl_{14}O_{25}:Eu^{2+}/Dy^{3+}$ phosphor ($0<y\leq4$) (Fluor.max. = Fluorescence maxima and Phos.max. = phosphorescence maxima).

Samples	Ca=0 (X_{Ca}=0)	Ca=0.2 (X_{Ca} =0.05)	Ca=0.4 (X_{Ca} =0.1)	Ca=0.6 (X_{Ca} =0.15)	Ca=0.8 (X_{Ca} =0.2)	Ca=2.0 (X_{Ca} =0.5)	Ca=3.2 (X_{Ca} =0.8)	Ca=1.0 (X_{Ca}=1.0)
Phases	$Sr_4Al_{14}O_{25}$	$Sr_4Al_{14}O_{25}$	$Sr_4Al_{14}O_{25}$	$Sr_4Al_{14}O_{25}$	$Sr_4Al_{14}O_{25}$	$CaAl_4O_7$ $Sr_4Al_{14}O_{25}$	$CaAl_4O_7$	$CaAl_4O_7$
2θ value D(220)	34.3 0.13681	34.32 0.13673	34.34 0.13667	34.38 0.13651	34.4 0.13643	34.52 0.13603	34.62 0.135698	34.82 0.13501
Fluor.max.	502	498.5	497	498	497	492, 438.5	440	442
Phos.max.	498.17	497.97	497.5	497.17	497	495.5	442,545	442
CIE (XY-value)	X=0.2022 Y=0.4381	X=0.1901 Y=0.4183	X=0.1850 Y=0.4028	X=0.1754 Y=0.3679	X=0.1667 Y=0.3562	X=0.1995 Y=0.2832	X=0.1595 Y=0.2217	X=0.148 Y=0.167

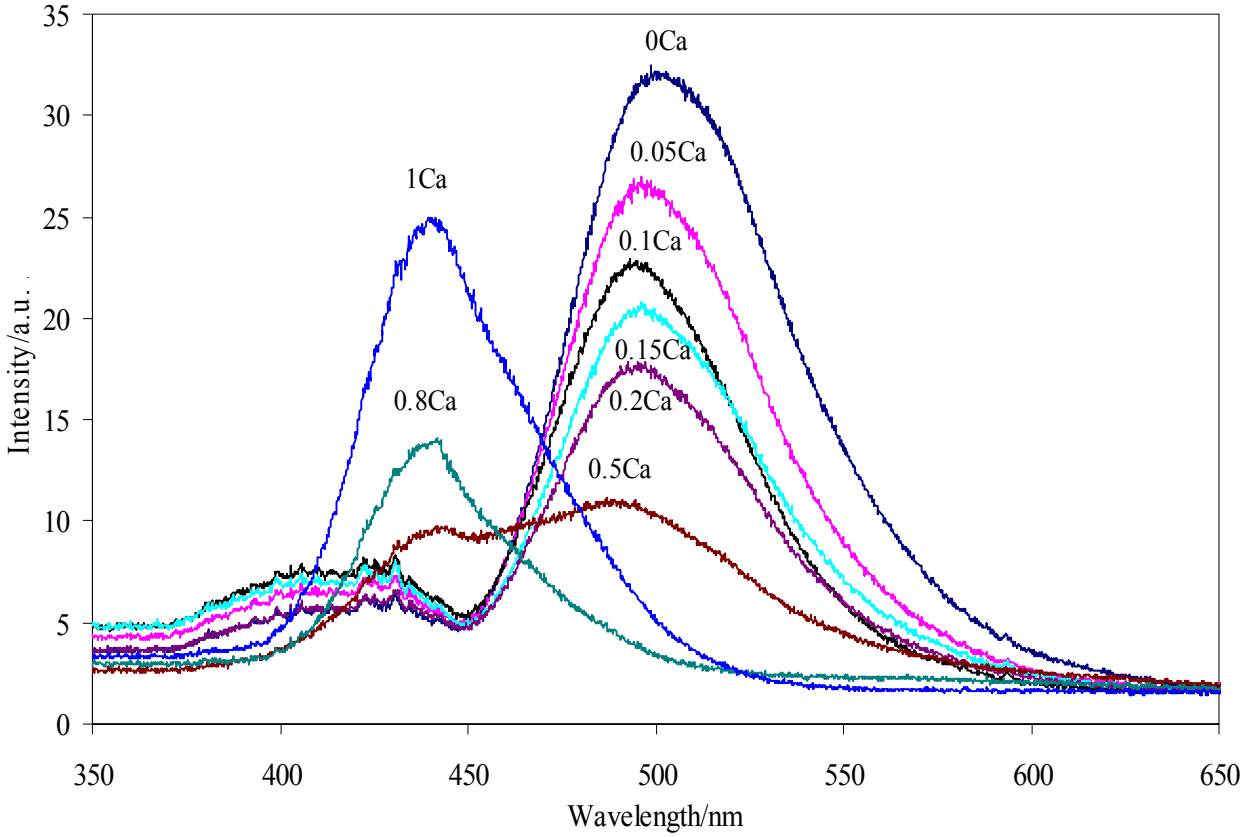

Fig. 2.25. Fluorescence spectra of $Sr_{4-y}Ca_yAl_{14}O_{25}:Eu^{2+}/Dy^{3+}$ phosphor substituted with various mole fractions of Ca ($0<y\leq4$).

Figure 2.26 shows the XYZ color coordinate diagram of $Sr_{4-y}Ca_yAl_{14}O_{25}:Eu^{2+}/Dy^{3+}$ phosphors substituted with different concentrations of calcium. By substituting small amount of Sr by Ca up to 0.2 mole fraction, there was gradual shift in the color co-ordinate values of the phosphor samples. However, there was abrupt change in the emission color of the phosphor on increasing Ca mole fraction from 0.2 to 0.5. This is due to appearance of a new phase ($CaAl_4O_7$). Further, it is found that on going from strontium aluminate compounds to calcium aluminate compounds, a bluish white color was observed when 0.7 to 0.8 mole fraction of Sr was substituted. Thus the emission color and the color and the color rendering index of the phosphor can be controlled by the control of host lattices.

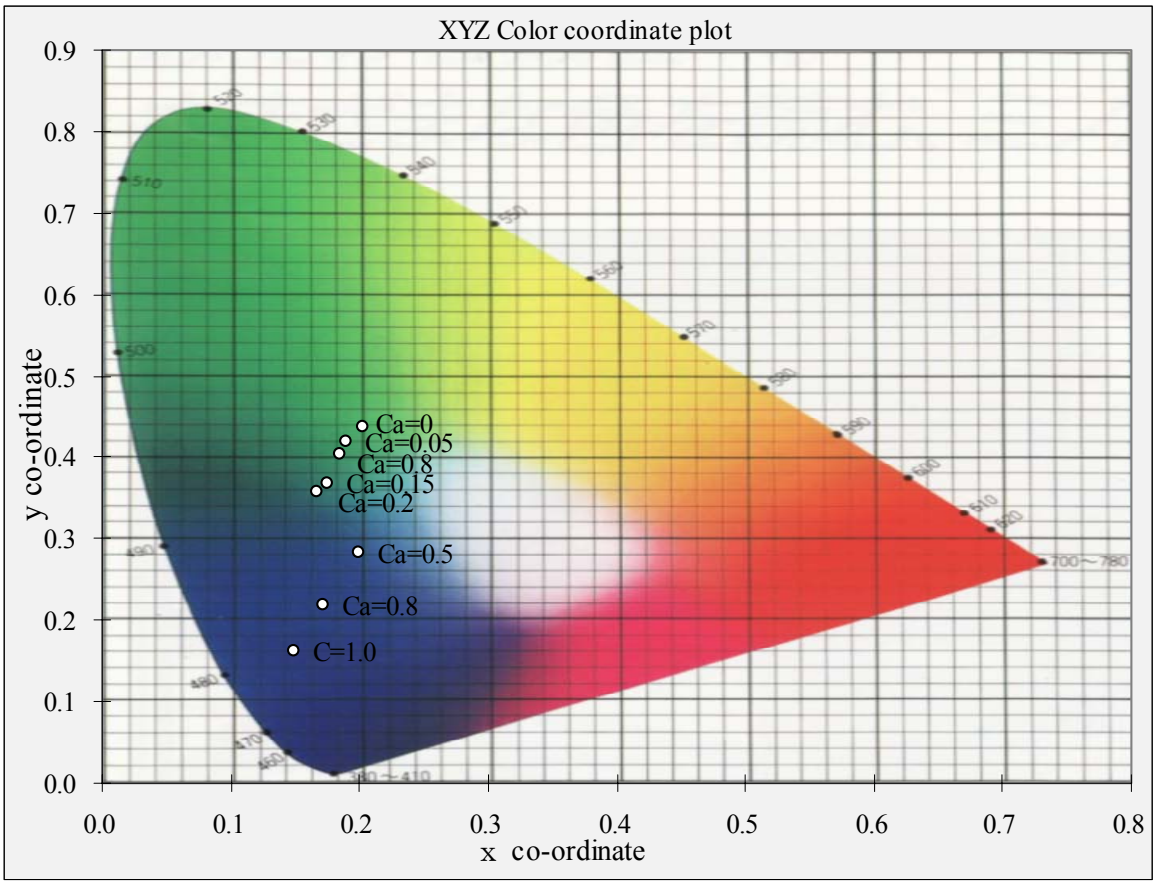

Fig. 2.26. XYZ color coordinates of various mole fraction of calcium substituted $Sr_{4-y}Ca_yAl_{14}O_{25}:Eu^{2+}/Dy^{3+}$ phosphors ($0<y\leq4$).

The digital images of $Sr_{4-y}Ca_yAl_{14}O_{25}:Eu^{2+}/Dy^{3+}$ phosphors substituted by various mole fractions of calcium are shown in Fig. 2.27 where Fig. (a) were images taken in presence of black light *i.e.* the fluorescence color whereas Fig. (b) were images taken in absence of black light (exposed to black light for 10 minutes before capturing the images) *i.e.* phosphorescence color. It is clearly seen that $Sr_4Al_{14}O_{25}:Eu^{2+}/Dy^{3+}$ phosphors exhibited blue-green emission while that of $CaAl_4O_7:Eu^{2+}/Dy^{3+}$ exhibited blue emission. The emission gradually changed from green to blue side of the spectrum on increasing the calcium concentration. The same trend was observed in the case of phosphorescence color (Fig. 2.27(b)). The interesting point is that on going from Sr rich samples to Ca rich samples, a bluish-white emission was observed, especially, in between 0.7 to 0.8 mole fraction of Ca substitution. The bluish-white emission was due to the mixing of the blue emission in $CaAl_4O_7:Eu^{2+}$ phosphor and green emission in $SrAl_2O_4:Eu^{2+}$ phosphor.

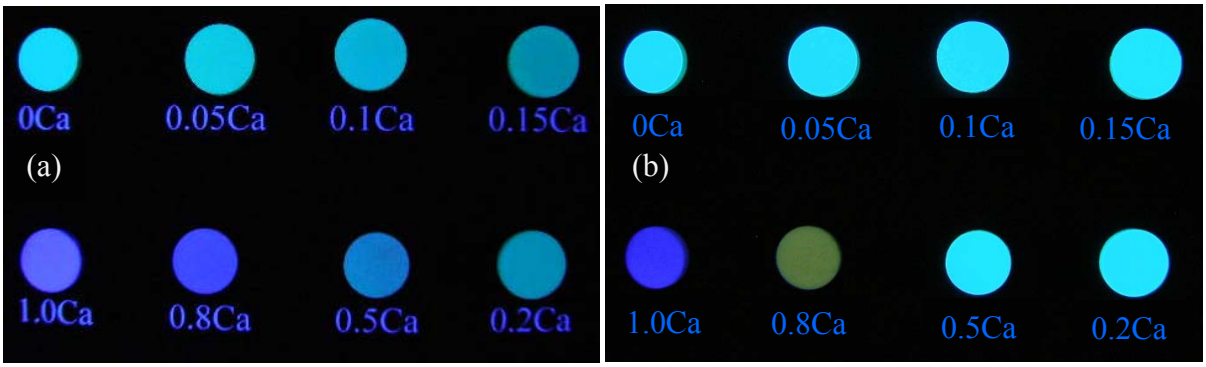

Fig. 2.27. Photographs of $Sr_{4-y}Ca_yAl_{14}O_{25}:Eu^{2+}/Dy^{3+}$ phosphors ($0<y\leq4$), (a) Fluorescence color in presence of excitation light and (b) phosphorescence color, after removing excitation light (the number indicates the mole fraction of calcium).

However, the phosphorescence intensity of the phosphor was very dim and faded rapidly remaining green afterglow within few seconds. It is reported that $CaAl_4O_7:Eu^{2+}$ phosphor exhibit very short afterglow. Thus, the blue component of the emission faded out within few seconds and remained only green emission. Further, it is found that the relative intensities of phosphorescence were dependent on the calcium content of the phosphor. Figure 2.28 shows that increasing concentration of calcium increased the phosphorescence intensity up to $X_{Ca} = 0.15$ without any change in spectral profile with peak maxima at 497 nm. It is reported that substitution of Sr^{2+} by RE^{3+} ions creates defects associated with interstitial oxygen that acts as phosphorescence killer [26, 43]. Insertion of small amount of Ca^{2+} ions replace these defects sites and enhance the afterglow intensity. However the phosphorescence intensity decreased on increasing the Ca^{2+} concentrations above the value of $X_{Ca} = 0.15$ and the decrease was due to the formation of other phases *viz.* $CaAl_2O_4$ and $CaAl_4O_7$ as seen in XRD profiles. These $CaAl_2O_4:Eu^{2+}/Dy^3$ and $CaAl_4O_7:Eu^{2+}/Dy^3$ phosphors exhibits lower phosphorescence intensity than that of the $Sr_4Al_{14}O_{25}:Eu^{2+}/Dy^3$ phosphor.

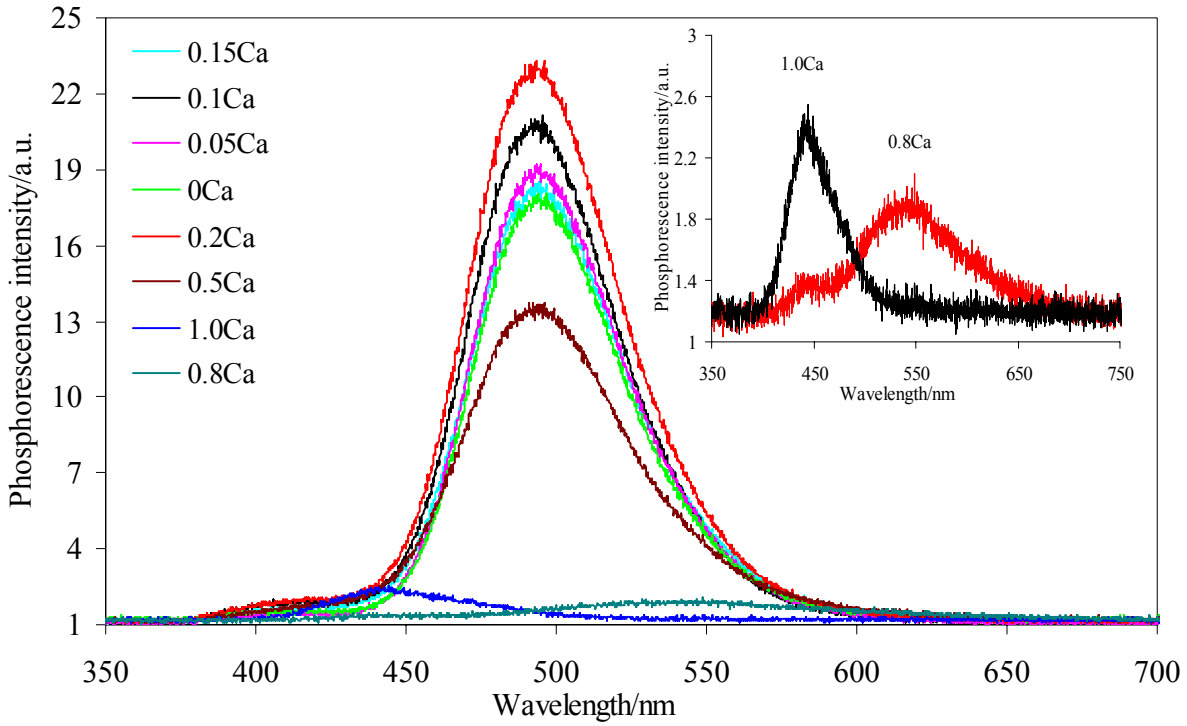

Fig. 2.28. Phosphorescence peaks (recorded 10s after source light was off) for various mole fractions of Ca substituted $Sr_{4-y}Ca_yAl_{14}O_{25}:Eu^{2+}/Dy^{3+}$ phosphors ($0<y\leq4$). The inset figure shows the enlarged phosphorescence curve of 1.0 and 0.8 mol fraction Ca substituted samples.

A similar study was carried out by substituting strontium by different mole fractions of barium varying from $X_{Ba}=0$ to 1. The fluorescence emission spectra of those barium substituted $Sr_{4-z}Ba_zAl_{14}O_{25}:Eu^{2+}/Dy^{3+}$ phosphor samples are shown in Fig. 2.29. Unlike calcium substitution, barium substitution decreased the emission intensity of the phosphor samples. On increasing barium concentration the emission intensity decreased sharply up to 0.8 mole fraction of barium substitution. However, the emission intensity was higher for pure barium aluminate phosphor than the mixture of Ba and Sr compounds. It is reported that when Eu^{2+} replaces larger cation (Ba^{2+}), reduction of the distance between Eu^{2+} and the coordinating anions will be unfavorable, since the site is too large for Eu^{2+} ions. Thus, the stability of europium ions is reduced that reduces the solubility of europium in the host and decreased the emission intensity. Further, with the increase of barium concentration, the emission maximum shifted towards the green side of the spectrum (red shift), but the trend was not smooth like calcium substitution. As explained above, at lower concentrations, substitution of strontium by barium ions reduces the covalency and $4f^65d^1$ band is shifted to

the lower energy side that led to the red shift in the emission maximum. However, at the higher barium concentrations, the $BaAl_2O_4$, $SrAl_2O_4$ and $BaAl_4O_7$ phases were formed, as seen in XRD patterns. The Eu^{2+} emits at higher wavelength side of the spectrum in these hosts than that of the $Sr_4Al_{14}O_{25}$ host [18, 22, 50].

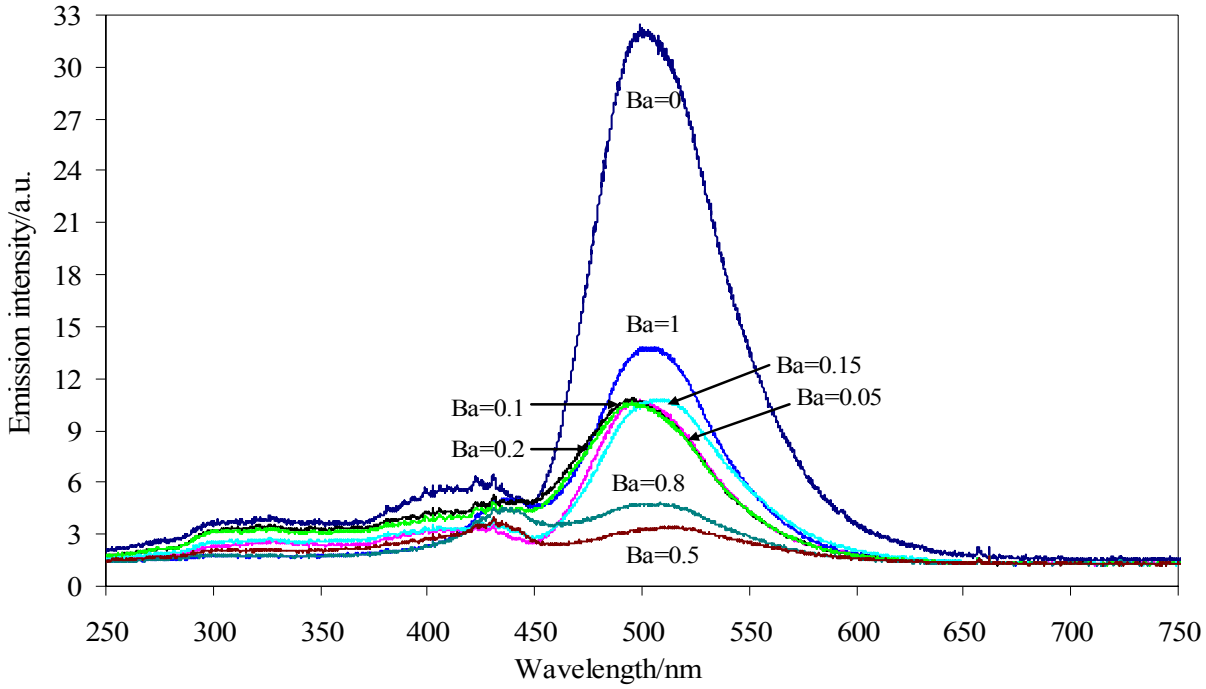

Fig 2.29 Fluorescence spectra of various mole fraction of Ba substituted $Sr_{4-z}Ba_zAl_{14}O_{25}:Eu^{2+}/Dy^{3+}$ phosphors ($0<z\leq4$).

Figure 2.29 shows the phosphorescence spectra of different mole fraction of barium substituted $Sr_{4-z}Ba_zAl_{14}O_{25}:Eu^{2+}/Dy^{3+}$ phosphors (recorded 10s after the excitation source was switched off). There was no any enhancement of phosphorescence intensity and afterglow duration by barium substitution. In the contrary, there was sharp decrease in the phosphorescence intensity and afterglow duration. On increasing the barium concentrations, both the phosphorescence intensity and the afterglow duration decreased. It indicates that unlike calcium, barium substitution is ineffective to remove the defects sites (supposed as phosphorescence killer) generated during the incorporation of Re^{3+} ions in the host. Further, substitution of larger ions (Ba^{2+}) to the strontium sites decreases the stability of Eu^{2+} and Dy^{3+} ions in the host that reduce the solubility of Eu^{2+} and Dy^{3+} in the host and hence the photoluminescence properties was reduced.

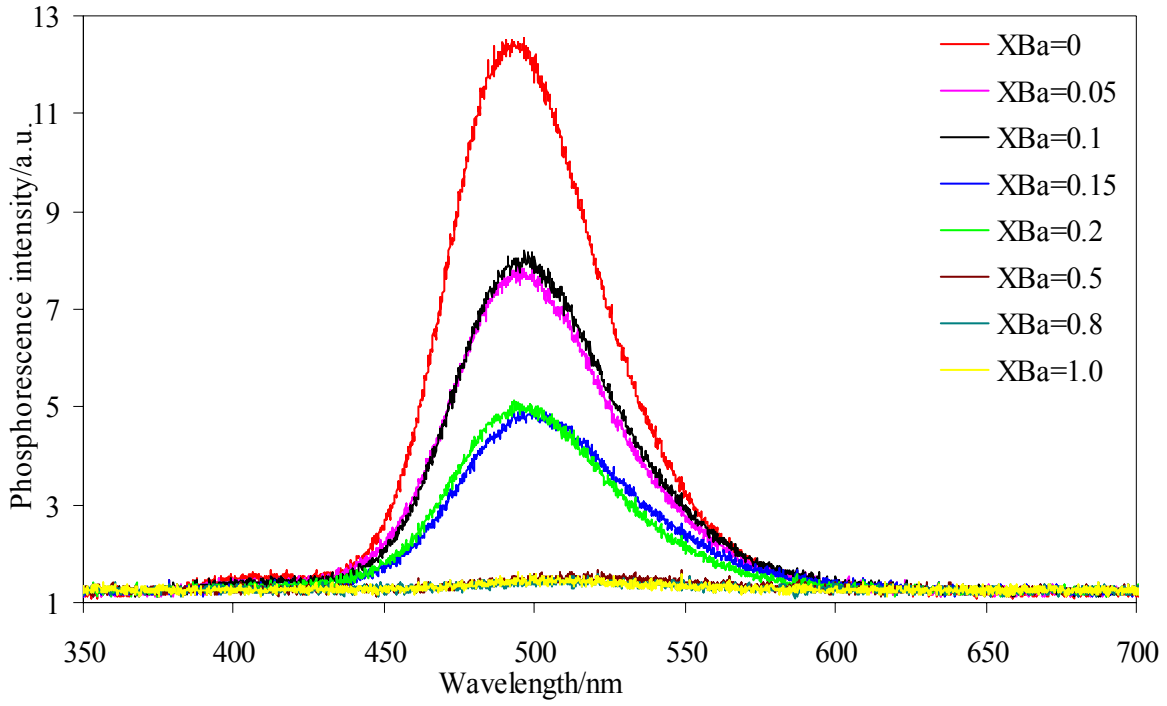

Fig 2.30 Phosphorescence spectra of different mole fraction of barium substituted $Sr_{4-z}Ba_zAl_{14}O_{25}:Eu^{2+}/Dy^{3+}$ phosphors ($0<z\leq4$).

Table 2.4. Summary of Ba substitution effects on the phase changes, lattice parameters and photoluminescence emission and afterglow properties of $Sr_{4-z}Ba_zAl_{14}O_{25}:Eu^{2+}/Dy^{3+}$ phosphors ($0<z\leq4$) (Fluor.max. = Fluorescence maxima and Phos.max. = phosphorescence maxima).

Samples	Ba=0 (X_{Ba}=0)	Ba=0.2 (X_{Ba}=0.05)	Ba=0.4 (X_{Ba}=0.1)	Ba=0.6 (X_{Ba}=0.15	Ba=0.8 (X_{Ba}=0.2)	Ba=2.0 (X_{Ba}=0.5)	Ba=3.2 (X_{Ba}=0.8)	Ba=1.0 (X_{Ba}=1.0)
Phases	$Sr_4Al_{14}O_{25}$	$Sr_4Al_{14}O_{25}$	$Sr_4Al_{14}O_{25}$	$Sr_4Al_{14}O_{25}$ $BaAl_4O_7$	$SrAl_2O_4$ $BaAl_4O_7$	$BaAl_4O_7$ $SrAl_2O_4$	$BaAl_4O_7$ $BaAl_2O_4$	$BaAl_4O_7$ $BaAl_2O_4$
2θ value D(220)	34.3 0.13680	34.24 0.136701	34.12 0.13744	34.02 0.13756	33.96 0.13800	33.94 0.13808	34.62 0.13652	34.82 0.13673
Fluo.max.	502	500	497	511	498	430, 520	440, 507	507
Phos.max.	497	498	499	502	495	521	514	510
CIE(XY-value)	X=0.2022 Y=0.4381	X=0.189 Y=0.399	X=0.1847 Y=0.3892	X=0.1786 Y=0.3297	X=0.1797 Y=0.3613	X=0.21644 Y=0.33038	X=0.1887 Y=0.2958	X=0.1738 Y=0.3735

2.3.7. Effect of size and type of starting alumina particles

Shape and size of phosphor particles plays important role for the photoluminescence properties. When the particle size reaches nano scale, new properties are appeared like the blue shift of emission intensity [52]. If the phosphor particles are regular and flat plate like, they are expected to give a better light absorption and form a dense compact by their orientation, resulting higher photoluminescence intensity. The shape and size of the phosphor particles can be controlled by selecting proper crystal type and particle size of starting materials as well as the methods of preparation. Control of particles shape and size has been already explored by many researchers using various methods of preparations like sol-gel method [53], chemical precipitation method [54], chemical combustion method [55] and many more. I will discuss the effect of synthetic methods on the control of particle shape and size of $Sr_4Al_{14}O_{25}:Eu^{2+}/Dy^{3+}$ phosphor in the next chapter. Here, I report the effect of raw Al_2O_3 powder type and its sizes on the control of phosphor morphology and the photoluminescence properties of $Sr_4Al_{14}O_{25}:Eu^{2+}/Dy^{3+}$ phosphor.

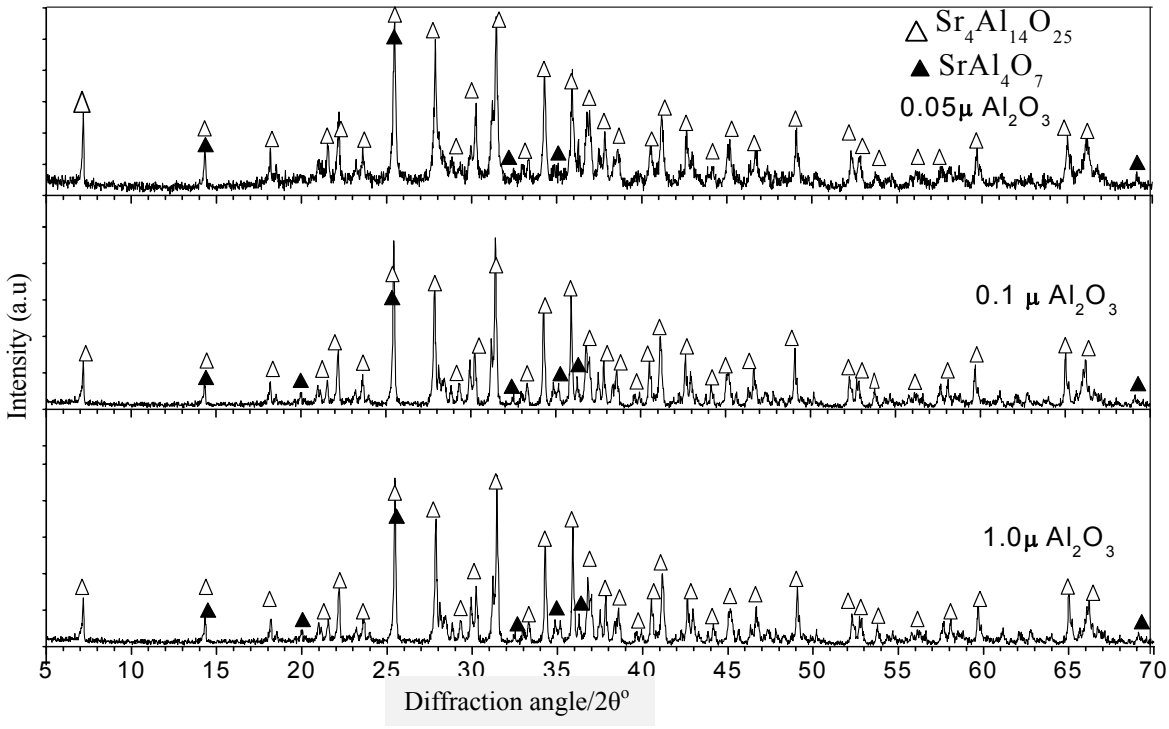

Fig. 2.31. X-ray diffraction pattern of $Sr_4Al_{14}O_{25}:Eu^{2+}/Dy^{3+}$ phosphor prepared using (a) 0.05μm, (b) 0.1μm and (c) 1.0μm alumina at 1350°C.

The X-ray diffraction patterns of the phosphor specimens prepared using three different types of Al_2O_3 (0.05 μm-γ-type, 0.1 μm - α-type and 1 μm - α-type) were same and all the peaks were well indexed with the JCPDS card value (52-1876) of pure $Sr_4Al_{14}O_{25}$ phase (Fig. 2.31). This result indicates that the change of particle size and crystal type of starting Al_2O_3 did not affect the $Sr_4Al_{14}O_{25}$ phase formation while keeping all other synthetic conditions constant.

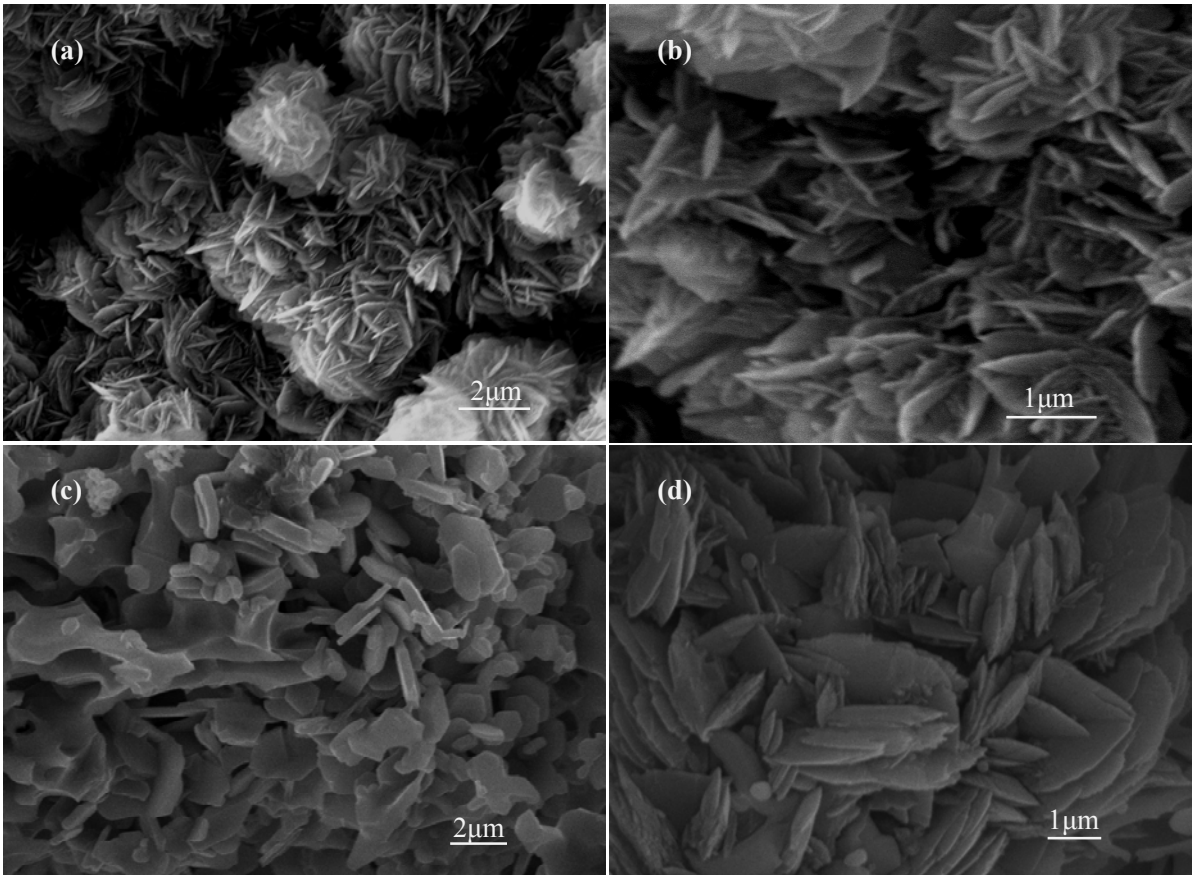

Fig. 2.32. SEM microstructure of $Sr_4Al_{14}O_{25}:Eu^{2+}/Dy^{3+}$ phosphor prepared using (a) 0.05μm; γ-Al_2O_3, (b) micrograph (a) at higher magnification, (c) 0.1μm; α-Al_2O_3 and (d) 1.0μm; α-Al_2O_3.

Figure 2.32 shows the SEM microstructure of these three samples prepared using Al_2O_3 of different particle sizes, (a) 0.05 μm (γ-type), (b) 0.1 μm (α-type) and (c) 1.0 μm (α-type). Although the same phase was observed (as in XRD observations), their microstructures were quite different. When γ-Al_2O_3 of smaller particle size was used as precursor powder, a ball like microstructure composed of spikes or elongated plates was observed. The average size of the plate like particle was roughly 1 μm long, 0.2 μm wide

and 20 nm thick. Due to formation of regular and smaller particles, these small plates overlapped with each other and formed compact ball like structure. The average size of these balls was about 3 μm in diameter. When 0.1μm α-Al_2O_3 was used, irregular porous microstructure composed of bigger and thicker hexagonal plates of nearly 1 μm long, 0.75 μm wide and 0.5 μm size was observed as shown in Fig. 2.32(b). These plates get connected with each other and formed walls, making a bit spongy structure. However, using α-Al_2O_3 of 1.0 μm particle size, much bigger but thinner, irregular flat plates of nearly 3 μm long 2 μm wide and 30 nm thick was observed as in Fig. 2.32(c). Due to the high aspect ratio of the irregular plates, much porous microstructure was formed. The porous microstructure was further supported by the density of the as prepared pellets that decreased on increasing the particle size of raw alumina powder and also the phosphor particles (0.05μ Al_2O_3 – 1.91 g/cm^3 > 0.1μ Al_2O_3 – 1.87 g/cm^3 > 1.0μ Al_2O_3 – 1.80 g/cm^3). The particle shape dependency according to the starting alumina powder may be explained on the basis of dissolution and precipitation mechanism [56]. The detail mechanism for the explanation of different shape according to the starting material is still unclear and left for the further work.

Figure 2.33 shows the absorption and phosphorescence spectra of $Sr_4Al_{14}O_{25}:Eu^{2+}/Dy^{3+}$ phosphor prepared using 0.05 μm, 0.1 μm and 1.0 μm Al_2O_3 as starting materials. All these phosphor samples prepared using these three types of Al_2O_3 were excited by the light of 220 to 440 nm wavelength. These samples gave similar emission spectra with emission maximum centered at 497 nm showing blue-green color. However, there was a small blue shift in the case of phosphor prepared using 0.05 μm Al_2O_3. It is obvious that decrease in particle size increases the surface energy, which results in the distortion of structure around the Eu^{2+}, consequently, the blue shift in the emission peak is possible [52]. The phosphorescence intensity of these phosphors, however, varied drastically according to the used raw alumina powder as shown in the Fig. 2.33. The phosphorescence intensity (recorded 10s after the excitation source was switched off) for the phosphor samples from 0.05 μm, 0.1 μm and 1.0 μm Al_2O_3 were 2316, 1379 and 1025 $mcd.m^{-2}$, respectively. The emission intensity increased with decreasing Al_2O_3 particle size and became highest for the phosphor prepared using 0.05 μm Al_2O_3. The decrease in phosphorescence intensity might be due to formation of bigger particles with much porous microstructure on increasing the Al_2O_3 particle size as explained in the SEM microstructure

observations and the schematic diagram in Fig. 2.34. As seen in Fig. 2.34, the surface structure and powder particle size greatly monitors the light absorption and hence the emission properties. If the surface is rough, it has higher absorption capacity than the smooth surface. Further, the bigger particles by their orientation scatter the emitted light in undesired direction that reduces the emission intensity in the desired directions. Obviously, as packing density decreases, the volume content of the phosphor decreases leading in the decrease of the emission intensity of the phosphor.

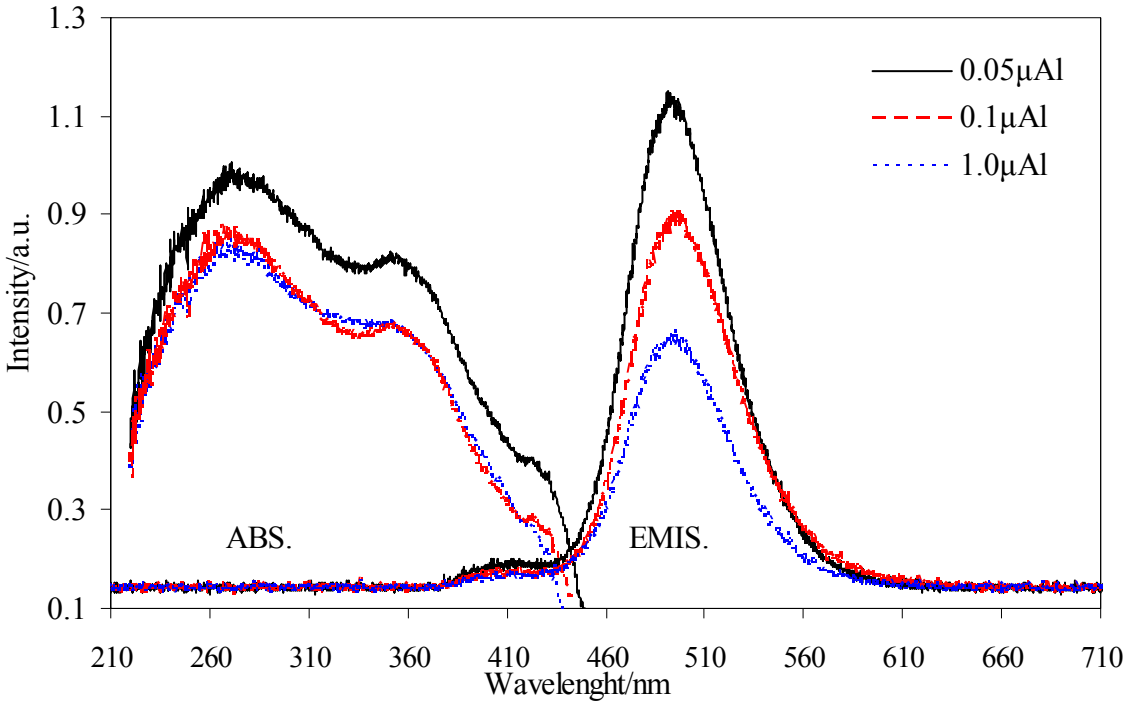

Fig. 2.33. Absorption and emission spectra of $Sr_4Al_{14}O_{25}:Eu^{2+}/Dy^{3+}$ phosphor prepared using (a) 0.05µm; γ-Al_2O_3, (b) 0.1µm; α-Al_2O_3 and (c) 1.0µm; α-Al_2O_3 as precursor powder.

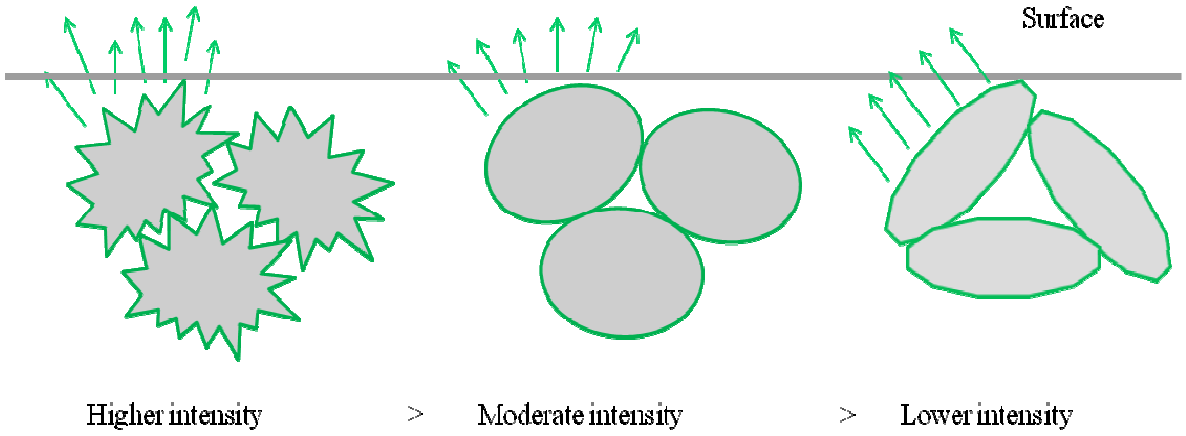

Fig. 2.34. Schematic diagrams to show the effect of phosphor particles shape and size on photoluminescence properties.

Figure 2.35 shows the change in the afterglow emission intensity and the decay speed of these phosphor products with time. The afterglow intensity was decreased by nearly $1/10^{th}$ of the initial intensity within few minutes. The afterglow intensity and persistent duration were higher for the phosphor prepared using 0.05 μm γ-Al_2O_3 and its afterglow duration was more than 20 h (over the value of 5 $mcd.m^{-2}$). The longer afterglow duration of the smaller particles phosphor may be explained as: upon exposure to light source, the direct excitation of Eu^{2+} due to $4f^7 \rightarrow 4f^65d^1$ transition occurs (Chapter I, Fig. 1.3), and a great numbers of holes are generated near the valence band. Some of these free holes are released thermally to the valence band, migrates through the valence band and captured by the Dy^{3+}-borate complex [24, 27]. When the excitation source is removed, the trapped holes are released thermally to the valence band, migrates to the excited Eu^{2+} ions and, consequently, the recombination take place, which leads to the long afterglow. So, the long afterglow duration depends on the number of captured holes. The numbers of captured holes, in turn, depends on the concentration of Dy-borate complexes and the trap depth of it. With decrease of particle size, the blue shift of the trap depth occurs [52] that leads to increase in the afterglow duration.

Table 2.5 shows the various properties of these three phosphors. The decay parameter, τ, calculated using the exponential curve fitting technique for these phosphor samples decreased on increasing the particle size of the phosphors. It is found that the decay parameter, τ value, was longest for the phosphor prepared using 0.05 μm γ-Al_2O_3 and

shortest for the phosphor prepared using 1.0 μm α-Al_2O_3. It has been normalized that higher the value of τ, the deeper was the trap depth becomes and hence the longer the persistent afterglow time duration of the phosphors.

Table 2.5 Optical properties and decay parameters of $Sr_4Al_{14}O_{25}:Eu^{2+}/Dy^{3+}$ phosphor prepared using (a) 0.05 μm γ-Al_2O_3, (b) 0.1 μm α-Al_2O_3 and (c) 1.0 μm α-Al_2O_3.

Phosphor samples	Used Al_2O_3 (size, type)	Maximum afterglow intensity	Persistent Time(h) (≥5mcd/m^{-2})	Used Al_2O_3 (size, type)	Decay parameter, τ (s)		
					τ_1	τ_2	τ_3
(a)	0.05 μ (γ)	2316	17	0.05 μ (γ)	19.7	190.0	2290
(b)	0.10 μ (α)	1379	14	0.10 μ (α)	13.73	139.3	1670
(c)	1.00 μ (α)	1025	10	1.00 μ (α)	11.85	95.0	1190

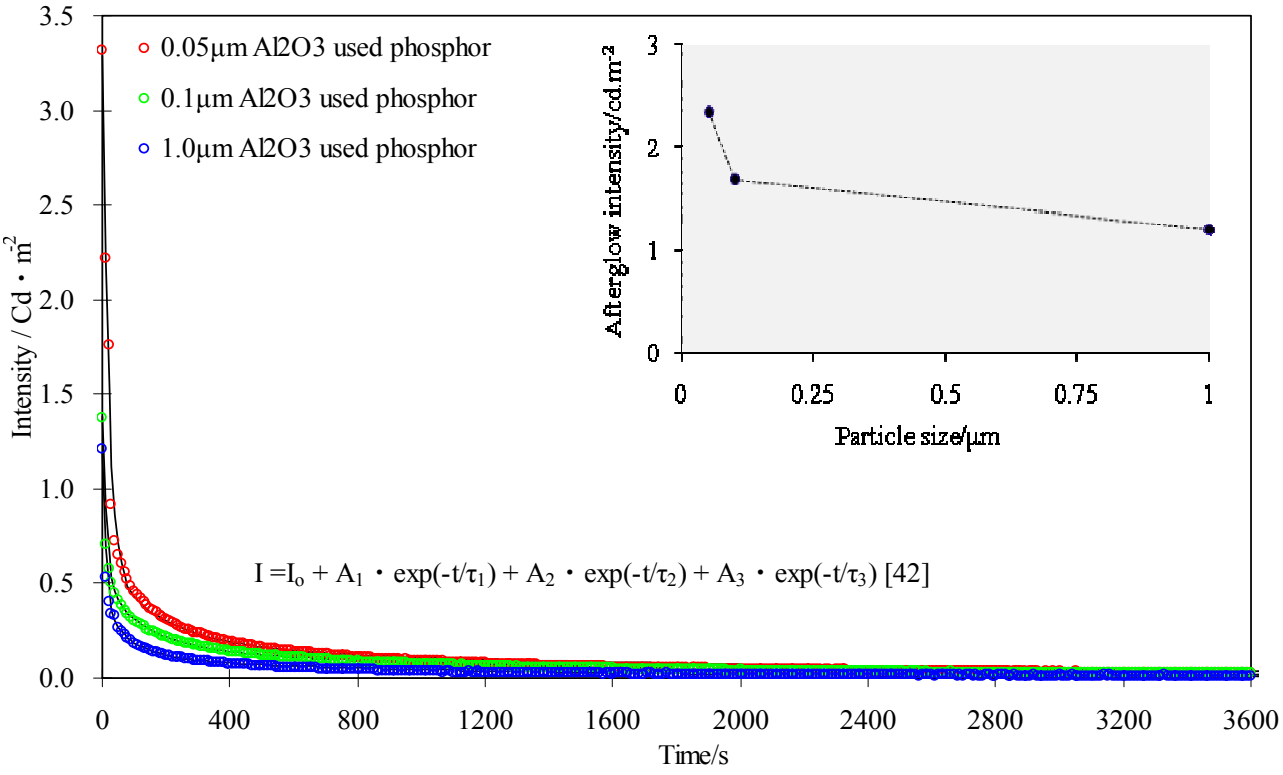

Fig. 2.35. Effect of Al_2O_3 particle size on the phosphorescence intensity and afterglow decay speed of $Sr_4Al_{14}O_{25}:Eu^{2+}/Dy^{3+}$ Phosphor (dots and solid lines are observed and fitted curves, respectively). Inset figure shows the variation of afterglow intensity of phosphor with Al_2O_3 particles size.

2.4. Conclusions

$Sr_4Al_{14}O_{25}:Eu^{2+}/Dy^{3+}$ phosphor with high brightness and long persistent phosphorescence was synthesized by the solid state reaction method at 1350^oC. Highly crystalline, single phase $Sr_4Al_{14}O_{25}$ phosphor was observed when 3.5 mol% boric acid was used as a flux. SEM results revealed that the particles shape and size was determined by the amount of boric acid as a flux. When 3.5 mol% boric acid was used, fine particles with higher angularity was obtained. EDX mapping results revealed that the Eu^{2+} and Dy^{3+} ions were homogeneously dispersed into the phosphor matrix when 3.5 mol% boric acid was used. Further, boric acid helps the Eu^{2+} and Dy^{3+} ions to disperse throughout the matrix and increased their concentration. The broad band UV-visible excited luminescence of the $Sr_4Al_{14}O_{25}:Eu^{2+}/Dy^{3+}$ phosphor was observed in the blue-green region (λ_{max} = 497 nm) due to transitions from the $4f^65d^1$ to the $4f^7$ configuration of the Eu^{2+} ion in the $Sr_4Al_{14}O_{25}$ crystal. The phosphorescence characteristics were highly influenced by the addition of small amounts of H_3BO_3 in the starting mixture and maximum photoluminescence properties were observed on adding 3.5 mol% boric acid. When the samples were preheated at 1000^oC and then reduced at 1350^oC in 10% H_2 and 90% N_2, better photoluminescence properties were observed. The optimum concentration of the emission center (Eu^{2+}) for higher brightness was found to be 4 at%. Out of various trivalent rare earth metal ions, Dy^{3+} was found to be the most affective to enhance the phosphorescence properties due to formation of suitable trap in the $Sr_4Al_{14}O_{25}$ matrix. When doped Eu^{2+} concentration was 4 at% and co-doped Dy^{3+} was 8 at%, the phosphor exhibited the highest phosphorescence intensity and longest afterglow persistency. The decay curve fitting results revealed that the phosphor with the aluminium to strontium ratio (Al/Sr) of 3.7 had deeper trap depths and hence showed the longer afterglow duration over other compositions. Addition of 3 mol% Ag^+ as charge compensator dramatically enhanced the brightness of the phosphor (greater than 2 fold) that may be due to removal of the lattice defects formed during replacement of strontium by trivalent rare metal ions. Use of γ-alumina of 0.05μm size as a raw powder during the synthesis of phosphor was found to be effective for the formation of regular particles with smaller particles size over the other alumina type (0.1 μ and 1.0 μ) and evinced better photoluminescence characteristics. Substitution of part or whole of Sr sites by Ca or Ba ions can effectively monitor the color of emission light and its CIE values. When 0.7 to 0.8 mole

fraction of Sr was substituted by Ca, bluish-white fluorescence was observed, however the persistent time of the bluish-white afterglow was very short and need to get improved before applications.

References

[1] F. Clabau, X. Rocquefelte, S. Jobic, P. Deniard, M.H. Whangbo, A. Garcia, T.L. Mercier, Chem. Mater. **17** (2005) 3904.

[2] Y. Lin, Z. Tang, Z. Zhang, Mater. Lett. **51** (2001) 14.

[3] H. Yamamoto, T. Matsuzawa, J. Lumin. **72** (1997) 287.

[4] Y.V. Zorchko, R.M. Turchak, W. Gryk, M. Grinberg, J. Lumin. **106** (2004) 313.

[5] B. Smets, J. Rutten et.al. J. Electrochem. Soc. **136** (1989) 2119.

[6] Y.X. Xu, L. Hao, W. Xie, Y.Wang, L. Yang, X. Yang, Mater. Lett. **63** (2009) 1511.

[7] T. Matsuzawa, Y. Aoki, N. Takeuchi, Y. Murayama, J. Electrochem. Soc. **143** (1996) 2670.

[8] Y. Gu, Q. Zhang, Y. Li, H. Wang, R-J. Xie, Mater. Lett. **63** (2009) 1448.

[9] X. Zhang, N. Choi, K. Park, J. Kim, Solid State Commun. **149** (2009) 1017.

[10] T. Aitasalo, J. Holsa, H.Jungner, J.C. Krupa, M. Lastusaari, J. Legendziewicz, J. Nittykoski, Radiation Measurements **38** (2004) 727.

[11] T. Aitasalo, P. Deren, H. Jungner, J.C. Krupa, M. Lastusaari,J. Legendziewicz, J. Niittykoski, J. Solid State Chem. **171** (2003) 114.

[12] G.Blasse, B. C. Grabmair, Luminescent Materials, Springer, Berlin, 1994.

[13] D. Haranath, P. Sharma, H. Chander, A. Ali, N. Bhalla, S.K. Halder, Mater. Chem. Phys. **101** (2007) 163.

[14] Y. Lin, Z. Tang, Z. Zhang, C. Nan, J. European Ceram. Soc. **23** (2003) 175.

[15] W.M. Yen, S. Shionoya, H. Yamamoto, Phosphor Hand Book, CRC press, 1995.

[16] D. Wang, M.Q. Wang, G.L. Lu, J. Mater. Sci. **34** (20) (1999) 4959.

[17] Z. X. Yuan, C. K. Chang, D.L. Mao, W. Ying, J. Alloys Compd. **377** (2004) 268.

[18] H. Yamamoto, T. Matsuzawa, J. Lumin. **72** (1997) 287.

[19] J.T.C Van Kemendo, G.P.F. Hoeka, Electrochem. Soc. Spring Meeting Abstract, San Francisco, 1983, Abstract No. 607.

[20] B.M.J. Smets, Mater. Chem. Phys. **16** (1978) 283.

[21] E. Nakazawa, T. Mochida, J. Lumin. **72-74** (1997) 236.

[22] T. Katsumata, T. Tanabe, K. Sasajima, S. Komuro, T. Morikawa, J. Electrochem. Soc. **144** (1997) L243.

[23] C.W. Thiels, H. Cruguel, Y. Sun, G. J. Lapeyre, R. M. Macfarlane, R. W. Equall, R. L. Cone, J. Lumin. **94-95** (2001) 1.

[24] E. Nakazawa, Y. Murazaki, S. Saito, J. Appl. Phys. **100** (2006) 113113.

[25] F. Clabau, X. Rocquefelte, S. Jobic, P. Deniard, M.H. Whangbo, A. Garcia, T. Le Mercier, Solid State Sci. **9** (2007) 608.

[26] N. Suriyamurthy, B.S. Panigrahi, J. Lumin. **128** (11) (2008) 1809.

[27] A. Nag, T.R.N. Kutty, J. Alloys Compd. **354** (2003) 221.

[28] C. Zhao, D. Chen, Mater. Lett. **61** (2007) 3673.

[29] D. Wang, Q. Yin, Y. Li, M. Wang, J. Lumin. **97** (2002) 1.

[30] Y.L. Chang, H.I. Hsiang, M.T. Liang, J. Alloys Compd. **461** (2008) 598.

[31] C. Chang, Z. Yuan, D. Mao, J. Alloys Compd. **415** (2006) 220.

[32] G.F.J. Garlick; Luminescent materials, Oxford university Press, UK, 1949, pp73

[33] S.D. Han, K. C. Singh, T.Y. Cho, H.S. Lee, D. Jakhar, J. P. Hulme, C.H. Han, J.D. Kim, I.S. Chun, J. Gwak, J. Lumin. **128** (2008) 301.

[34] M.L. Ruiz-Gonzalez, J.M. Gonzalez-Galbet, M. Vallet-Regi, E. Crondoncillo, P. Escribano, J.B. Carda, M. Marchal, J. Mater. Chem. **12** (2002) 1128.

[35] F. Clabau, X. Rocquefelte, S. Jobic, P. Deniard, M.H. Whangbo, A. Garcia, T. Le Mercier, Chem. Mater. **17** (2005) 3904.

[36] N. Peng, Z. Pei, G. Hong, Q. Su, Chem. Phys. Lett. **371** (2003)1.

[37] D.L. Dexter, J. Chem. Phys. **21** (1953) 836.

[38] G. Blasse, B.C. Grabmailer, Luminescent Materials, Springer-Verlag, 1994.

[39] H. He, R. Fu, X. Song, D. Wand, J. Chen, J. Lumin. **128** (2008) 489.

[40] F. Clabau, X. Rocquefelte, T. Le Mercier, P. Deniard, S. Jobic, M.H. Whangbo, Chem. Mater. **18** (2006) 3212.

[41] A. Nag, T.R.N. Kutty, Mater. Res. Bull. **39** (2004) 331.

[42] R. Sakai, T. Katsumata, S. Komuro, T. Morikawa, J. Lumin. **85** (1999) 149.

[43] R. Grasser, J. Lumin. **40-41** (1988) 389.

[44] W.M. Yen *et al.,* Phosphor with long persistent green phosphorescence, US Patent 6267911 B1 (2001).

[45] Y.J. Chen F. Cao, Y. Tian, L. Xiao, L. Li, Physica B **405** (2009) 435.

[46] J. Kuang, Y. Liu, J. Lumin. **118** (2006) 33.

[47] C. Liu, Y. Yang, Y. Hu, R. Chen, F. Liao, J. Alloys. Compd. **470** (2009) 473.

[48] J.L. Pascal, Z. Barandiaram, L. Seijo, Phys. Rev. B **76** (2007) 104109.

[49] D. Jia, J. Zhu, B. Wu, J. Lumin. **93** (2001) 107.

[50] H. Ryu, B.K. Singh, K.S. Bartwal, Physica B **403** (2008) 126.

[51] W.B. Im, Y-II Kim, H.S. Yoo, D.Y. Jeon, Inorg. Chem. **48** (2009) 557.

[52] Z. Tang, F. Zhang, Z. Zhang, C. Huang, and Y. Lin, J. Euro. Ceram. Soc. **20** (2000) 2129.

[53] C.H. Lu, W.T. Hsu, C.H. Huang, S.V. Godbole, B.M. Cheng, Mater. Chem. Phys. **90** (2005) 62.

[54] Y. Chen, J. Wang, M. Gong, Q. Su, J. Solid State Chem. **180** (2007) 1165.

[55] S. Wu, S. Zhang, J. Yang, Mater. Chem. Phys. **102** (2007) 80.

[56] R. M. German, “Liquid phase sintering,” Plenum Press, New York, USA, 1985, pp. 23.

Chapter III

Comparative investigation on the synthesis and photoluminescence properties of $Sr_4Al_{14}O_{25}:Eu^{2+}/Dy^{3+}$ phosphor

3.1. Introduction

Of the phosphors, the alkali earth aluminates containing rare earth ions are functional inorganic materials with strong luminescence in the range from blue to red regions of the spectrum [1-3]. These materials are widely used for such devices "glow-in-dark" items as; safe helmets, direction indicators and signs, robber shoe soles, varieties of toys and the like due to their better safe, chemical stability, excellent photo resistance, very bright and long-lasting afterglow with no radio-active radiations and hence forms the important materials in various ceramics industries [4].

In recent years, $SrAl_2O_4$ and $Sr_4Al_{14}O_{25}$ phosphors doped with Eu^{2+} and Dy^{3+} ions have been regarded as excellent phosphors and attracted the researcher's interest [1-6]. For the improvement of phosphorescent properties, research has been focused on regarding additives, molar ratio of constituents and the preparation methods [4-6]. Z. Wu *et al.* reported the control of particle size by adopting the sol-gel and co-precipitation methods [6]. It was found that the shape and size of phosphor particles plays important role for the fluorescence properties of $Sr_4Al_{14}O_{25}:Eu^{2+}$ phosphor. When the particle size reaches the nano scale, new properties are appeared like the blue shift of emission intensity [7]. If the phosphor particles are flat plate like, they are expected to give a better light absorption and form a dense compact by their orientation, resulting higher photoluminescence intensity.

The solid state reaction process has been used intensively for phosphor synthesis in spite of its poor homogeneity leading to irregular morphology, high calcinations temperature and long time of calcinations. Furthermore, the phosphor particles prepared by this method is much bigger in the range of several tens of micrometers. To get smaller particle powder high energy grinding is required that destroy the crystal structure and hence the photoluminescence properties.

Phosphor of smaller particles size can be synthesized by the liquid phase reaction methods like sol-gel [8-10], co-precipitation [11] microwave [12] and combustion [13] synthesis methods. In the liquid phase synthesis methods, each component (especially, activator ions) can be accurately controlled and uniformly dispersed throughout the phosphor materials, which is of prime importance for the phosphor properties. Further, the liquid phase synthesis methods like sol-gel, chemical combustion, and chemical co-precipitation methods are often used as low temperature routes to incorporate the activator ions into the phosphor host lattices. Use of surfactants and capping agents like glycerol *etc* can aid in the precise control of a chemical reaction and hence the morphology of the phosphor particles.

The solution combustion method to prepare rare earth activated alkaline earth aluminates is an efficient and facile method which takes hardly few minutes and has been extensively used for the preparation of various oxides and aluminates materials [12-15]. Further, combustion method is a liquid phase synthesis method in which each component can be accurately controlled and uniformly mixed to get the homogenous materials. The combustion synthesis technique makes use of heat released during the redox exothermic reactions between nitrate precursors and fuels like urea at relatively lower temperatures [16]. The excessive heat released during combustion reaction completes the reaction in very short time producing small particles with high crystallinity. Further, the Eu^{3+} ions can be easily reduced to Eu^{2+} at relatively lower sintering temperature, which otherwise needs very high temperature and slightly reducing environment.

Sol-gel method is one of the most important techniques for the synthesis of various functional materials, especially, phosphors because it offers many advantages over solid state method such as higher uniformity in mixing in solution form and hence homogeneous particle size distribution, non agglomeration due to use of dispersing agents like glycerol leading to formation of smooth and homogenous particles and hence higher excitation and emission intensities. The surface area of powders produced from sol-gel method is very high that provides better thermal conductivity when excited with high energy photons [17]. In general, different preparation method may greatly influence the crystallization, morphology, particle size, and luminescence characteristics of phosphor materials.

Thus, in this chapter, I aim to report the preparation of $Sr_4Al_{14}O_{25}:Eu^{2+}/Dy^{3+}$ phosphor samples by solid state, sol-gel and chemical combustion methods. Then, the comparative studies on the morphology and photoluminescence properties of these phosphor samples have been explained in detail.

3.2. Experimental

3.2.1. Synthesis of $Sr_4Al_{14}O_{25}:Eu^{2+}/Dy^{3+}$ phosphor by solid state method

The starting materials, strontium carbonate ($SrCO_3$; Aldrich, 99.9+ %), aluminum oxide (Al_2O_3; Baikalox, ultrapure nano-powder), europium oxide (Eu_2O_3; Aldrich, 99.9+ %) and dysprosium oxide (Dy_2O_3; Aldrich, 99.9+ %) with molar ratio of 3.88:14.00:0.04:0.08 for Sr:Al:Eu:Dy were mixed thoroughly using mortar and pestle using a little ethanol. Small amount (3.5 mol %) of boric acid (Aldrich, AR) was added as a flux to accelerate the reaction. Pellets were prepared and heated in ambient air atmosphere at 1000^oC for 4 h. The product was pulverized and again prepared in the form of pellet and then heated in reducing atmosphere of 10% H_2 and 90% N_2 by flowing 20 ml/min H_2 and 180 ml/min N_2. The product was hard solid material that was grinded finely and used for characterization and photoluminescence measurements.

3.2.2. Synthesis of $Sr_4Al_{14}O_{25}:Eu^{2+}/Dy^{3+}$ phosphor by combustion method

The stoichometric compositions of the redox mixture for solution combustion were calculated using total oxidizing and reducing valences of the species which serves as the numerical coefficients for the stoichometric balance so that equivalent ratio of oxidant to reductant is unity [18]. Thus, the stoichometry for the $Sr_4Al_{14}O_{25}$ matrix becomes $3.38Sr(NO_3)_2 + 14Al(NO_3)_3 + NH_4NO_3 + 42CO(NH_2)_2$. In the typical experiment, the combustion synthesis of $Sr_4Al_{14}O_{25}:Eu^{2+}/Dy^{3+}$ is as follows: 5.66g $Sr(NO_3)_2$ + 35.5g $Al(NO_3)_3$ + 0.54g NH_4NO_3 + 0.112g $Eu(NO_3)_3$ + 0.234g $Dy(NO_3)_3$ + 0.165g H_3BO_3 + 17.10g urea were dissolved in minimum amount of pure water at 70^oC by stirring for 2 h. Then the beaker containing the mixture was inserted inside the muffle furnace maintained at 530^oC. Initially, the solution boiled, frothed, foamed and caught fire. Then the fire propagates to its own leading to the completion of reaction in less than five minutes. The white foamy voluminous product (precursor powder) was crushed and used for characterization such as phase analysis, crystallinity, color co-ordinate and

photoluminescence properties. To get the highly crystalline phosphor, the precursor powder was again sintered in the form of small pellets in slightly reducing atmosphere of 10 % H_2 in N_2 for 3-5 h at higher temperatures.

3.2.3. Synthesis of $Sr_4Al_{14}O_{25}:Eu^{2+}/Dy^{3+}$ phosphor by sol-gel method

A mixed solutions with a molar ratio of 3.38:14.00:0.04:0.08 for Sr:Al:Eu:Dy using corresponding metal nitrates was prepared and mixed thoroughly in a magnetic stirrer. Then the solution was added drop wise to the citric acid solution under stirring so that the molar ratio of metal to citric acid was 1:3. A small amount of ethylene glycol was added to avoid the agglomeration. After evaporating the solution at 80^{o}C water bath for 5 h, a transparent light yellow viscous gel was formed. The gel was then heated at 150^{o}C for 12 h to get a dry yellowish precursor powder. Subsequently, this solid precursor powder was calcined at 800^{o}C for 5 h. Then the white powder obtained was mixed with little (3.5 mol%) boric acid and finely grounded using mortar and pestle and sintered at 1200^{o}C for 4 h in weak reducing atmosphere of 10% H_2 and 90% N_2 to get the final phosphor product.

3.2.4. Characterizations

Phase identification was carried out using a Shimadzu XRD-630D instrument with Cu-K_α radiation at room temperature. Scanning Electron Microscopy (SEM) observations were carried out using a Hitachi S-3000N SEM instrument. Photoluminescence (PL) spectra were measured using USB 4000 UV-VIS miniature fiber optic spectrometer (Ocean optics). The decay curves were obtained using a brightness meter (Konica Minolta LS-100). Before afterglow measurements, the phosphor samples were exposed to 15W xenon lamp for 20 minutes. All the measurements were carried out at room temperature.

3.3. Results and discussion

XRD patterns of the phosphor samples synthesized by sol-gel (SG), combustion (CB) and solid state (SS) methods are shown in Fig. 3.1. The different peaks can be indexed to the $Sr_4Al_{14}O_{25}$ phase (JCPDS 52-1876), which has been refined to be orthorhombic crystal structure with *Pmma* space group and cell parameters of a = 24.785 *Å*, b = 8.487 A$^\circ$ and c = 4.866 A$^\circ$, and are in good agreement with the literature values [19]. The combustion powder prepared at 530^{o}C (CB-530) showed some peaks of $SrAl_2O_4$ due to low reactive

temperature but the post annealed combustion powder at 1350°C (CB-1350) can be well indexed to the pure $Sr_4Al_{14}O_{25}$ phase. From the diffraction intensity, it can be seen that the order of crystallization degree for the phosphor is CB-1350≈SS>SG>CB-530. This is also in accordance with the firing temperature, since the crystallinity increases with the increase of firing temperatures.

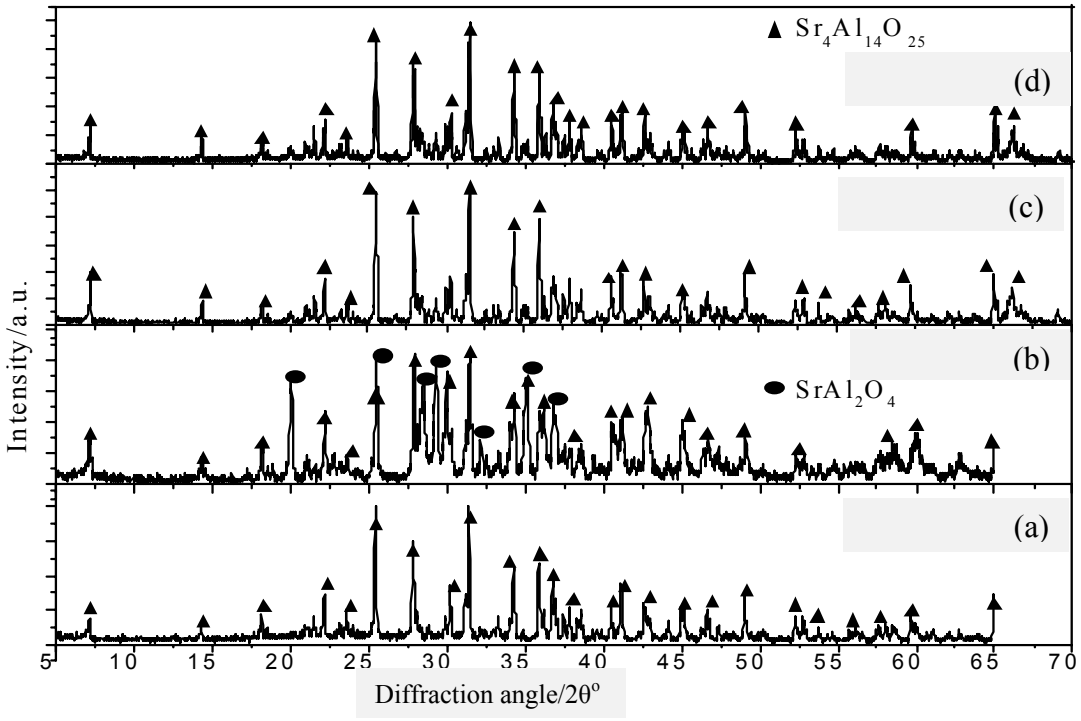

Fig. 3.1. XRD profiles of $Sr_4Al_{14}O_{25}:Eu^{2+}/Dy^{3+}$ phosphor prepared by (a) Sol-gel (SG-1200), (b) Combustion at 530°C (CB-530), (c) CB-530 powder post annealed at 1350°C (CB-1350) and (d) Solid state (SS) methods.

In Fig. 3.2, SEM images of $Sr_4Al_{14}O_{25}:Eu^{2+}/Dy^{3+}$ phosphor prepared by solid state, chemical combustion and sol-gel methods are presented. The phosphor particles prepared by sol-gel method appeared regular, cylindrical solid structures with 5-10 μm long and 1-2 μm in diameter. This is the benefits of the sol-gel method where particles with regular morphology can be achieved due to liquid phase synthesis. The precursor powder prepared by combustion method showed irregular network like structures with lots of voids, pores and networks. The pores and voids were produced during the escaping of gaseous products during the combustion of nitrates and fuel. Even though, a bit rough and irregular morphology, the particle size was tremendously smaller in the nano order. The particles connected together forming bigger network like structure. The combustion precursor powder

(CB-530) post annealed at 1350^{o}C (CB-1350) showed irregular but highly crystalline structure with average particle size of 1 to 2 μm whereas the particles prepared by solid state method (SS) showed spherical ball like structures connected with each other and thoroughly covered by the molten glasses on the surface. The average particle size was bigger than 5 μm. The highly agglomerated big particles formation is the main drawbacks of solid state method even if good crystallinity and easy way of preparations. Even though the sintering temperature was same for SS and CB-1350 samples, the later showed highly crystalline particles with greatly reduced particles size which is the benefits of chemical combustion method.

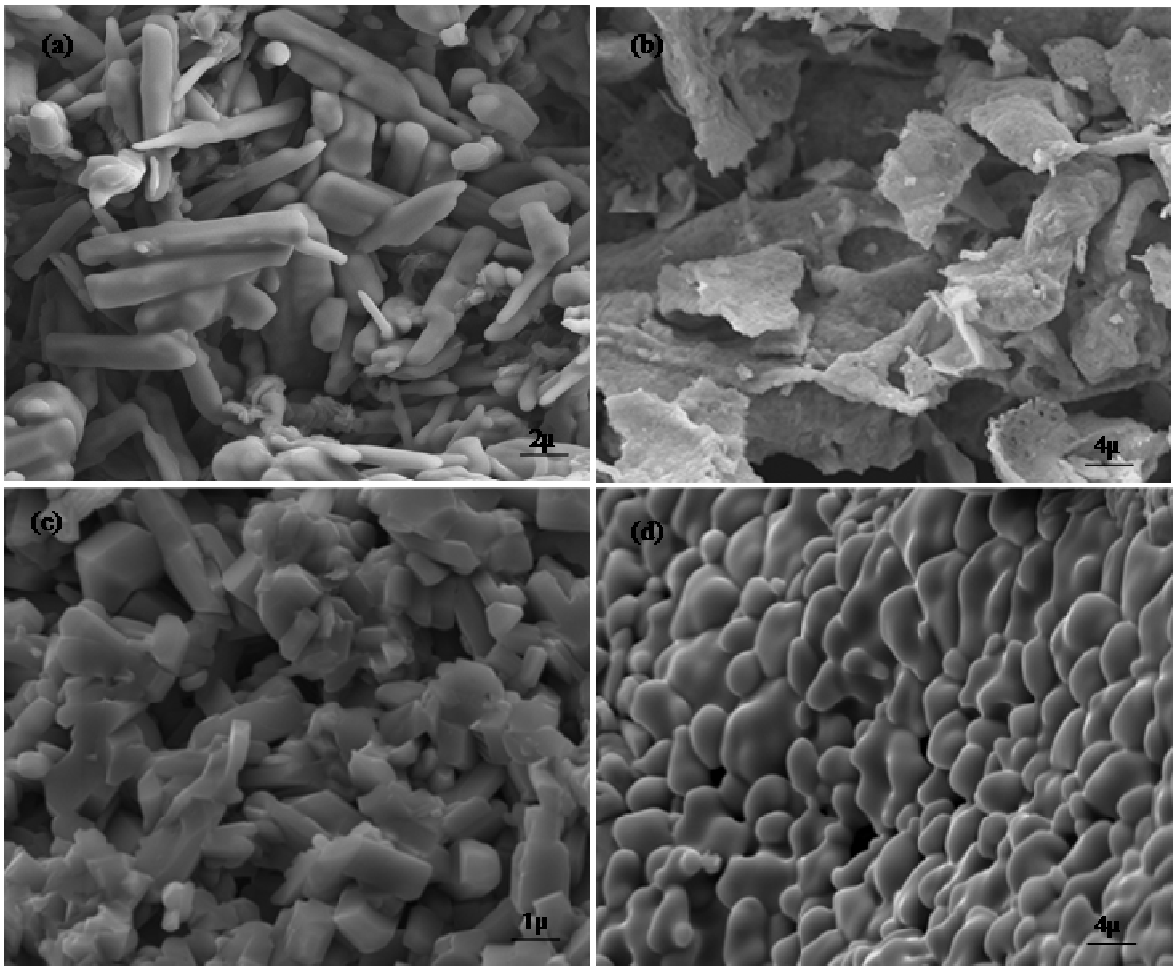

Fig. 3.2. SEM micrographs of $Sr_4Al_{14}O_{25}:Eu^{2+}/Dy^{3+}$ phosphor prepared by (a) Sol-gel, (b) Combustion at 530^{o}C, (c) Combustion powder annealed at 1350^{o}C and (d) Solid state (SS) at 1350^{o}C methods.

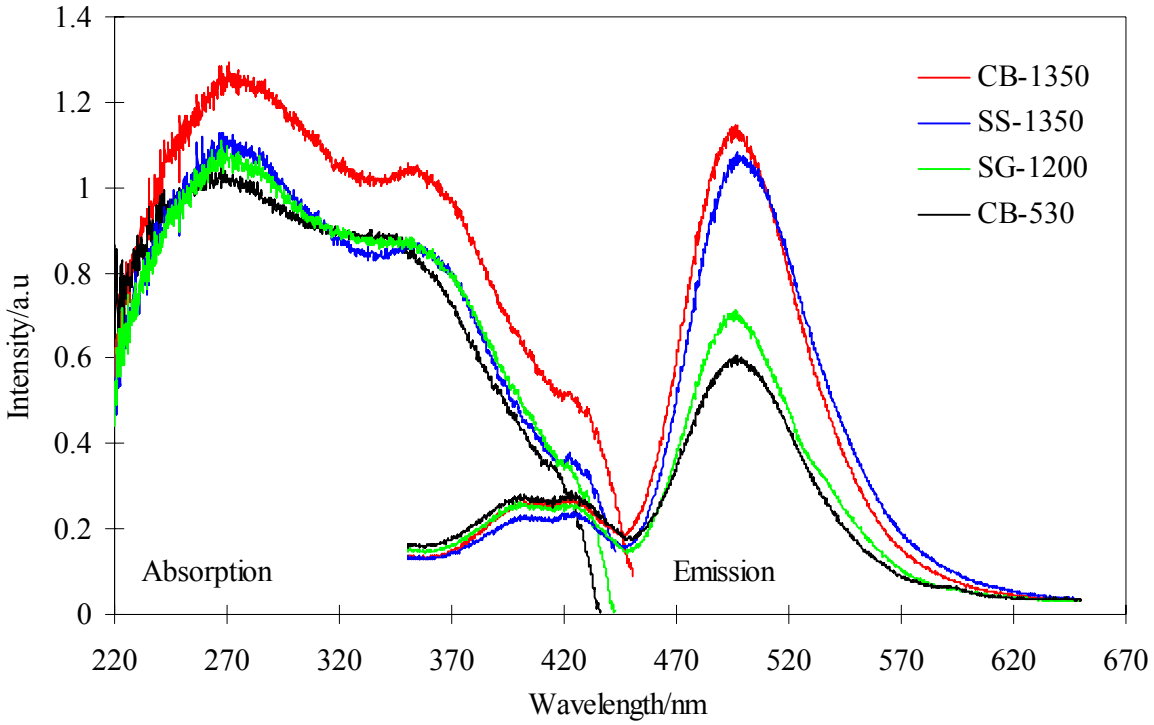

Fig. 3.3. Absorption and emission spectra of $Sr_4Al_{14}O_{25}:Eu^{2+}/Dy^{3+}$ phosphor samples prepared by solid state, sol-gel and chemical combustion methods.

Figure 3.3 shows the absorption and emission spectra of $Sr_4Al_{14}O_{25}:Eu^{2+}/Dy^{3+}$ phosphor prepared by different methods. As seen in the figure, the phosphor samples can be excited by the light of near UV to visible light of 220~430 nm wavelengths. The absorption spectrum consists of a broad range with maxima at 270 and 365 nm. This signifies that the sample can be excited by variety of light sources, especially, by the most common natural sun shine. Since the host $Sr_4Al_{14}O_{25}$ hardly shows any absorption between 300 and 450 nm, the excitation band is attributed to the transition from $4f^7$ ground state to the $4f^65d^1$ excited state of doped Eu^{2+} ions. The emission spectra of SG, CB-530, CB-1350 and SS samples are also presented in Fig. 3.3. All these samples gave the broad band emission with the maxima at around 500 nm showing blue-green color. The emissions in these samples were attributed to the typical $4f^65d^1 \rightarrow 4f^7$ transition of Eu^{2+} ions in the $Sr_4Al_{14}O_{25}$ host. No emission peaks of Eu^{3+} were observed in the emission spectra, indicating that Eu^{3+} ions in the samples have been completely reduced to Eu^{2+} ions. However, there was a small blue shift in the case of phosphor prepared by sol-gel and combustion methods, which is more pronounced in SS and CB-1350 phosphor samples. It is reported that the decrease of particles size increases

the surface energy and results in the distortion of atomic structure around the Eu^{2+} ions in the lattice; consequently, the blue shift in the emission peak is possible [20]. Thus, the blue shift in the combustion and sol-gel samples was due to the smaller size of the phosphor particles.

The afterglow emission intensity was found to be in the order of CB-1350>SS>SG> CB-530. It is the fact that the emission intensity depends on the number of excited luminescent ions and its recombination efficiency in the host lattice. The liquid phase synthetic method like combustion and sol-gel method makes the activator and co-activators ions, here Eu^{2+} and Dy^{3+}, respectively, homogenously disperse throughout the $Sr_4Al_{14}O_{25}$ host increasing its concentration and produced higher emission intensity. Further, as seen in SEM micrograph, the phosphor particles of SS sample was completely covered by non emissive glassy phase that suppress the emission intensity of the phosphor. However, the reduced emission intensity in the case of CB-530 and SG samples was due to the very low sintering temperature. At high sintering temperature fine crystallinity would be expected and which in turn increase the emission intensity.

Figure 3.4 shows the afterglow decay curves of the SG, CB-530, CB-1350 and SS-1350 phosphor samples. It is clearly seen in the figure that the CB-1350 sample showed maximum phosphorescence intensity of 3.68 $Cd.m^{-2}$ that decreased in the order of CB-1350>SS-1350>SG-1200>CB-530, which is in accordance with the crystallinity and the sintering temperatures. All the phosphor samples exhibited a similar afterglow decay spectra. The decay curves consisted of three parts, in the first part, the intensity sharply reduces to nearly $1/10^{th}$ within few seconds, in the second part the decrease of afterglow emission intensity is slow that persists for several minutes and in the third part the there was almost constant afterglow emission intensity that last for more than 10 hours.

It is reported that the decay behavior can be fitted by an empirical equation stated as below [21]:

$$I = I_0 + A_1 \exp(t/\tau_1) + A_2 \exp(t/\tau_2) + A_3 \exp(t/\tau_3) \qquad 3.1$$

Where, I represents the phosphorescence intensity, I_0, A_1, A_2, A_3 are constants, t is time and τ_1, τ_2, τ_3 are the exponential decay components, respectively. Using the fitting functions,

these parameters τ_1, τ_2 and τ_3 can be calculated by simulating the decay curves of the phosphors prepared by different methods. The decay curves obtained in the experiments well fitted the above equations. According to the literature [21] that reports the long lasting mechanism of $CaAl_2O_4:Eu^{2+}/Dy^{3+}$, $SrAl_2O_4:Eu^{2+}/Dy^{3+}$ and $BaAl_2O_4:Eu^{2+}/Dy^{3+}$ phosphors according to the decay parameters τ, greater the value of τ, the longer is the afterglow duration. Three different values of τ obtained by simulating the decay curves indicate that there are three different types of traps and hence three kinds of decay processes. The largest value of τ_3 can be related to the deepest trap center and slowest the decay process. The value of τ_1, τ_2, and τ_3 for the samples are in the order of CB-1350>SS-1350>SG>CB-530, indicating that high temperature sintering helps to increase the emission centers, trap centers and deepen the trap centers that increase the afterglow duration.

Table 3.1. Phosphorescence intensity and its exponential decay parameters of $Sr_4Al_{14}O_{25}:Eu^{2+}/Dy^{3+}$ phosphor prepared by solid state, sol-gel and solution combustion methods.

Samples	Decay parameters						
	I_o	A_1	τ_1	A_2	τ_2	A_3	τ_3
CB-1350	3.68	2.4	13.50	0.95	155	0.350	1600
SS-1350	3.31	1.97	11.20	0.6	115	0.240	1200
SG-1200	0.64	0.35	8.75	0.2	145	0.075	900
CB-530	0.23	0.27	7.35	0.19	130	0.070	790

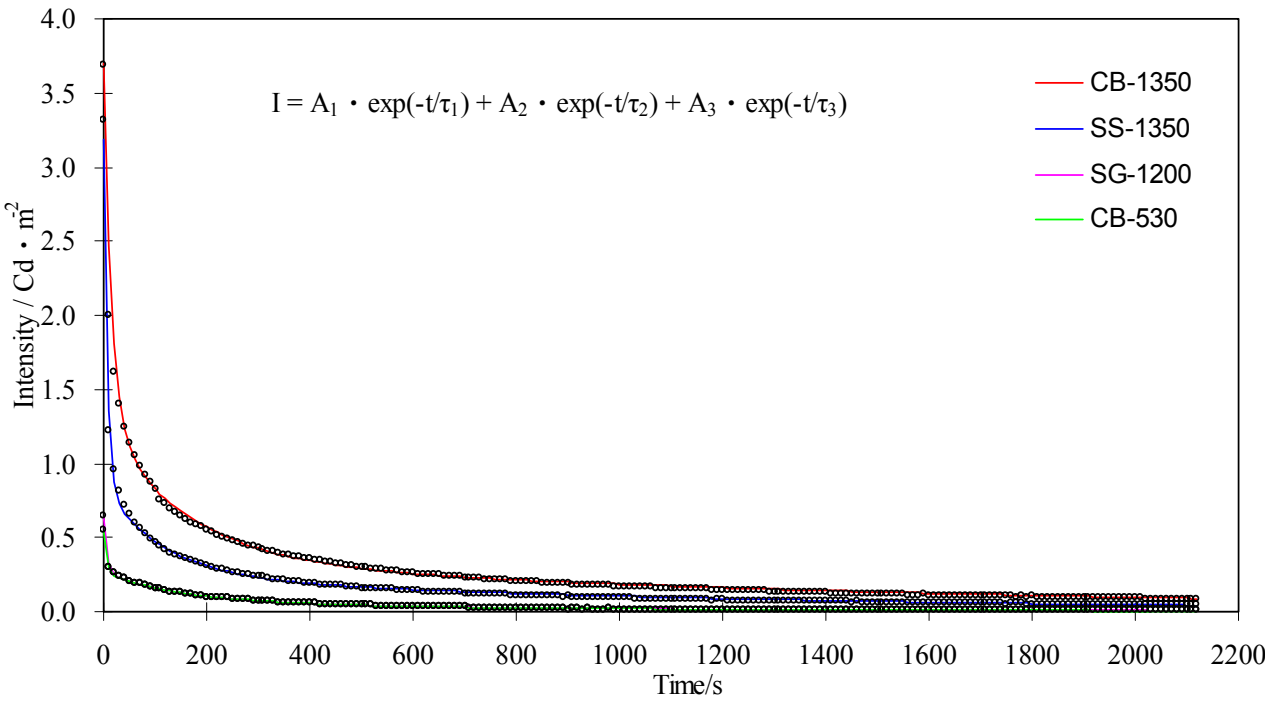

Fig. 3.4. Afterglow decay curves of $Sr_4Al_{14}O_{25}:Eu^{2+}/Dy^{3+}$ phosphors prepared by solid state, sol-gel and combustion methods (dots and solid lines are observed and fitted curves, respectively).

The mechanism of long persistent phosphorescence is shown in Fig. 3.5. The long persistent mechanism can be explained as; upon exposure to UV or visible light, the excitation transition of Eu^{2+} ions *i.e.* $4f^7 \rightarrow 4f^65d^1$ occurs immediately, causing large number of holes near the valence band and electrons near the conduction band. Some of the holes are transferred to the valence band and captured by Dy^{3+} ions located around the valance band to form Dy^{4+} ions. When the excitation light source is removed, the transition between $4f^65d^1 \rightarrow 4f^7$ is partly allowed. The holes trapped by Dy^{3+} are thermally released to valence band, since the trap depth of Dy^{3+} ions from valence band is shallow enough to liberate trapped holes at room temperatures, migrate these holes through valence band to the Eu^{1+} ions to form excited $(Eu^{2+})^*$ ions, and consequently, the recombination takes place leading to the long afterglow. Thus, the afterglow intensity depends on the number of holes released at room temperature and it's recombination with the excited europium ions $(Eu^{2+})^*$. On the other hand the afterglow life time depends on the depth of the holes trapped by the Dy^{3+} ions and hence the release rate of these trapped holes to the valence band. Higher the depth of hole traps, slower is the release rate and longer will be the afterglow time.

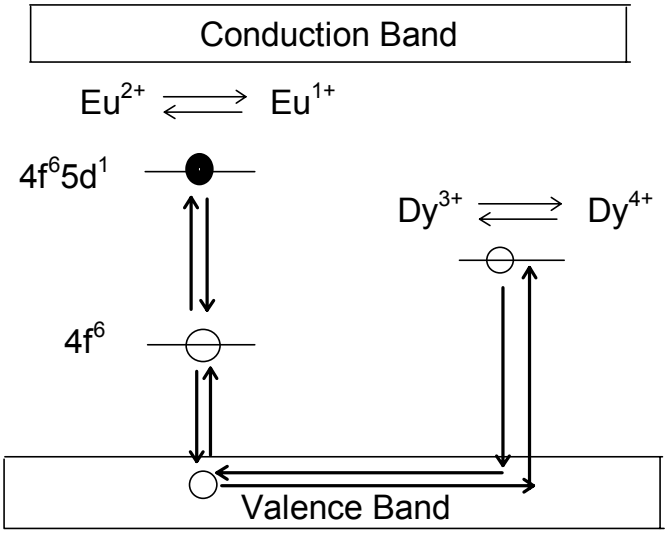

Fig. 3.5. Mechanism of long afterglow of $Sr_4Al_{14}O_{25}:Eu^{2+}/Dy^{3+}$phosphor according to the Matuzawa's model.

3.4. Conclusions

$Sr_4Al_{14}O_{25}:Eu^{2+}/Dy^{3+}$ phosphor was synthesized by sol-gel, chemical combustion and solid state reaction methods. At very low synthesis temperature (CB-530), some impurities of $SrAl_2O_4$ phase existed but at higher calcinations temperatures, pure $Sr_4Al_{14}O_{25}$ phase was observed, irrespective of the synthesis methods used. Relatively smaller particles size, regular morphology and narrow size distribution was achieved by wet chemical methods (sol-gel and chemical combustion). Even at the same sintering temperatures, the chemical combustion method can be used to generate smaller particles with regular particles morphology. By the chemical combustion method, activator ions can be homogenously dispersed throughout the phosphor matrix leading to the higher excitation, emission and afterglow intensities. Thus, chemical combustion method can be used for the large scale production of phosphor materials.

References

[1] J. Holsa, H. Jungner, M. Lastusaari, J. Niittykoski, J. Alloys Compd. **326** (2001) 323.

[2] W.Y. Jia, H.B. Yuan, L.Z. Lu, H.M. Liu, W.M. Yen, J. Cryst. Growth **200** (1999) 179.

[3] M. Peng, Z.W. Pei, G.G. Hong, Chem. Phys. Lett. **371** (2003) 1.

[4] Y.H. Lin, Z.T. Zhang, F. Zhang, Z.L. Tang, Q.M. Chen, Mater. Chem. Phys. **65** (2000) 103.

[5] A. Nag, T.R.N. Kutty, J. Alloys Compd. **354** (2003) 221.

[6] V. Shankar, H. Chander, H. Divi, P.K. Ghosh, US Patent 0183807 A1.

[7] D. Jia, Opt. Mater. **22** (2003) 65.

[8] T. Peng, L. Huajun, H. Yang, C. Yan, Mater. Chem. Phys. **85** (2004) 68.

[9] C.H. Lu, W.T. Hsu, C.H. Huang, S.V. Godbole, B.M. Cheng, Mater. Chem. Phys. **90** (2005) 62.

[10] Y. Pan, M. Wu, Q. Su, Mater. Sci. Eng. B **106** (2004) 251.

[11] Y. Chen, J. Wang, M. Gong, Q. Su, J. Solid State Chem. **180** (2007) 1165.

[12] Z. Chen, Y. Yan, J. Liu, Y. Yin, H. Wen, J. Zao, D. Liu, H. Tian, C. Zhang, S. Li, J. Alloys Compd. **473** (2009) L13.

[13] S. Wu, S. Zhang, J. Yang, Mater. Chem. Phys. **102** (2007) 80.

[14] C. Zhao, D. Chen, Y. Yuan, M. Wu, Mater. Sci. Eng. B **133** (2006) 200.

[15] H. Song, D. Chen, W. Tang, Y. Peng, Displays **29** (2008) 41.

[16] A. Saberi, F. Golestani-Fard, H. Sarpoolaky, M. Willert-Porada, T. Gerdes, R. Simon, J. Alloys Compd. **462** (2008) 142.

[17] R. P. Rao, J. Electrochem. Soc. **143** (1) (1996) 189.

[18] S.Ekambaram, M. Maaza, J. Alloys Compd. **395** (2005) 132.

[19] T.N. Nanzhina, E. A. Pobedimskaya, N.V. Belov, Krystallografiya **25** (1980) 938.

[20] Z. Tang, F. Zhang, Z. Zhang, C. Huang, Y. Lin, J. Eur. Ceram. Soc. **20** (2001) 14.

[21] Y.H. Lin, Z.T. Zhang, F. Zhang, Z.L. Tang, Mater. Chem. Phys. **70** (2000) 156.

Chapter IV

Synthesis and photoluminescence properties of Cr^{3+} doped $Sr_4Al_{14}O_{25}:Eu^{2+}/Dy^{3+}$ blue-green and red phosphor

4.1. Introduction

Recently, strontium aluminate phosphors activated by Eu^{2+} and Dy^{3+} ions have attracted a lot of attentions since they show excellent properties such as high quantum efficiency, long persistence of phosphorescence, good stability, suitable emitting color and no radio-active radiations, unlike previous Co or Pm co-doped ZnS based phosphors [1-7]. Due to excellent properties, Eu^{2+} and Dy^{3+} doped alkaline earth aluminates viz. $xSrO.yAl_2O_3:Eu^{2+}/Dy^{3+}$ phosphor result in wide potential applications in many fields. To highlight a few, one may include emergency signs and low level lightening escape systems, military applications, textile fibers, textile printings, lightening apparatus and switches, exit signboards, electronic instrument dial pads and other more [8-9]. For the better photoluminescence properties of these strontium aluminate phosphors, researches regarding the addition of various rare metal ions [10], other metal ions [11] and boric oxide [4] have been performed. However, the emission centers are limited in the rare earth metal ions, which are extremely expensive. Trivalent chromium (Cr^{3+}) is the most stable oxidation state of chromium, therefore widely used as luminescent dopant as well as luminescent sensitizer in various materials. Because of its low cost, deep color and bright luminescent properties, the potential application of Cr^{3+} in such phosphor materials is very high. Various Cr^{3+} doped host materials has been widely investigated and its emission in various compounds like YAG [12], $MgAl_2O_4$ [13], Mg_2SiO_4 [14], $ZnAl_2S_4$ [15] and many others [16] have been studied. However, there are very few reports [17] on the persistent emission of Cr^{3+} that may be used as persistent phosphors. Blue and green long persistent phosphors have been obtained using aluminates host system but better red persistent phosphors are still in search.

Zhong *et al.* [17] reported the existence of red phosphorescence by persistent energy transfer from Eu^{2+} to Cr^{3+} in strontium aluminates system. They used the solid state method

to prepare the phosphor. However, the solid state reaction method has been extensively used for the phosphor synthesis in spite of its poor homogeneity, high calcinations temperatures and long time of calcinations [18]. Furthermore, the phosphor particles prepared by this method is much bigger in the range of several tens of micrometers. To get smaller particle powder high energy grinding is required that destroy both the crystal structure and the photoluminescence properties.

Phosphor with smaller particles size can be synthesized by the liquid phase reaction methods like sol-gel, co-precipitation [19], microwave [20] and combustion [21] *etc*. The combustion method to prepare rare earth activated alkaline earth aluminates is an efficient and facile method, which takes hardly few minutes and has been extensively used for the mass production of various oxides and aluminates materials [21-24]. Further, combustion method is a liquid phase synthesis method in which each component can be accurately controlled and uniformly mixed to get the homogenous materials. The combustion synthesis technique makes use of heat released during the redox exothermic reactions between metal nitrate precursors and fuels like urea [25] and completely reduces Eu^{3+} to Eu^{2+} at relatively low temperature, unlike high temperature solid state reaction method. So in this chapter, a rapid, facile combustion synthesis method has been applied to prepare the $Sr_4Al_{14}O_{25}:Eu^{2+}/Dy^{3+}/Cr^{3+}$ nano powder. The effect of compositions of starting materials, boric acid as flux, Eu^{2+}, Dy^{3+} and Cr^{3+} as dopants-co-dopants in the $Sr_4Al_{14}O_{25}$ host on the optical properties of the phosphor has been presented in detail.

4.2. Experimental

4.2.1. Sample preparation

Synthesis of strontium aluminate phosphors doped with Eu^{2+}, Dy^{3+} and Cr^{3+} ions by aqueous chemical combustion method involves rapidly heating the aqueous solution containing stoichometric amounts of corresponding metal nitrates, ammonium nitrate and urea at 530^{o}C temperature. Stoichometric compositions of the redox mixture for solution combustion were calculated using total oxidizing and reducing valences of the species which serves as the numerical coefficients for the stoichometric balance so that equivalence ratio of oxidant to reductant is unity [25]. Thus the stoichometry for the $Sr_4Al_{14}O_{25}$ material becomes 4 $Sr(NO_3)_2$ (Aldrich, 99.9+ %) + 14 $Al(NO_3)_3$(Aldrich, 99.9%) + NH_4NO_3

(Aldrich, >99%) + 42 NH_2CONH_2 (Aldrich, 99.9%). In the typical experiment, the combustion synthesis of $Sr_4Al_{14}O_{25}:Eu^{2+}/Dy^{3+}/ Cr^{3+}$ is as follows; 5.66g $Sr(NO_3)_2$ + 35.5g $Al(NO_3)_3$ + 0.54g NH_4NO_3 + 0.028g $Eu(NO_3)_3$ + 0.0585g $Dy(NO_3)_3$ + 0.11g $Cr(NO_3)_3$ + 0.165g H_3BO_3 + 17.10g urea were dissolved in minimum amount of distilled water at 70°C by stirring for 2 h. Then the beaker containing the mixture was inserted inside a muffle furnace maintained at 530°C for nearly 10 minutes. Initially, the solution boiled, frothed, foamed and caught fire. Then the fire propagates to its own leading to the completion of reaction in less than five minutes. The final foamy voluminous product was crushed and used for characterization such as phase analysis, crystallinity, morphology and photoluminescence properties. To get the highly crystalline persistent red phosphor, the precursor powder was again sintered at 1300°C in the form of small pellets in slightly reducing atmosphere of 10 % H_2 and 90 % N_2 for 3 h. The whole synthetic process can be explained by the flow chart in Fig. 4.1.

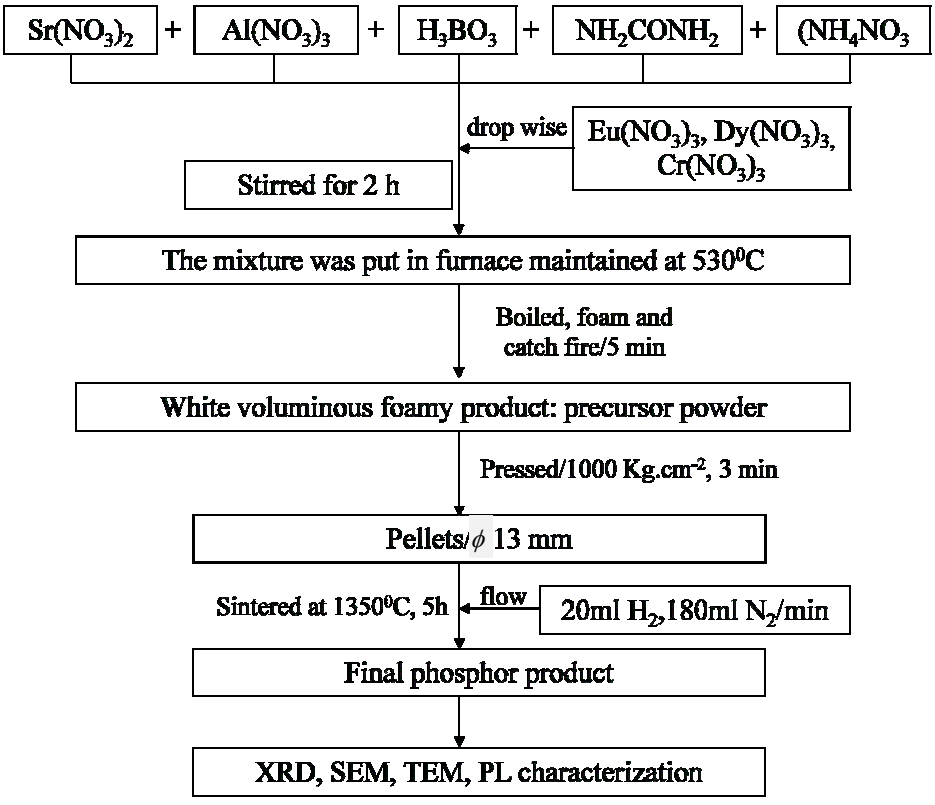

Fig. 4.1 Preparation of $Sr_4Al_{14}O_{25}:Eu^{2+}/Dy^{3+}/Cr^{3+}$ nanometer powder by solution combustion method.

4.2.2. Characterization

Phase identification was carried out using a Shimadzu XRD-630D X-ray diffractometer with Cu-Kα radiation. The morphology of the phosphor particles were characterized by scanning electron microscopy (SEM) and transmission electron microscopy (TEM). SEM measurements were conducted using a Hitachi S-3000N SEM instrument. TEM image was obtained on a Hitachi H-800MU microscope. Photoluminescence (PL) spectra (absorption and emission) were recorded using USB 4000-UV-VIS fiber optic spectrometer (Ocean optics). The afterglow decay curves were obtained by using a brightness meter (Konica Minolta LS-100) equipped with RS232C Comm. Before phosphorescence and afterglow decay curves measurements each phosphor samples were excited by 15W Xenon lamp for 20 minutes and measurements were recorded 10 seconds after the excitation light was removed. All the measurements were carried out at room temperatures.

4.3. Results and discussion

A typical X-ray diffraction pattern of the precursor powder prepared by combustion method at 530^{o}C (for 10 minutes) and combustion powder post annealed phosphor at 1300^{o}C (for 3 h) were shown in Fig. 4.2(a and b), respectively. In Fig 4.2(a), the diffraction peaks of $Sr_4Al_{14}O_{25}$ phase (JCPDS; 52-1876) along with the peaks of $SrAl_2O_4$ (JCPDS; 34-0379) and $SrAl_4O_7$ (JCPDS; 30-1276) were observed. Even though the starting materials were mixed according to the chemical composition of $Sr_4Al_{14}O_{25}$, other phases like $SrAl_2O_4$ and $SrAl_4O_7$ could be formed at low-temperature combustion process. So the precursor powder was further annealed at 1300^{o}C for 3 h in a reducing atmosphere of 10% H_2 and 90% N_2 to get highly crystalline, pure $Sr_4Al_{14}O_{25}$ phase. The $Sr_4Al_{14}O_{25}$ phosphor consists of orthorhombic crystal structure with *Pmma* space group [26]. The cell parameters calculated from X-ray results were a = 24.78$\dot{A}$, b = 8.48$\dot{A}$ and c = 4.86$\dot{A}$. These values are in good agreements with the literature values [26].

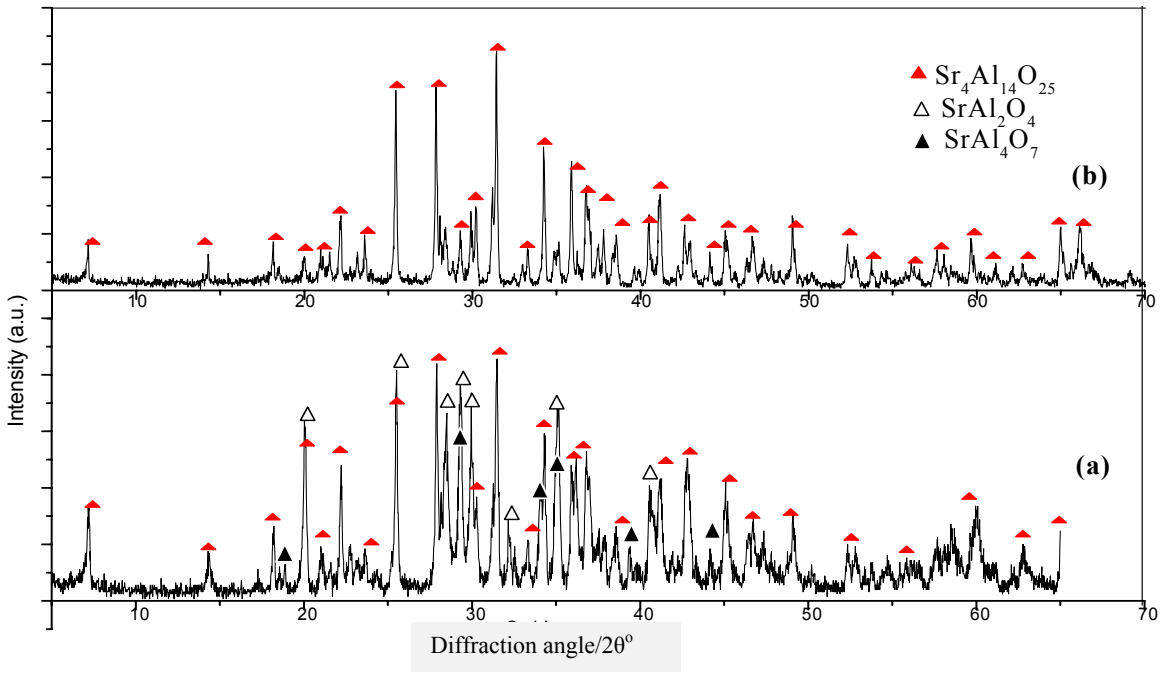

Fig. 4.2. XRD spectra of 4 at% Cr^{3+} doped $Sr_4Al_{14}O_{25}$:Eu^2/Dy^{3+} phosphor powders (a) precursor powder prepared at 530°C (b) target powder post annealed at 1300°C.

Figure 4.3 (a-d) shows the SEM and TEM micrographs of the as prepared precursor powder at 530°C and the post annealed phosphor powder at 1300°C. The precursor powder showed irregular to hexagonal particles with lots of cracks, voids and pores on the surface formed due to escaping of various gases like CO_x, NO_x, NH_3 during the combustion of precursor nitrates and fuels. The mean grain size of the precursor powders was about 200 nm. Further, the shape and size of the precursor powder was confirmed by TEM micrograph as shown in Fig. 4.3(d). The particle was of octahedral shape with edge length of nearly 200 nm. Compared with the phosphor prepared by traditional solid state reaction method, the particle size was greatly reduced but the crystallinity was poor due to low firing temperature. To get better crystallinity, the precursor powder was post annealed at 1350°C in 10% H_2 and 90%N_2. Even though, the post annealing at 1350°C sharply increased the mean particle size from 200 nm to nearly 2 μm, the octahedral shape retained same as precursor powder. The post annealed phosphor particles were highly crystalline with sharp boundaries as shown in Fig. 4.3(b). Even though post annealing at high temperature increased the phosphor particles roughly 10 times than the precursor powder, the phosphor particles are much smaller than the particles prepared by solid state reaction method at the same temperature and it had regular morphology as revealed in the Fig. 4.3. Thus, chemical

combustion method can be used to generate fine particles with higher crystallinity at relatively lower temperature than solid state reaction method.

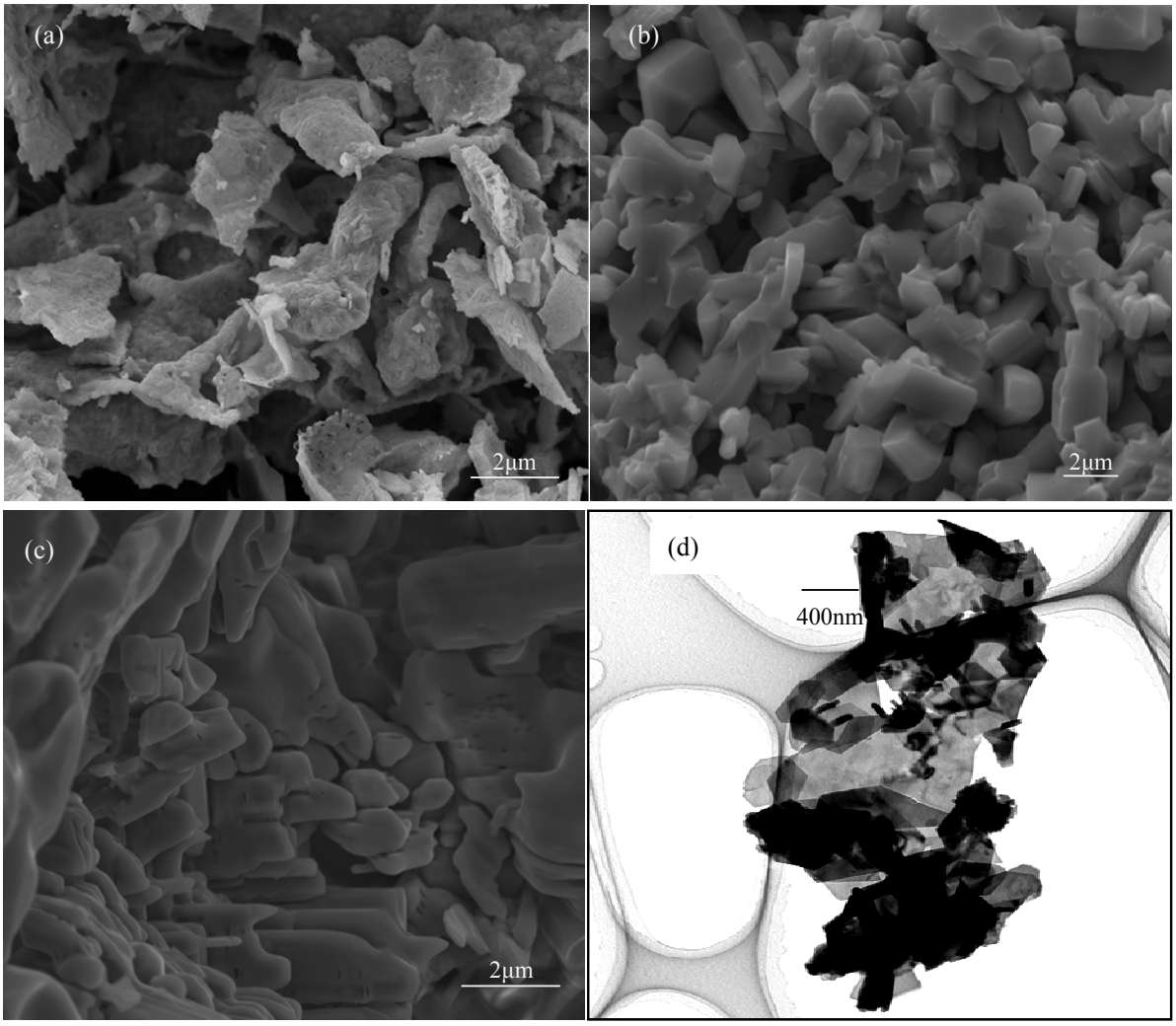

Fig. 4.3. SEM micrograph of 4 at% Cr doped $Sr_4Al_{14}O_{25}:Eu^{2+}/Dy^{3+}$ phosphor: (a) precursor powder derived via combustion method at 530^{o}C, (b) post annealed phosphor at 1300^{o}C, (c) solid state at 1300^{o}C and (d) TEM microstructure of precursor powder.

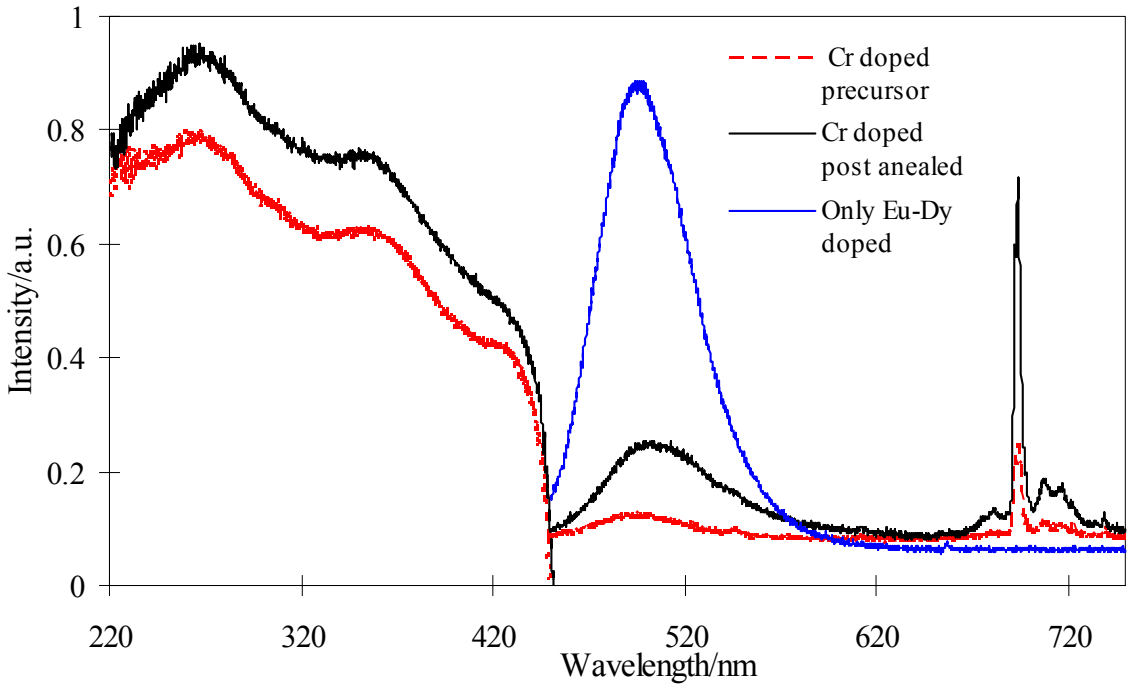

Fig. 4.4. Absorbance and emission spectra of $Sr_4Al_{14}O_{25}$:4 at% $Cr^{3+}/Eu^{2+}/Dy^{3+}$ phosphor compared with $Sr_4Al_{14}O_{25}:Eu^{2+}/Dy^{3+}$ phosphor (dotted lines and solid lines represents precursor powder and post annealed phosphors, respectively.

Absorption and emission spectra of the $Sr_4Al_{14}O_{25}:Cr^{3+}/Eu^{2+}/Dy^{3+}$ phosphors are shown in Fig. 4.4. The absorption spectrum was a broad band ranging from 220 nm to 430 nm, with maxima at 270 and 367 nm. The excitation spectrum is attributed to the typical f to d transition of Eu^{2+} ions in the $Sr_4Al_{14}O_{25}$ matrix. The emission spectrum of $Sr_4Al_{14}O_{25}$:4 at%Eu^{2+}/8 at% Dy^{3+} phosphor prepared at 1300^{o}C consists of a strong broad band emission centered at 497 nm. However, Cr^{3+} doped precursor powder and the post annealed $Sr_4Al_{14}O_{25}$:4 at% $Cr^{3+}/Eu^{2+}/Dy^{3+}$ phosphor consists of a strong broad band emission at 497 nm and a sharp emission peak at 695 nm. The broad band emission at 497 nm in these samples was attributed to a typical $4f^65d^1 \rightarrow 4f^7$ transition of Eu^{2+} ions in the $Sr_4Al_{14}O_{25}$ host [26]. No any emission peaks of Eu^{3+} were observed in the emission spectra, indicating that Eu^{3+} ions in these samples were completely reduced to Eu^{2+}. The sharp emission peak at 695 nm in these Cr^{3+} doped phosphors besides the broad band emission at 497 nm was due to the $^2E_2$-$^4A_2$ transition in the Cr^{3+} ions doped in the $Sr_4Al_{14}O_{25}$ phosphor [17]. It is clear from Fig. 4.4 that the emission intensity at 497 nm was sharply reduced by addition of Cr^{3+} ions,

the reason of that will be discussed later. Further, the emission intensity of post annealed phosphor was higher than the combustion precursor powder due to the higher crystallinity and pure $Sr_4Al_{14}O_{25}$ phase formation as observed in the XRD results. It is reported that 200-400 nm UV light can excite only Eu^{2+} but not Cr^{3+}, since Cr^{3+} excitation consists of the $^4A_2$-$^4T_1$ absorption at 420 nm and $^4A_2$-$^4T_2$ absorption at 570 nm [17]. Thus, the strong red emission at 695 nm should be the result of energy transfer from Eu^{2+} to Cr^{3+} in the $Sr_4Al_{14}O_{25}$ phosphor.

Figure 4.5 depicts the emission spectra of $Sr_4Al_{14}O_{25}:Eu^{2+}/Dy^{3+}/Cr^{3+}$ phosphor according to the Eu^{2+} ions concentration while maintaining 4 at% Cr^{3+} ions concentration. From the figure, it is seen that the red emission of Cr^{3+} at 695 nm increased with Eu^{2+} ions concentrations from 0.5 at% to 4 at%. This strongly indicates the energy transfer from Eu^{2+} to Cr^{3+} in $Sr_4Al_{14}O_{25}:Eu^{2+}/Dy^{3+}/Cr^{3+}$ phosphor increased with the Eu^{2+} ions concentration. A similar result was obtained by Zhong *et al.* [17] in solid state samples of the same $Sr_4Al_{14}O_{25}:Eu^{2+}/Dy^{3+}/Cr^{3+}$ phosphor. Fig. 4.5 also shows the effect of Eu^{2+} concentrations on the emission intensities of Eu^{2+} at 497 nm. The effect was highly pronounced in the emission in the blue-green emission (497 nm) than in red which increased on increasing Eu^{2+} concentrations, attained maximum at 4 at% Eu^{2+} and then on further increasing Eu^{2+} concentrations, it started decreasing. The decrease in emission intensity beyond 4 at% Eu^{2+} concentrations might be due to the concentration quenching process. Increased Eu^{2+} ions in the $Sr_4Al_{14}O_{25}:Eu^{2+}/Dy^{3+}$ phosphor decreased the distance between these ions and leads efficient energy transfer from one Eu^{2+} ion to another Eu^{2+} ion and finally to the non luminescent center leading to the quenching of the emission [27].

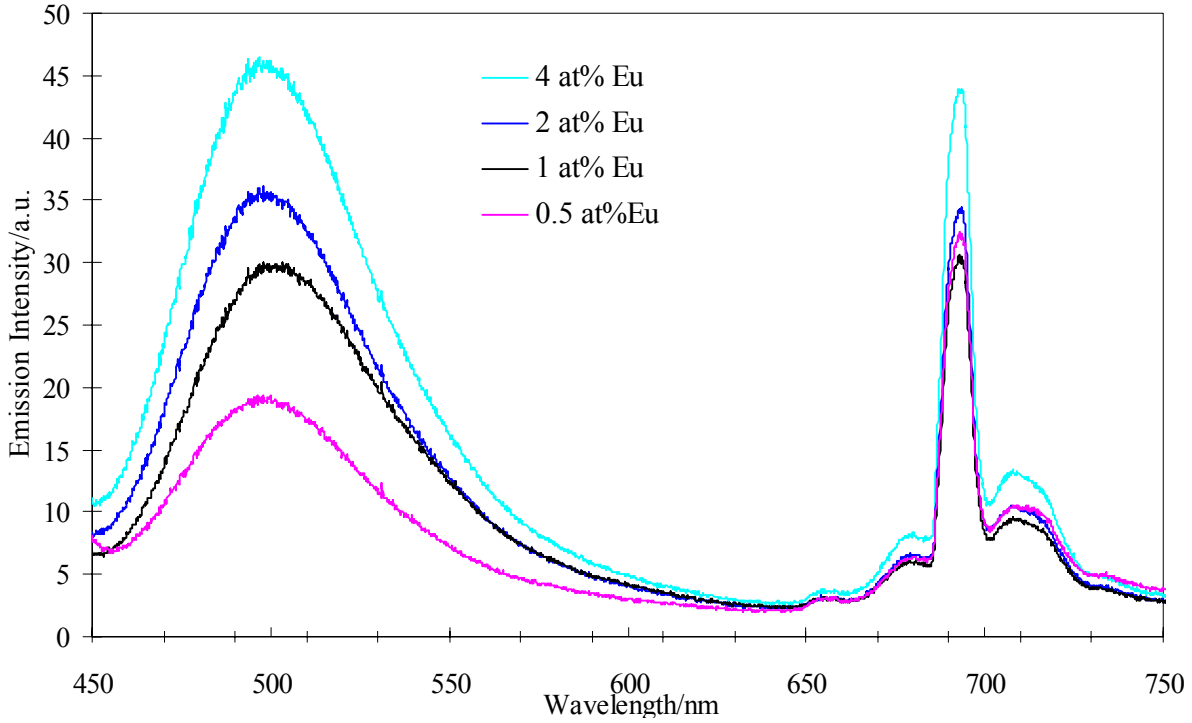

Fig. 4.5. Effect of Eu^{2+} ions concentrations on the emission intensity of 4 at% Cr^{3+} doped $Sr_4Al_{14}O_{25}:Eu^{2+}/Dy^{3+}$ phosphor derived via combustion method at 1300°C.

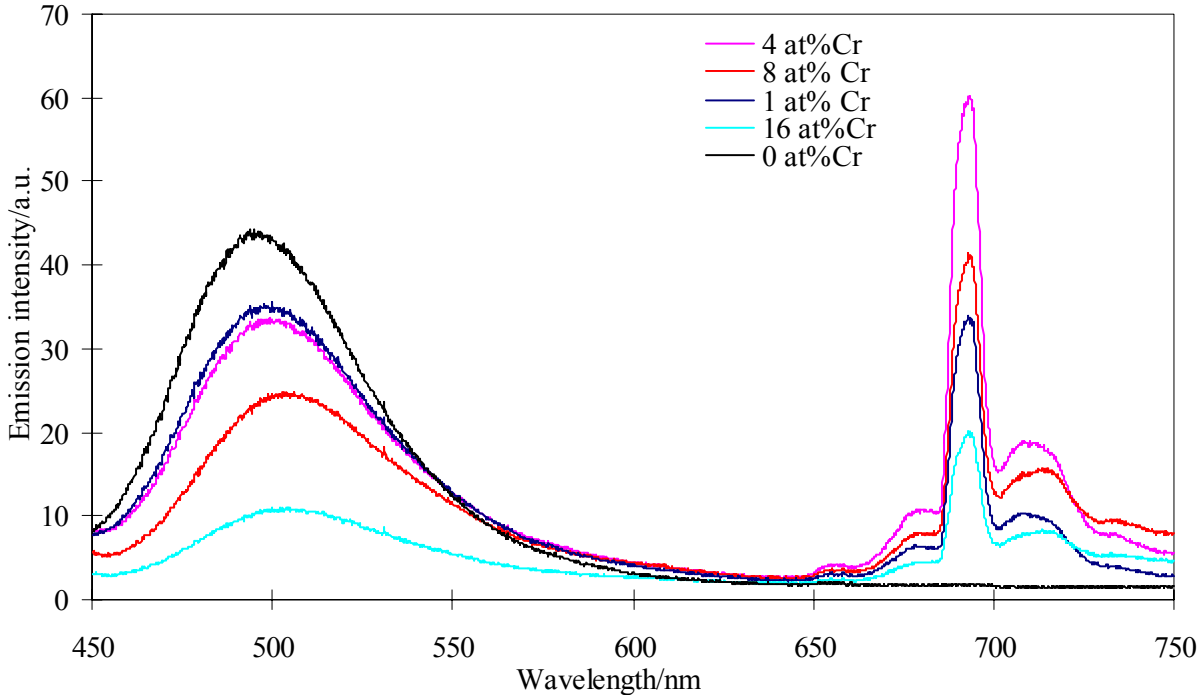

Fig. 4.6. Effect of Cr^{3+} ion concentration on the emission intensity of the $Sr_4Al_{14}O_{25}$:x at%Cr^{3+}/1 at% Eu^{2+}/2 at% Dy^{3+} phosphor prepared via combustion method at 1300°C.

Figure 4.6 shows the emission spectra of $Sr_4Al_{14}O_{25}$: 1 at% Eu^{2+}/2 at% Dy^{3+}/x at% Cr^{3+} (x=0, 1, 4, 8 and 16) phosphor. While maintaining 1 at% Eu^{2+} and 2 at% Dy^{3+} ions concentration and increasing the Cr^{3+} ions concentration, the red emissions at 695 nm enhanced gradually, indicating the increase of Eu^{2+} to Cr^{3+} energy transfer efficiencies. As the Cr^{3+} ions concentrations increased, the distance between Eu^{2+} to Cr^{3+} ions decreased that increased energy transfer process. While changing the concentrations of Cr^{3+} ions, the shapes and positions of the emission bands had exhibited no obvious change. The Cr^{3+} ion concentration might be low enough to shift the peak position at the present study. Further, addition of Cr^{3+} ions concentration decreased the emission intensity of Cr^{3+} at 695 nm and it became almost non-emissive when doped Cr^{3+} concentration was very high (~ 50 at%). The critical quenching concentration of Cr^{3+} is defined as the concentration of doped Cr^{3+} ions at which the emission intensity begins to decrease. From the Fig. 4.6, it is concluded that the critical concentration of Cr^{3+} is 4 at% in the $Sr_4Al_{14}O_{25}$:Eu^{2+}/Dy^{3+}/Cr^{3+} phosphor. The quenching mechanism might be explained as; with the increase of Cr^{3+} ions concentration, the distance between nearby Cr^{3+} ions decreases and hence increases the mutual interaction between it. This lead to the migration of excitation energy from one activator center to another and eventually to an imperfection which may acts as energy sink and results in killing of its luminescence [28].

Figure 4.7 shows the effect of boric acid (as a flux) concentration on the emission intensities of $Sr_4Al_{14}O_{25}$:Eu^{2+}/Dy^{3+}/Cr^{3+} phosphor containing 4 at% Cr^{3+}, 1 at% Eu^{2+} and 2 at% Dy^{3+}. On increasing boric acid concentration, the emission intensity first increased, attained maximum at 3.5 mol% and then decreased again when it was further increased. As described in chapter II, addition of boric acid flux promotes the formation of $Sr_4Al_{14}O_{25}$ and helps the dopants to disperse homogeneously throughout the host lattice [29]. If boric acid concentration was very low there was formation of $SrAl_2O_4$ phase together with $Sr_4Al_{14}O_{25}$ phase. The Eu^{2+} ions in $SrAl_2O_4$ host emits at 520 nm, which was reflected in the emission curve in Fig. 4.7 by the red shift in the emission maximum. When boric acid concentration was 3.5 mol%, highly crystalline single phase $Sr_4Al_{14}O_{25}$ phosphor was formed and hence produced higher emission intensity. However, as boric acid concentration was increased to 8.5 mol%, there was formation of strontium aluminoborate and glassy phases along with the $Sr_4Al_{14}O_{25}$ phase. The former two are non emissive. As a result, there was decrease in the

emission intensity. The detailed study on the effect of flux on the photoluminescence properties of strontium aluminate phosphor has been explained in chapter II.

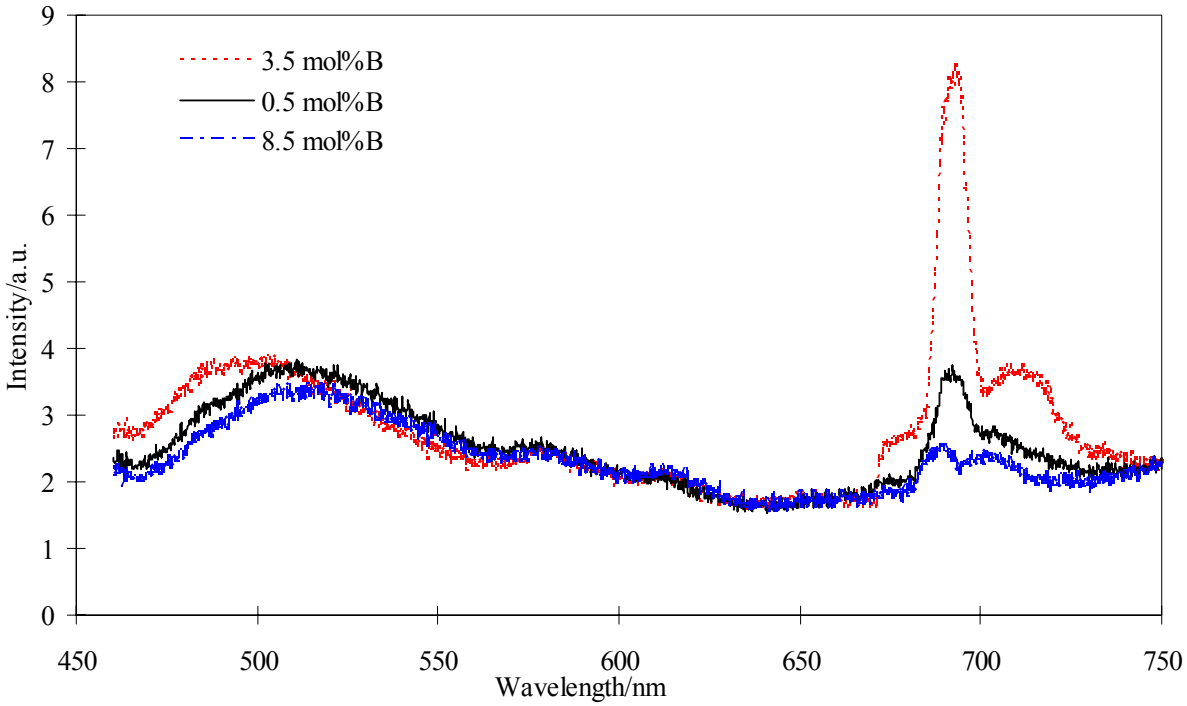

Fig. 4.7. Effect of boric acid contents as a flux in the photoluminescence intensity of 4 at% Cr^{3+} doped $Sr_4Al_{14}O_{25}$: Eu^{2+}/Dy^{3+} phosphor prepared via combustion method at 1300°C.

Figure 4.8 shows the afterglow decay curves of the blue-green emission at 495 nm and the red emission at 695 nm in the post annealed $Sr_4Al_{14}O_{25}$:4at% Cr^{3+}/1at% Eu^{2+}/2at% Dy^{3+} phosphor after irradiation with 15W xenon lamp for 20 minutes. The afterglow decay curves in both the cases decreased rapidly at the first part of the decay curves that reduced the phosphorescence intensity to about $1/10^{th}$ within few seconds. The decrease in the second part was slow which persists for several minutes and in the third part of the spectrum, the decay of the afterglow intensity was very slow. Further, the afterglow decay rate of the red phosphorescence was much faster than that of the blue-green one. The blue-green phosphorescence persisted for longer than 10 h but red phosphorescence elapsed within few seconds.

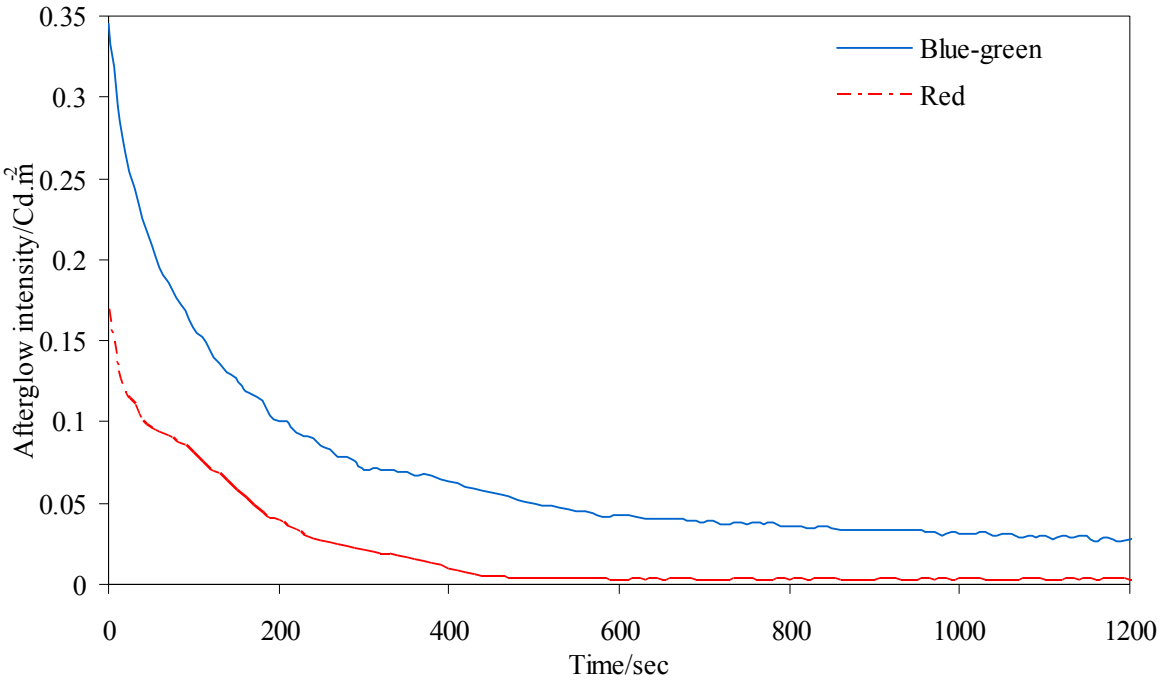

Fig. 4.8. Afterglow decay curves for blue green and red emission of 4 at% Cr^{3+} doped $Sr_4Al_{14}O_{25}:Eu^{2+}/Dy^{3+}$ phosphor derived via combustion method at 1300°C.

In the $Sr_4Al_{14}O_{25}:Eu^{2+}/Dy^{3+}/Cr^{3+}$ phosphor, Dy^{3+} acts as trap centers, capturing the free holes similar in other aluminates system [29-31]. On adding impurities or additives (Eu^{2+}, Dy^{3+} and Cr^{3+}), Eu^{2+} and Dy^{3+} replace Sr^{2+} site while Cr^{3+} occupy Al site by replacing it [17, 26], there exist two types of Dy^{3+}, one surrounded all around by Al, called Dy1 and another by at least one near neighboring Cr (came from replacement of Al), called Dy2. Incorporation of Cr^{3+} ions in the host produces shallow hole traps nearby Dy traps. It is suggested that the former trap is deeper than the later *i.e.* Dy1 traps are deeper than Dy2 traps [17]. For simplicity, the energy transfer process from Eu^{2+} to Cr^{3+} ions may be considered as two parts, the first part being the short range energy transfer between Eu^{2+} and Cr^{3+} ions. In this case, Eu^{2+} ion is surrounded by both Dy1 and Dy2 at a short distance, leading both Dy1 and Dy2 to contribute to phosphorescence. The second part is named as long range energy transfer between two ions. In this case, Eu^{2+} is surrounded by Dy1 at short distance leading only Dy1 for phosphorescence. Due to the efficient energy transfer in short distance, the red afterglow is mainly generated by those Cr^{3+} ions close to Eu^{2+} ions and negligibly by those far from it. Therefore, the red phosphorescence decays faster as

determined by the incorporation of Dy1 and shallow trap Dy2 induced by Cr^{3+} ions. The detail mechanism is shown in Fig. 4.9.

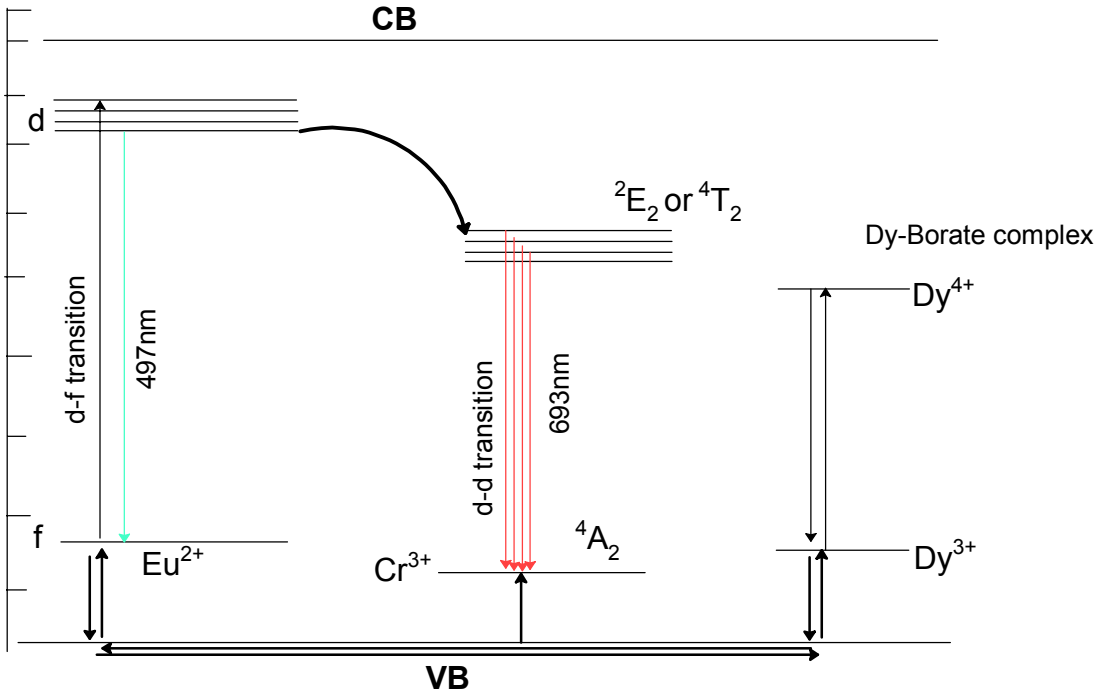

Fig. 4.9. Mechanism of blue green and red emissions and their afterglow in Cr^{3+} doped $Sr_4Al_{14}O_{25}:Eu^{2+}/Dy^{3+}$ phosphor.

4.4. Conclusions

Cr^{3+} co-activated $Sr_4Al_{14}O_{25}:Eu^{2+}/Dy^{3+}$ persistent phosphor was synthesized by rapid chemical combustion method. As compared to the solid reaction state method, combustion method generates particles with smaller particles size and regular morphology. The red emission of Cr^{3+} at 695 nm and blue-green emission of Eu^{2+} at 495 nm were observed in this phosphor. The blue-green emission was due to the $4f^65d^1 \rightarrow 4f^7$ transition of Eu^{2+} ions in the $Sr_4Al_{14}O_{25}$ host while the red emission in Cr^{3+} was observed due to energy transfer from Eu^{2+} to nearby Cr^{3+} ions. As the concentration of Eu^{2+} and Dy^{3+} were fixed, the red emission intensity of Cr^{3+} increased on increasing Cr^{3+} ions concentration and attained maximum at 4 at%, beyond that it decreased due to concentration quenching process. The energy transfer process was found to be more efficient when the doped Eu^{2+} ions concentration was 4 at%. When the phosphor was prepared by adding 3.5 mol% boric acid as a flux better

photoluminescence properties were observed. The phosphor exhibited red phosphorescence at 695 nm and blue-green phosphorescence at 497 nm similar to the fluorescence spectra. The red phosphorescence decayed much faster than the blue-green phosphorescence. The faster decay speed of red phosphorescence in the Cr^{3+} was due to existence of shallow traps nearby Cr^{3+} ions. The persistent time for blue-green emission was more than 10 h but that of red was comparatively very short.

References

[1] J. Lin, Y. Huang, J. Zhang, F. Shi, S. Wei, J. Gao, Z. Huang, X. Ding, C. Tang, Mater. Chem. Phys. **10** (2008) 440.

[2] W.Y. Jia, H.B. Yuan, L.Z. Lu, H.M. Liu, W.M. Yen, J. Cryst. Growth **200** (1999) 179.

[3] J. Holsa, H. Jungner, M. Lastusaari, J. Niittykoski, J. Alloys Compd. **323-324** (2001) 326.

[4] Y.L. Chang, H.I. Hsiang, M.T. Liang, J. Alloys Compd. **461** (2008) 598.

[5] A. Nag, T.R.N. Kutty, J. Alloys Compd. **354** (2003) 221.

[6] M.Y. Peng, Z.W. Pei, G.G. Hong, Chem. Phys. Lett. **371** (2003) 1.

[7] Y.H. Lin, Z.T. Zhang, F. Zhang, Z.L. Tang, Q.M. Chen, Mater. Chem. Phys. **65** (2000) 103.

[8] D. Jia, Opt. Mater. **22** (2003) 65.

[9] V. Shankar, H. Chander, H. Divi, P.K. Ghosh, US Patent 0183807 A1.

[10] R. Chen, Y. Wang, Y. Hu, Z. Hu, C. Liu, J. Lumin. **128** (2008) 1180.

[11] S.D. Han, K.C. Singh, T.Y. Cho, H.S. Lee, D. Jakhar, J.P. Hulme, C.H. Han, J.D. Kim, I.S. Chun, J. Gwak, J. Lumin. **128** (2008) 301.

[12] Z. Ruixia, Z. Jiahua, S. Lu, W. X. Jun, J. Lumin. **119-120** (2006) 327.

[13] T. L. Phan, M. H. Phan, S. C. Yu, Phys.Stat.Sol. (b) **241** (2004) 434.

[14] S.M. Kaczmarek, W. Chen, G. Boulon, Cryst. Res. Technol. **41** (2006) 41.

[15] E. Broussell, L. Fortina, S. Kulyuk, A. Popov, R. Anedda, J. Appl. Phys. **84** (1998) 531.

[16] V. Singh, R.P.S. Chakradhar, J.L. Rao, J. J. Zhu, Mater. Chem. Phys. **111** (2008) 143.

[17] Z. Ruixia, Z. Jiahua, S. Lu, W. Xiao-jun, Appl. Phys. Lett. **88** (2006) 201916.

[18] L.S. Cavalcante, A.Z. Simões, J.C. Sczancoski, V.M. Longo, R. Erlo, M.T. Escote, E. Longo, J.A. Varela, Solid State Sci. **9** (2007) 1020.

[19] Z. Wu, M. Gong, J. Shi, Q. Su, J. Alloys Compd. **458** (2007) 134.

[20] S. Wu, S. Zhang, J. Yang, Mater. Chem. Phys. **102** (2007) 80.

[21] C. Zhao, D. Chen, Y. Yuan, M. Wu, Mater. Sci. Eng. B, **133** (2006) 200.

[22] H. Song, D. Chen, W. Tang, Y. Peng, Displays **49** (2008) 41.

[23] A. Saberi, F. Golestani-Fard, H. Sarpoolaky, M. Willert-Porada, T. Gerdes, R. Simon, J. Alloys Compd. **462** (2007) 142.

[24] Y. Pan, M. Wu, Q. Su, Mater. Sci. Eng. B **106** (2004) 251.

[25] S.Ekambaram, M. Maaza, J. Alloy Compd. **395** (2005) 132.

[26] G. Blasse, B.C. Grabmailer, Luminescent Materials, Springer, (1994) 120.

[27] D. Wang, Q. Yin, Y. Li, M. Wang, J. Lumin. **97** (2002) 1.

[28] D.L. Dexter, J. Chem. Phys. **22** (1954) 1063.

[29] C.K. Chang, L. Jiang, D.L. Feng, Ceramics International **30** (2004) 285.

[30] Y. Lin, Z. Tang, Z. Zhang, Mater. Lett. **52** (2001) 14.

[31] T. Aitasalo, P. Deren, J. Hosla, H. Jungner, J.C. Krupa, M. Lastusaari, J. Legendziewicz, J. Niittykoski, W. Strek, J. Solid state Chem. **171** (2003) 114.

Chapter V

Preparation of a novel $Sr_4Al_{14}O_{25}:Sm^{3+}$ phosphor and its optical investigations

5.1. Introduction

Of the phosphors, the alkali earth aluminates containing rare earth ions are functional inorganic materials with strong luminescence in the blue to red regions of the spectrum [1-3]. These materials are widely used in the illumination, the displays, storage devices, medical instruments and many more [4]. To highlight a few, one may include "glow-in-dark items" as; safe helmets, direction indicators and signs, plasma display panel, cathode ray tubes, vacuum fluorescent display, scintillators, optical fibers, amplifiers and the like due to their better safe, chemical stability, excellent photo resistance, high quantum yield, very bright and long-lasting afterglow with no radio-active radiations and hence forms the important materials in various ceramics industries [5]. In recent years, strontium aluminates, especially $SrAl_2O_4$ and $Sr_4Al_{14}O_{25}$, doped with rare earth ions (Eu^{2+}, Ce^{3+}, *etc.*) have been regarded as an excellent phosphor due to their excellent luminescence, long persistent time and very high quantum yield and are already in some applications [6]. Many reports have been already published regarding preparations and improvements on the photoluminescence properties of these phosphors [1-3, 7]. However, Sm^{3+}-doped materials are less studied compared to the other trivalent rare earths metal ions and in particular, the spectroscopic studies of Sm^{3+} ions in the aluminates host are rarely reported [8-11]. To the best of our knowledge, there is no report on the $Sr_4Al_{14}O_{25}:Sm^{3+}$ phosphor which emits in the orange-red region. From the practical applications point of view, the longer wavelength side (orange-red) of the emission is more suitable source for illuminating devices, and is applicable for various displays. This motivated me to explore the photoluminescence properties of Sm^{3+} ions in the well known $Sr_4Al_{14}O_{25}$ phosphor. In this chapter, the effect of calcinations temperature, proper amount of flux and appropriate concentrations of dopant and co-dopant for the optimum photoluminescence properties has been explained in detail.

Experimental

5.1.1. Sample preparation

Strontium aluminate phosphor doped with Sm^{3+} ions ($Sr_4Al_{14}O_{25}:Sm^{3+}$) was synthesized by the reaction between strontium carbonate ($SrCO_3$; Aldrich, 99.9+ %), aluminium oxide (Al_2O_3 Baikalox ultrafine powder) and samarium oxide (Sm_2O_3; Aldrich, 99.9+ %). Bismuth oxide (Bi_2O_3; Aldrich, 99.9+ %), neodymium oxide (Nd_2O_3; Aldrich, 99.9+ %) and dysprosium oxide (Dy_2O_3; Aldrich, 99.9+ %) were used as co-dopant. Small amount of boric acid (H_3BO_3; AR) was added in the mixture as a high temperature flux. These powders were mixed according to the nominal composition of (4-x)$SrCO_3$ + 7Al_2O_3 + 0-10 mol % B (as H_3BO_3) + x at% Sm (x = 1, 2, 4 and 8 at %). The mixing was performed thoroughly by mortar and pestle with the help of ethanol and dried to get fine powder. Pellets were prepared and preheated in air atmosphere at 1000^oC for 4 h, followed by 1300^oC for 5 h in 10% H_2 and 90% N_2 atmosphere.

5.1.2. Characterization

Phase identification was carried out using a Shimadzu XRD-630D instrument with Cu-Kα radiation. Scanning Electron Microscopy (SEM) observations were carried out using a Hitachi S-3000N SEM instrument. Elemental analysis and mass percentage of the doped ions was estimated using EDX coupled with SEM. Before SEM measurements, the sample was coated roughly 5 nm in thickness with platinum using Hitachi E-1030 ion sputter. Photoluminescence absorption and emission spectra were recorded using USB 4000 UV-VIS-NIR miniature fiber optic spectrometer (Ocean optics). The afterglow intensity and decay curves were recorded by a brightness meter (Konica Minolta LS-100). Before decay curves measurement, each sample was exposed to normal 15W Xenon lamp for 20 minutes. All the measurements were carried out at room temperature.

5.2. Results and discussion

The X-ray diffraction patterns of the as prepared $Sr_4Al_{14}O_{25}:Sm^{3+}$ phosphor is shown in Fig. 5.1. The diffraction peaks coincide well with the standard JCPDS card database number 52-1876 of $Sr_4Al_{14}O_{25}$ phase. The peaks of Sm_2O_3 were not observed in the

diffractogram indicating that all the Sm^{3+} ions occupied Sr^{2+} sites in the $Sr_4Al_{14}O_{25}$ matrix. The ionic radius of Al^{3+}, Sr^{2+} and Sm^{3+} ions in the $Sr_4Al_{14}O_{25}$ matrix are 67 pm, 112 pm, and 102 pm, respectively. Thus, the Sm^{3+} ions are expected to occupy Sr^{2+} sites rather than Al^{3+} sites. However, due to the nonequivalent substitution, an excess of positive charge in the lattice must be compensated. The most possible way is that two Sm^{3+} ions replace three Sr^{2+} ions to balance the charge of the phosphor that creates two $Sm_{Sr}^{\cdot}$ positive defects and one $V_{Sr}^{''}$ negative defect. The XRD patterns of 0, 1.75, 3.5 and 8.75 mol% H_3BO_3 containing phosphor powder were also recorded. From the XRD results it was found that 3.5 mol% H_3BO_3 containing phosphor showed pure $Sr_4Al_{14}O_{25}$ phase, however, if less or more concentration of H_3BO_3 was used as a flux, some impurity phases *viz.* $SrAl_2O_4$ and $SrAl_2B_2O_7$ were formed, respectively. The detail result on the effect of flux on pure phase formation of $Sr_4Al_{14}O_{25}$ phosphor has been explained in chapter II. Average crystallite size was estimated from the full width at half maximum of the diffraction peak by the sheerer equation and was estimated to be 2-3 μm in diameter.

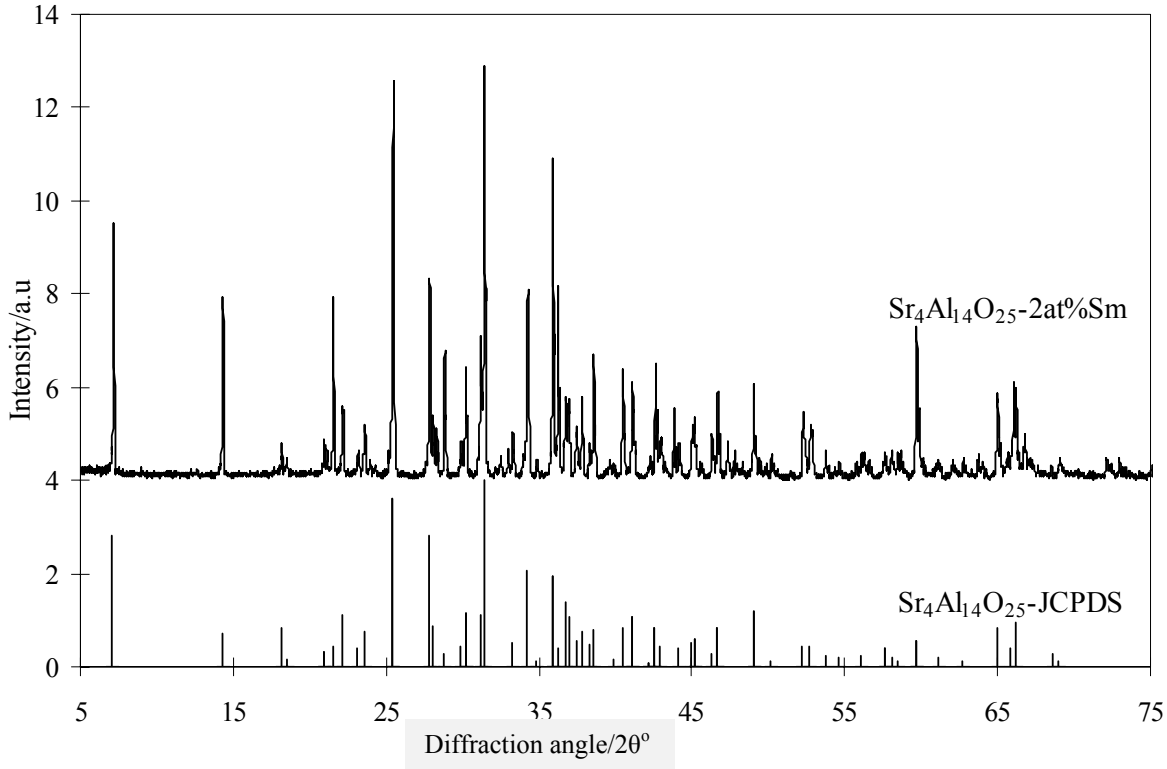

Fig. 5.1. XRD patterns of $Sr_4Al_{14}O_{25}$:2at% Sm phosphor compared with standard JCPDS value (52-1876) of $Sr_4Al_{14}O_{25}$ crystal.

SEM images along with energy dispersive X-ray spectroscopy (EDX) mapping of the $Sr_4Al_{14}O_{25}:Sm^{3+}$ phosphor samples are as shown in Fig. 5.2. These images revealed that spherical particles connected with each other forming a porous microstructure in the phosphor sample prepared without flux (0B). The average particle size was nearly 0.5 μm in diameter. When the phosphor sample was prepared adding small amount of flux (3.5 mol%), particles growth took place rapidly forming particles with the sharp edges and fixed corners. The average particles size was found to be nearly 2 μm, which is same as calculated from the XRD peaks. However, when the boron concentration was increased above 4 mol %, much bigger particles grew (~4 μm). Each particle showed smooth boundaries, indicating formation of glassy phase. Further, the glass completely covered the surface of the phosphor making it smooth. The EDX analysis was carried out to confirm the presence of Sm^{3+} ions in the phosphor and the results confirmed their presence (Fig 5.2d). From the EDX intensity calculation, it was found that nearly 1.55 at% Sm^{3+} was incorporated into the $Sr_4Al_{14}O_{25}$ matrix while originally added Sm^{3+} ions concentration was 2 at%.

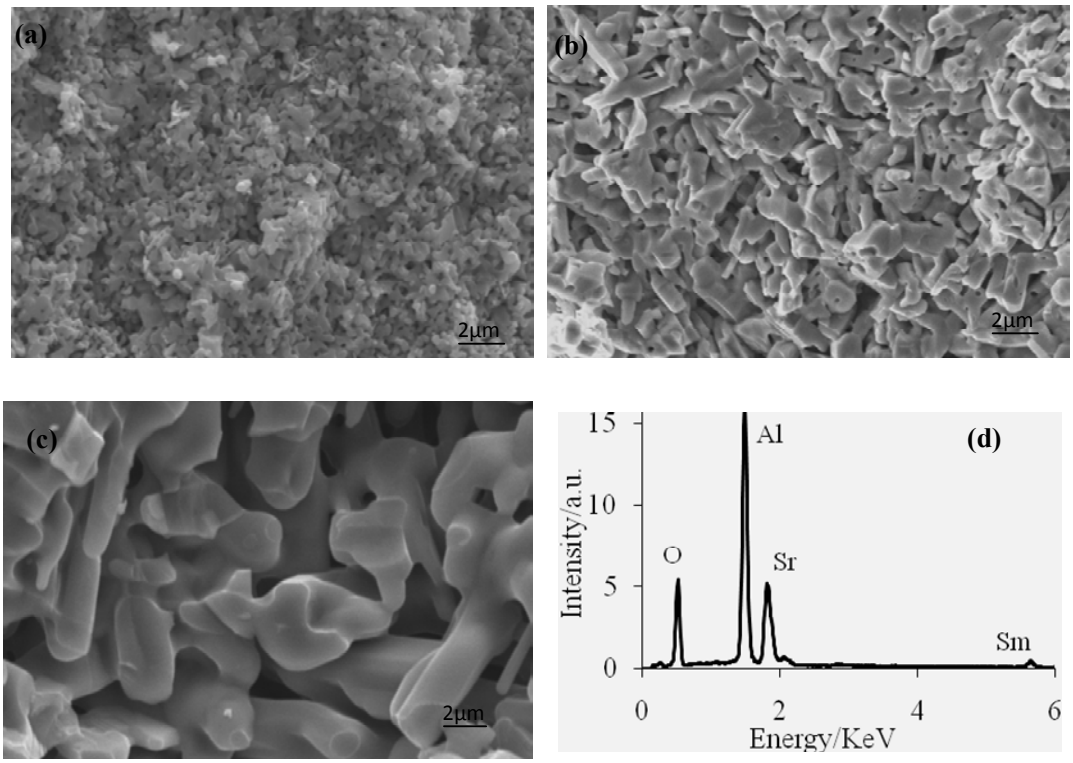

Fig. 5.2. SEM images of $Sr_4Al_{14}O_{25}:Sm^{3+}$ phosphors containing; (a) 0 mol%, (b) 3.5 mol %, (c) 8.75 mol % boric acid and (d) EDX spectrum of 2at% Sm doped $Sr_4Al_{14}O_{25}$ phosphor.

Room temperature photoluminescence (absorption and emission) spectra of $Sr_4Al_{14}O_{25}$:2at% Sm^{3+} phosphor was taken for the characterization of the optical properties. The absorption spectrum consists of a broad band from 220 to 440 nm. The excitation spectra of Sm^{3+} is obviously complicated, composed of charge transfer transitions from $O^{2-} \rightarrow Sm^{3+}$, f-f transitions, f-d transitions and absorption due to host lattice. The strong absorption peak of $Sr_4Al_{14}O_{25}$:Sm^{3+} were located at 230 nm, 330 nm, 400 nm and 420 nm. These peaks were corresponding to the $Sr_4Al_{14}O_{25}$ host absorption and that of the $^6H_{5/2} \rightarrow {}^{2S+1}L_J$ transitions of the Sm^{3+} ion. The emission spectrum of $Sr_4Al_{14}O_{25}$:2 at% Sm^{3+} phosphor measured at room temperature are shown in Fig. 5.3. The phosphor showed orange red emission when illuminated by UV light. The orange red emission of the phosphor was resulted from the mixture of four emissions peaks located at 560, 598, 640 and 700 nm instead of a monochromatic emission having a single peak in the spectrum. The emission spectra are contributed of the forbidden f-f orbital transition from $^4G_{5/2}$ level to the $^6H_{5/2}$, $^6H_{7/2}$, $^6H_{9/2}$ and $^6H_{11/2}$ levels of Sm^{3+} ion [12]. Among these emissions, the strongest emission ($^4G_{5/2} \rightarrow {}^6H_{7/2}$) is located at 598 nm. Particularly, the emission lines located at 598, 640 and 700 nm are the most important parts of the emissions because they are located at the longer wavelength (orange red) region of the spectrum.

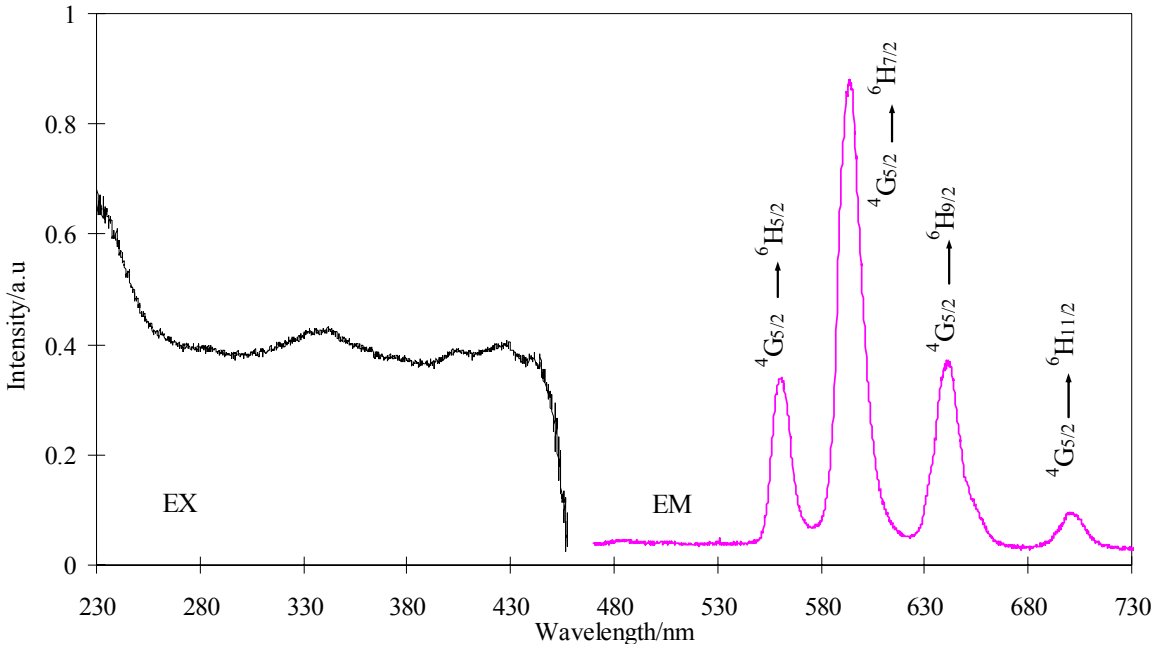

Fig. 5.3. Room temperature absorption and emission spectra of $Sr_4Al_{14}O_{25}$:2 at% Sm^{3+} phosphor.

Figure 5.4 shows the effect of flux (H_3BO_3) on the emission intensity of the $Sr_4Al_{14}O_{25}$:2 at% Sm^{3+} phosphor. It is clear that the emission intensity increased on increasing the flux concentration. It is the flux that can properly facilitate the entry of activator ions into the crystal lattice and aids in the formation of the luminescent centers [13]. Due to liquid boron oxide as high temperature flux, distribution of the rare ions becomes random and deep throughout the lattice as well as the flux enforce the Sm^{3+} ions to replace the Sr site in the lattice [14]. This increases the Sm^{3+} concentrations in the lattice. Further, the flux helps the Sm^{3+} ions to distribute uniformly throughout the host lattice and causes steep increase in the emission intensity. The maximum intensity was observed in the phosphor sample prepared using 3.5 mol% boric acid. Above 4 mol% boric acid concentration, the emission intensity started decreasing, that might be due to the formation of non emissive glassy phases on the surface that covers the surface and protects the phosphor from emission as observed in XRD profiles and SEM image (Fig. 5.2c).

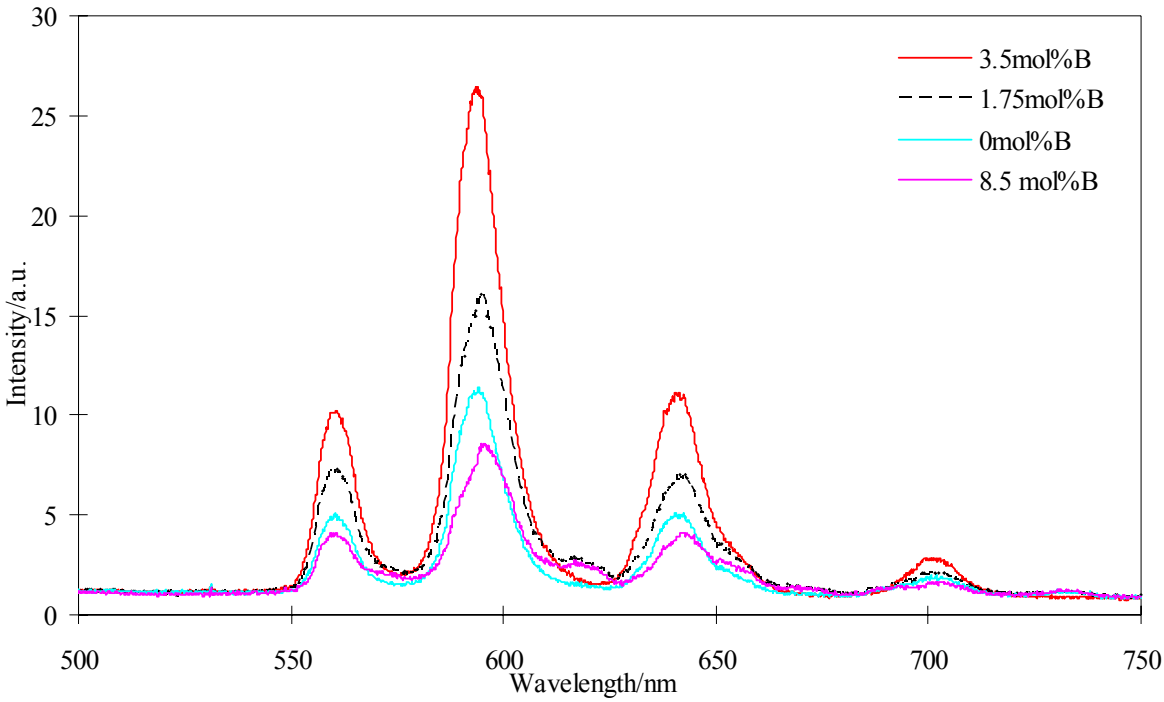

Fig. 5.4. Variation of fluorescence intensity of the $Sr_4Al_{14}O_{25}$:2 at% Sm^{3+} phosphor with various boric acid concentrations.

To study the effect of Sm^{3+} ions concentrations on the emission intensity of the $Sr_4Al_{14}O_{25}$:Sm^{3+} phosphors, a series of samples with different Sm^{3+} ions concentrations

ranging from 1 at% to 8 at% were prepared, keeping all other processing conditions constant. Fig. 5.5 shows the variation of emission intensity according to the Sm^{3+} ions concentrations. From the figure it is clear that on increasing the Sm^{3+} ions concentrations, the emission intensity first increased, attained maximum emission at 2 at% Sm^{3+} concentration, and thereafter, again decreased. The decrease in the emission intensity at higher Sm^{3+} ions concentration might be due to the concentration quenching process [15]. With the increase of the activator concentration, here Sm^{3+} ions, the distance between the nearby Sm^{3+} ions becomes shorter and the interaction between them increases. Thus it is easier to transfer the excitation energy from one activated ions to another and that finally transfers to the non emitting centers leading to quenching of the emission.

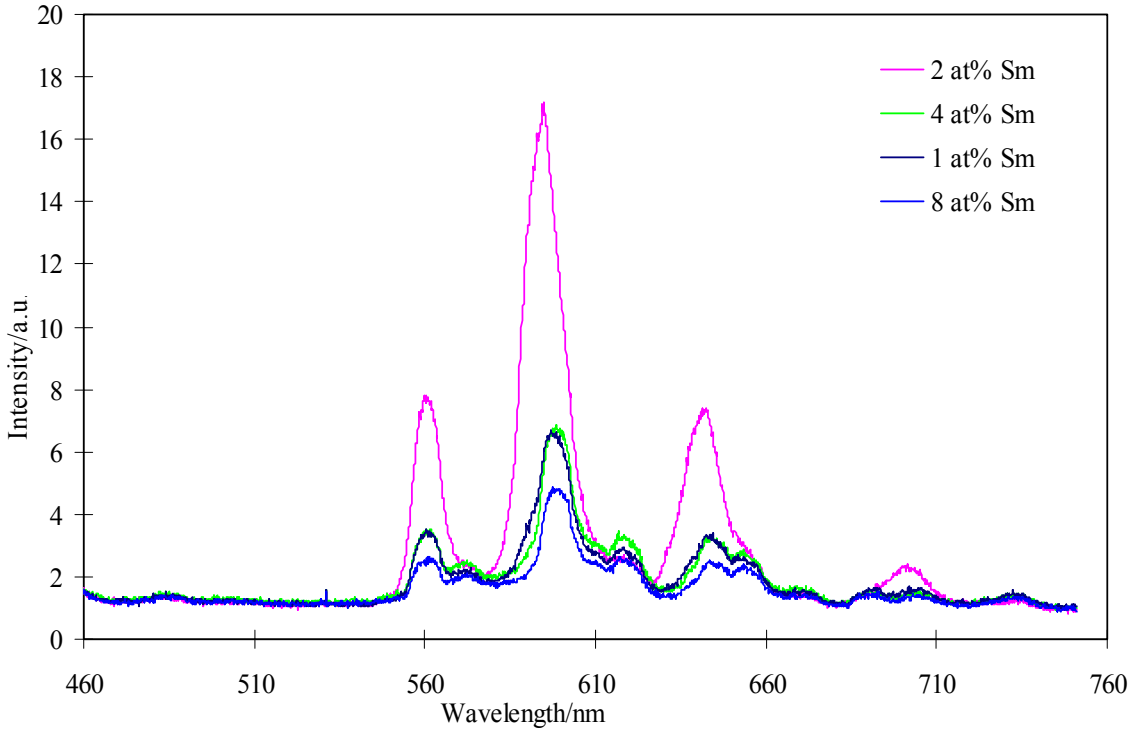

Fig. 5.5. Variation of emission intensity of the $Sr_4Al_{14}O_{25}:Sm^{3+}$ phosphor with various Sm^{3+} ions concentrations.

Figure 5.6 shows the effects of M^{3+} ions co-dopant (M = Bi, Dy and Nd; each being 2 at%) on the photoluminescence emission phenomena. Co-doping of these M^{3+} ions were not found to change the emission band position of the phosphor. Thus, it can be assumed that the emission is mainly originated from the Sm^{3+} emission center rather than these co-doped M^{3+} ions. However, addition of Bi^{3+} increased the emission intensity drastically, the increase by Dy^{3+} was not so pronounced, but Nd^{3+} suppressed it. It should be noted that

addition of Dy^{3+} and Bi^{3+} besides increasing the emission intensity at these 4 peaks, the shoulder peak at 596 nm was observed with much higher intensity then the other peaks. To confirm, whether the new peak at 596 nm was either form Bi^{3+} or Dy^{3+} ions, $Sr_4Al_{14}O_{25}:Bi^{3+}$ or Dy^{3+} phosphor samples with same amount of Bi^{3+} or Dy^{3+} ions were prepared independently. However, no any emission peaks were observed in the samples $Sr_4Al_{14}O_{25}:Bi^{3+}$ and $Sr_4Al_{14}O_{25}:Dy^{3+}$. Thus, the emission peak of the $Sr_4Al_{14}O_{25}:Sm^{3+}/Bi^{3+}$ phosphor at 596 nm should be due to splitting of the emission peak at 598 nm. It is possible that addition of Bi^{3+} and Dy^{3+} ions change the crystal field around the Sm^{3+} ions and splits the $^4G_{5/2}$ to $^6H_{7/2}$ peaks into duplets with unequal intensities [16]. The reason of the increase in emission intensity by Dy^{3+} or Bi^{3+} co-doping might be due to the fact that Bi^{3+} and Dy^{3+} ions efficiently absorbs the excitation energy than other ions used in the present study and transfers it efficiently to the Sm^{3+} ions [17], consequently, increased the emission intensity.

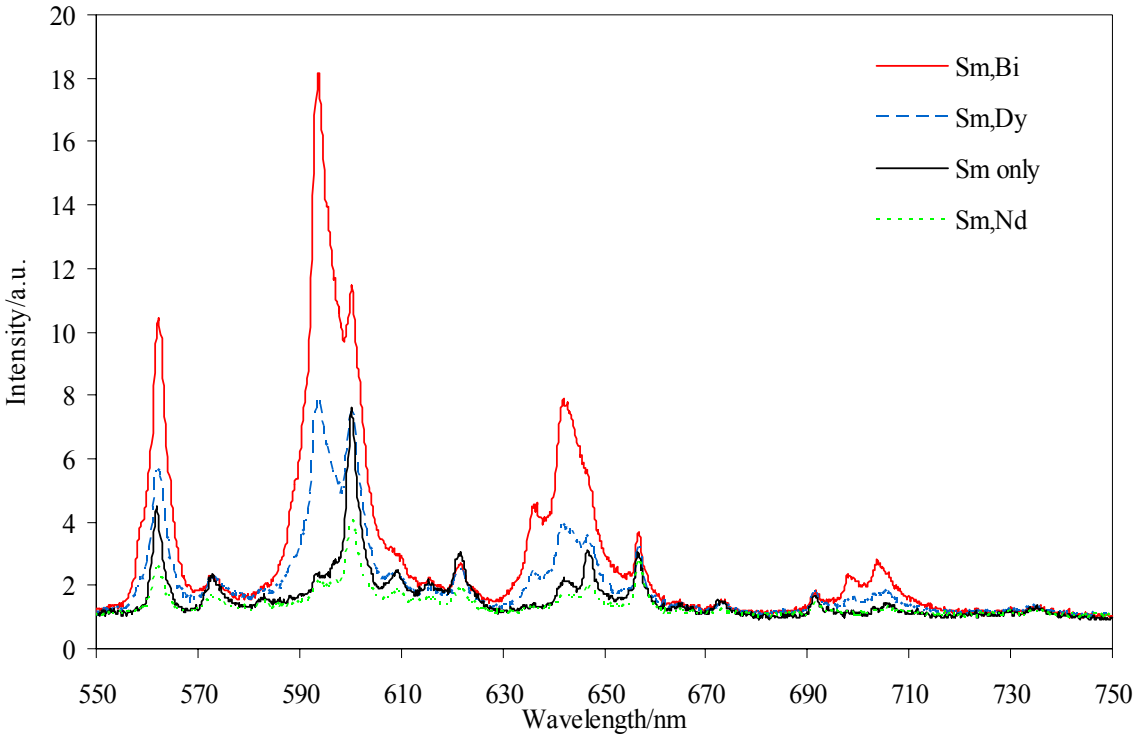

Fig. 5.6. Effect of M^{3+} (Bi^{3+}, Dy^{3+} and Nd^{3+}) co-dopants on the emission spectra of $Sr_4Al_{14}O_{25}$:2 at% Sm^{3+} phosphors.

It is well known that Bi^{3+} is good sensitizers of luminescence in many hosts [18]. It can efficiently absorb the UV-light and transfer the absorbed energy to the luminescent center; as a result, the emission intensity of the luminescent center would be strengthened.

Fig. 5.6 shows the effect of Bi^{3+} ions concentrations on the emission intensity of $Sr_4Al_{14}O_{25}$:2 at% Sm^{3+}/x at% Bi^{3+} phosphor. On increasing Bi^{3+} ions concentrations, the emission intensity gradually increased and reached maximum when doped Bi^{3+} ions concentration was 2 at%, after that it started decreasing and became almost non emissive when it was 16 at%. Thus, at optimum concentration, the excitation energy is transferred to the Sm^{3+} ions, however, at higher concentration, it transfers from one another and finally to non-emitting centers, leading to quenching of the emission.

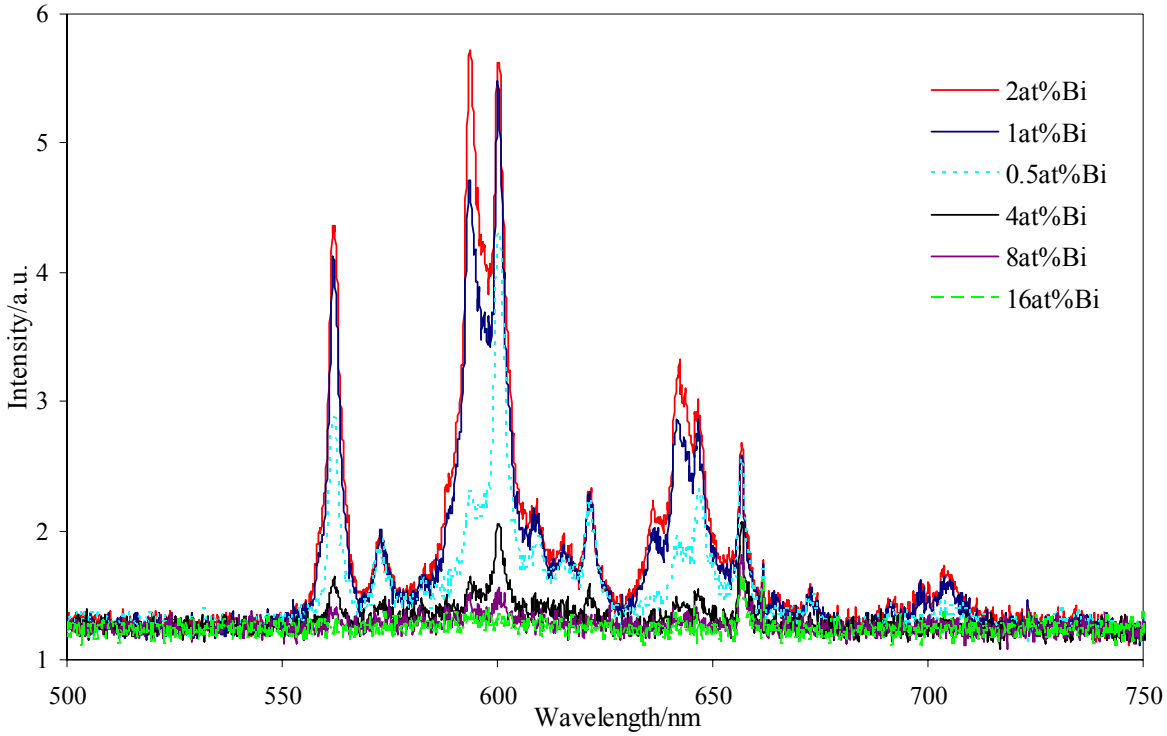

Fig. 5.7. Effect of Bi^{3+} ions concentration on the emission intensity of $Sr_4Al_{14}O_{25}$:2 at% Sm^{3+}/ x at% Bi^{3+} phosphor(x= 0.5, 1, 2, 4, 8 and 16).

The afterglow decay time of the orange red emission of the $Sr_4Al_{14}O_{25}:Sm^{3+}$, $Sr_4Al_{14}O_{25}:Sm^{3+}/Bi^{3+}$ and $Sr_4Al_{14}O_{25}:Sm^{3+}/Dy^{3+}$ phosphor samples were recorded at room temperature and presented in Fig. 5.8. From the figure it is clear that addition of Dy or Bi increased the phosphorescence intensity and the afterglow decay time of the phosphors, however, the increase was incremental. The phosphor samples showed very low phosphorescence intensity immediately after turning off the excitation light source that is hard to detect by the human eyes (naked human eye can detect phosphorescence intensity

more than 10 $mCd.m^{-2}$) and the afterglow faded away very fast, even faster than 10 sec.

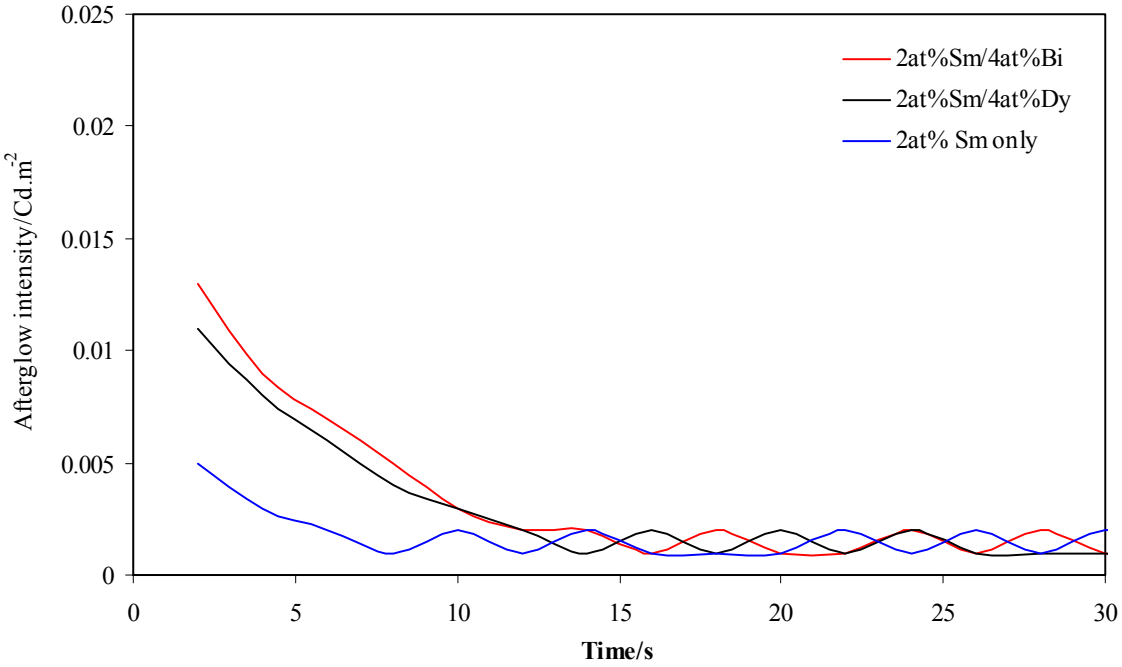

Fig. 5.8. Afterglow decay curves of M^{3+} (Bi^{3+}or Dy^{3+}) ions doped and undoped $Sr_4Al_{14}O_{25}$:2 at% Sm^{3+} phosphor.

5.3. Conclusion

A novel Sm^{3+} doped $Sr_4Al_{14}O_{25}$ phosphor was prepared by solid-state reaction method at 1350°C. It exhibited orange-red emission consisting of four emission maxima peaking at 560, 595, 640 and 700 nm, respectively. Introduction of H_3BO_3 as a flux significantly increased the fluorescence performance of the phosphor. The fluorescence intensity increased on increasing the H_3BO_3 flux concentration up to 4 mol % above that it decreased, the decrease is due to formation of impurity phases and the glasses. The fluorescence intensity of the phosphor increased on increasing the Sm^{3+} ions concentration up to 2 at% and then decreased. The decrease in emission intensity at higher Sm^{3+} ions concentration might be due to concentration quenching process. Addition of Bi^{3+} ions increased the emission intensity almost two times, the increase by Dy^{3+} was not so pronounced, but Nd^{3+} suppressed the emission intensity. The increase of emission intensity by Bi^{3+} co-doping might be due to efficient energy transfer to the Sm^{3+} emission centers from the excitation source. The optimum concentration of Bi^{3+} to enhance the emission intensity was found to be 2 at%.

References

[1] C.K. Chang, D.L. Mao, J.F. Shen, J. Alloys Compd. **348** (2003) 224.

[2] T. Aitasalo, J. Holsa, H. Jungnerd, H. Jungner, M. Lastusaari, J. Niittykoski, J. Lumin. **94-95** (2001) 59.

[3] R. Zhong, J. Zhang, S. Lu, X.J. Wang, Appl. Phys. Lett. **88** (2006) 201916.

[4] V. Shankar, H. Chander, H. Divi, P.K. Ghosh, US patent 0183807 A1.

[5] G. Blasse, B.C. Grabmaier, Luminescent Materials, Springer, Berlin (1994) 123.

[6] http://www.nemoto.co.jp/en/products/luminova/pdf/lumonova-BG.pdf (accessed: 2009-01-13).

[7] Z. Wu, M. Gong, J. Shi, Q. Su, J. Alloys Compd. **458** (2008) 134.

[8] B. Lei, Y. Liu, J. Liu, Z. Ye, C. Shi, J. Solid State Chem. **177** (2004) 1333.

[9] G.B. Kumar, S. Buddhudu, Physica B, **403** (2008) 4146.

[10] W.M. Yen, S. Shionoya, H. Yamamoto, Phosphor Hand Book, CRC press, New York (1998) 483.

[11] B.M.S. Smets, J. Rutten, G. Hokes, J. Verlijsdonk, J. Electrochem. Soc. **136** (1989) 2119.

[12] G.S.R. Raju, S. Buddhudu, Spectrochimica Acta A, **70** (2008) 601.

[13] G.F.J. Garlick, Luminescent materials, Oxford university Press, UK (1949) 73.

[14] Y. Lin, Z. Tang, Z. Zhang, Mater. Lett. **51** (2001) 14.

[15] D. Wang, Q. Yin, Y. Li, M. Wang, J. Lumin. **97** (2002) 1.

[16] H.M. Farok, G.A. Saunders, W.C.K. Poon, J. Crain, H. Vass, W. Honle, E. Schonherr, J. Mater. Sci. **34** (1999) 2389.

[17] R.K. Datta, J. Electrochem. Soc. **114** (1967)1057.

[18] W. Jia, A. Perez-Anhujar, I. Rivera, J. Electrochem. Soc. **150** (2003) H161.

Chapter VII

General conclusion

$Sr_4Al_{14}O_{25}:Eu^{2+}/Dy^{3+}$ phosphor with high brightness and long persistent afterglow was synthesized by the solid state reaction method at 1350°C. Highly crystalline, single phase $Sr_4Al_{14}O_{25}$ phosphor was obtained when 3.5 mol% boric acid was used as a flux. The SEM results revealed that particles shape and size could be controlled by the use of appropriate amount of flux. When 3.5 mol% boric acid was used as a flux, fine particles with higher angularity were observed. The EDX mapping results revealed that the Eu^{2+} and Dy^{3+} ions were homogeneously dispersed in the phosphor matrix. The broad band UV-visible excited luminescence of the orthorhombic $Sr_4Al_{14}O_{25}:Eu^{2+}/Dy^{3+}$ phosphor was observed in the blue-green region (λ_{max} = 497 nm) due to transitions from $4f^65d^1$ to $4f^7$ configuration of the Eu^{2+} ion. The photoluminescence characteristics were highly influenced by the addition of small quantities of H_3BO_3 (flux) in the starting mixture and maximum phosphorescence properties were observed at 3.5 mol% boric acid. When the samples were preheated at 1000°C and then reduced at 1350°C in 10% H_2 and 90% N_2, better photoluminescence properties were observed. The optimum concentration of the emission center (Eu^{2+}) for the higher brightness was found to be 4 at%. Out of various trivalent rare earth ions, Dy^{3+} was found to be affective to enhance the phosphorescence properties due to formation of suitable traps in the $Sr_4Al_{14}O_{25}$ matrix. When doped Eu^{2+} concentration was 4 at% and co-doped Dy^{3+} 8 at%, the phosphor showed better phosphorescence intensity and longer afterglow persistency. The decay curve fitting results revealed that the phosphor with the aluminium to strontium ratio (Al/Sr) of 3.7 had deeper trap depths and hence showed the higher phosphorescence intensity. Addition of 3 mol% Ag^+ as a charge compensator dramatically enhanced the brightness of the phosphor (almost 2 fold) that may be due to removal of the lattice defects formed during replacement of strontium by trivalent rare metal ions. Use of γ-alumina of 0.05μm size as a raw powder during the synthesis of phosphor was found to be effective for the formation of regular particles with smaller particles size over other alumina type and showed the better photoluminescence characteristics.

Substitution of part or whole of strontium sites by calcium or barium ions can effectively monitor the luminescence color and CIE values of the phosphor. When 0.7 to 0.8 mole fraction of calcium was used in place of strontium, a bluish-white luminescence was observed due to the mixing of the blue emission in $CaAl_4O_7:Eu^{2+}$ phosphor and green emission in $SrAl_2O_4:Eu^{2+}$ phosphor, however the persistent time of the bluish-white afterglow was very short due to short life time of blue emission in $CaAl_4O_7:Eu^{2+}$ phosphor.

The $Sr_4Al_{14}O_{25}:Eu^{2+}/Dy^{3+}$ phosphor was synthesized by Pechini sol-gel, chemical combustion and solid state reaction methods and their microstructure and photoluminescence characteristics were compared. At very low synthetic temperature (CB-530^oC), impurities of $SrAl_2O_4$ existed but at higher synthetic temperature ($\geq$1200^oC) pure $Sr_4Al_{14}O_{25}$ phase was observed. Relatively smaller particles size, regular morphology and narrow size distribution could be achieved by wet chemical methods (sol-gel and chemical combustion). Thus, the particle shape and size can be controlled by sol-gel and chemical combustion methods. Even at the same sintering temperatures, the combustion method can be used to generate smaller particles with higher crystallinity. By the chemical combustion method, activator ions can be homogenously dispersed throughout the phosphor matrix leading to the higher excitation, emission and afterglow intensities.

Cr^{3+} co-activated persistent $Sr_4Al_{14}O_{25}:Eu^{2+}/Dy^{3+}$ phosphor was synthesized by the chemical combustion synthesis method. The red emission in Cr^{3+} at 695 nm and blue-green emission in Eu^{2+} at 495 nm was observed in the same $Sr_4Al_{14}O_{25}$ host doped with Eu^{2+} and Cr^{3+} ions together. The blue-green emission was due to the $4f^65d^1 \rightarrow 4f^7$ transition of Eu^{2+} ions in the $Sr_4Al_{14}O_{25}$ host while the red emission in Cr^{3+} was observed due to energy transfer from Eu^{2+} to Cr^{3+}. As the concentration of Eu^{2+} and Dy^{3+} were fixed, the red emission intensity in Cr^{3+} was increased on increasing Cr^{3+} ions concentrations and attained maximum at 4 at%, beyond that it was decreased due to quenching process. Boric acid as flux (4 mol%) and proper amount of rare earth metal ions (4 at% Eu^{2+} and 8 at% Dy^{3+}) played important role for the improvement of the photoluminescence characteristics. The red phosphorescence decayed much faster than the blue-green phosphorescence. The faster decay speed of red phosphorescence in the Cr^{3+} was due to existence of shallow traps nearby Cr^{3+} ions. The persistent time for blue-green emission was more than 10 h but that of red was comparatively very short.

A novel Sm^{3+} doped $Sr_4Al_{14}O_{25}$ phosphor was prepared by solid-state reaction method at 1350^oC. The phosphor showed orange-red emission consisting of four main emission peaks at 560, 595, 640 and 700 nm, respectively. Introduction of H_3BO_3 as a flux significantly increased the emission performance of the phosphor. The fluorescence intensity increased by increasing the concentration of H_3BO_3 up to 4 mol% above that it decreased. The phosphor samples were prepared doping 1, 2, 4 and 8 at% Sm^{3+} ions. The emission intensity increased with the Sm^{3+} concentration up to 2 at% and then decreased, that might be due to concentration quenching process. Addition of 2 at% Bi^{3+} ions increased the emission intensity drastically, the increase by Dy^{3+} was not so pronounced but Nd^{3+} suppressed it. The increased emission intensity of the phosphor by Bi^{3+} co-doping was found to be due to efficient energy transfer to the Sm^{3+} emission centers.

Overall, the $Sr_4Al_{14}O_{25}$ phosphor with various emission colors was synthesized by incorporating different emission centers or substituting one of the host ions, *viz.* $Sr_4Al_{14}O_{25}:Eu^{2+}/Dy^{3+}$ (blue-green), $Sr_4Al_{14}O_{25}:Cr^{3+}/Eu^{2+}/Dy^{3+}$ (red and blue-green), $Sr_4Al_{14}O_{25}:Sm^{3+}$ (orange-red) and $Sr_{0.8}Ca_{3.2}Al_{14}O_{25}:Eu^{2+}/Dy^{3+}$ (white). The microstructure and the photoluminescence characteristics can be controlled by the methods of synthesis, addition of various additives (fluxes, emission centers, charge compensators, rare metal ions), composition and quality of starting materials. The phosphor showed bright intensity and long persistent time and hence can be used in various display applications, especially 'glow in dark items'.

List of Publications

1. H. N. Luitel, T. Watari, T. Torikai, M. Yada, R. Chand, "Highly Water Resistant Surface Coating by Fluoride on Long Persistent $Sr_4Al_{14}O_{25}:Eu^{2+}/Dy^{3+}$ Phosphor", Applied Surface Science, 256 (2010) 2347–2352.

2. H. N. Luitel, T. Watari, T. Torikai, M. Yada, "Luminescent properties of Cr^{3+} doped $Sr_4Al_{14}O_{25}:Eu^{2+}/Dy^{3+}$ blue-green and red phosphor", Optical Materials **31** (2009) 1200–1204.

3. H. N. Luitel, T. Watari, T. Torikai, M. Yada, "Effects of Particle Size and Type of Alumina on the Morphology and Photoluminescence properties of $Sr_4Al_{14}O_{25}$: Eu^{2+}/Dy^{3+} Phosphor", Research Letter in Materials Sciences **Vol. 2009**, Article ID–475074.

4. H. N. Luitel, T. Watari, T. Torikai, M. Yada, "Preparation and characterization of Eu and Dy doped $Sr_4A_{l14}O_{25}$ Phosphor", Materials Science Forum **569** (2008) 249–252.

5. R. Chand, H.N. Luitel, T. Watari, K. Inoue, T. Torikai, M. Yada, "Chemical modification of carbonized wheat and barley straw using HNO_3 and the adsorption of Cr(III)", Journal of Hazardous Materials **15** (2009) 319–324.

6. R. Chand, T. Watari, K. Inoue, H.N. Luitel, D. Parajuli, T. Torikai, M. Yada, "Selective adsorption of precious metals from hydrochloric acid solutions using porous carbon prepared from barley straw and rice husk", Minerals Engineering, **22** (2009) 1277–1282.

Academic Activities and Paper Presentations

1. H. N. Luitel, T. Watari, T. Torikai, M. Yada, "Preparation of $Sr_4Al_{14}O_{25}$ Phosphor and Protective Coating by Ammonium fluoride", Japan-China-Korea (CJK2009) Seminar & Summer Workshop, 2009, Jeju, Korea.

2. T. Watari, H.N. Luitel, "Preparation and Characterization of (Ca-Sr)Aluminate: Eu^{2+}, Nd^{3+} phosphors", The CJK2009 Seminar and Summer Workshop, June 2009, Jeju, Korea.

3. H. N. Luitel, T. Watari, T. Torikai, M. Yada, C.N. Xu, N. Kazuhiro, "Development and Application of New Luminescent Materials-Mechanoluminescence and Long Persistent Phosphor" 12th Saga University-AIST joint seminar, 2009, Saga, Japan.

4. H. N. Luitel, T. Watari, T. Torikai, M. Yada, "Development and Applications of $Sr_4Al_{14}O_{25}:Eu^{2+}/Dy^{3+}$ Long Persistent Phosphor", The 21st JSPS-KOSEF CUP Seminar between Japan & Korea, Dec. 2008, Awaji Japan.

5. T. Watari, H. N. Luitel, T. Torikai, M. Yada, "Fabrication of Ceramic Phosphors by Penetration process using Ceramic Plate", The 21st JSPS-KOSEF CUP Seminar between Japan & Korea, Dec. 2008, Awaji, Japan.

6. H. N. Luitel, T. Watari, T. Torikai, M. Yada, "Effect of particle size and type of alumina on the morphology and photoluminescence properties of $Sr_4Al_{14}O_{25}:Eu^{2+}/Dy^{3+}$ phosphor", The 21st International Symposium on Chemical Engineering, Dec. 2008, Saga University, Japan.

7. H. N. Luitel, T. Watari, T. Torikai, M. Yada, "Improvement of Phosphorescence characteristics of Strontium Aluminates phosphor", 10th Saga University-AIST joint seminar, 2008, Saga, Japan.

8. H. N. Luitel, T. Watari, T. Torikai, M. Yada, "Effect of Flux and Rare metal ions on the Phosphorescence properties of $Sr_4Al_{14}O_{25}$ Phosphor", The 1st Workshop on New Trends in Chemistry and Biology, Jan. 2008, Saga University, Japan.

9. H. N. Luitel, T. Watari, T. Torikai, M. Yada, "Preparation & properties of $Sr_4Al_{14}O_{25}:Eu^{2+}/Dy^{3+}$ Phosphor", 9th international Symposium on Eco- Materials Processing and Design, 2008, Changwon, Korea.

10. H. N. Luitel, T. Watari, T. Torikai, M. Yada, "Improvement on Phosphorescence characteristics of $Sr_4Al_{14}O_{25}$: Eu^{2+}/Dy^{3+} Phosphor" The 1st Workshop on New Trends in Chemistry and Biology, 2008, Saga University, Japan.

Resume

Name: Hom Nath Luitel

Nationality: Nepali

Date and Place of Birth: 1979/10/15, Ladhavir-2, Sindhuli, NEPAL.

Gender/ Marital Status: Male/ Married

Academic qualification:

2007 – 2010 – Ph. D., Saga University, Japan

2002 – 2005 – M. Sc., Tribhuvan University, Nepal

1999 – 2002– B. Sc., Amrit Science College, Tribhuvan University, Nepal

1997 – 1999 – I. Sc., R.R.M. Campus, Tribhuvan University, Nepal

Area of Research:

Materials Chemistry: Preparation & Characterization of various Inorganic Luminescent Materials

Major List of Publications:

1. H. N. Luitel *et al.*, Applied Surface Science, **256** (2010) 2347–2352.
2. H. N. Luitel *et al.*, Optical Materials **31** (2009) 1200–1204.
3. H. N. Luitel *et al.*, Research Letter in Materials Sciences, **Vol. 2009**, Article ID-475074.
4. H. N. Luitel *et al.*, Materials Science Forum **569** (2008) 249-252.
5. Rumi Chand, H.N. Luitel *et al.*, Journal of Hazardous Materials **15** (2009) 319-324.

Reference:

Prof. Dr. Takanori WATARI

Department of Applied Chemistry, Saga University, Saga, JAPAN

watarit@cc.saga-u.ac.jp

Tel: +81-952-28-8683